拓扑量子相变

刘 伍 明

(中国科学院物理研究所)

Email: wmliu@iphy.ac.cn

Supported by NSFC, MOST, CAS

Collaborators

强关联系统：

Yao-Hua CHEN（陈耀桦）

Heng-Fu LIN（林恒福）

Hai-Di LIU（刘海迪）

Hong-Shuai TAO（陶红帅）

Wei WU（吴为）

自旋-轨道耦合系统：

Ming YANG（杨明）

Tian ZHANG（张田）

Xiao-Long ZHANG（张晓龙）

目 录

1、概况：量子相变

A phase transition between different quantum phases, Contrary to classical phase transitions, quantum phase transitions can only be accessed by varying a physical parameter—such as magnetic field or pressure—at absolute zero temperature.

Transverse Ising Chain $H = -J \sum_{\langle i,j \rangle} \sigma_i^z \sigma_j^z + h \sum_i \sigma_i^x$

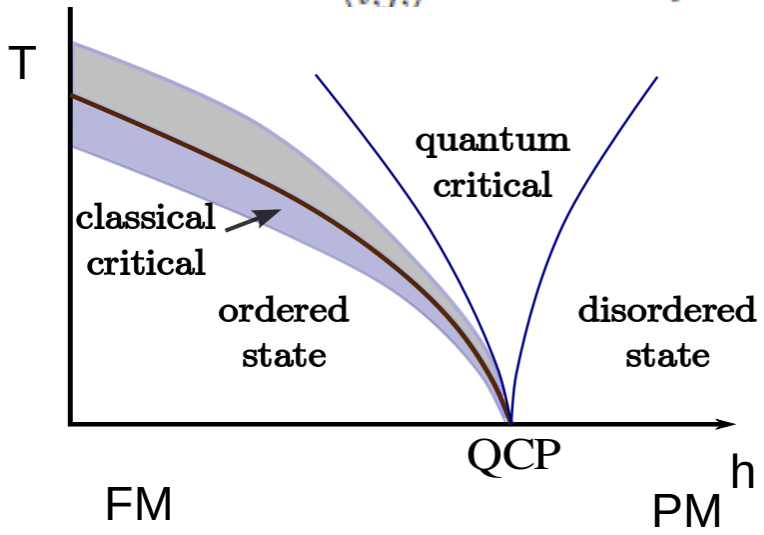

Finite-T phase diagram of the *d* = 1 quantum Ising model

1、概况： 拓扑量子相变

拓扑量子相变往往临近于某个拓扑态，需要引入规范场以及分数化的自由度。

使用陈数、Berry相等描述拓扑量子相变，包括拓扑绝缘体、拓扑超导体、拓扑量子计算、自旋量子霍尔效应等。

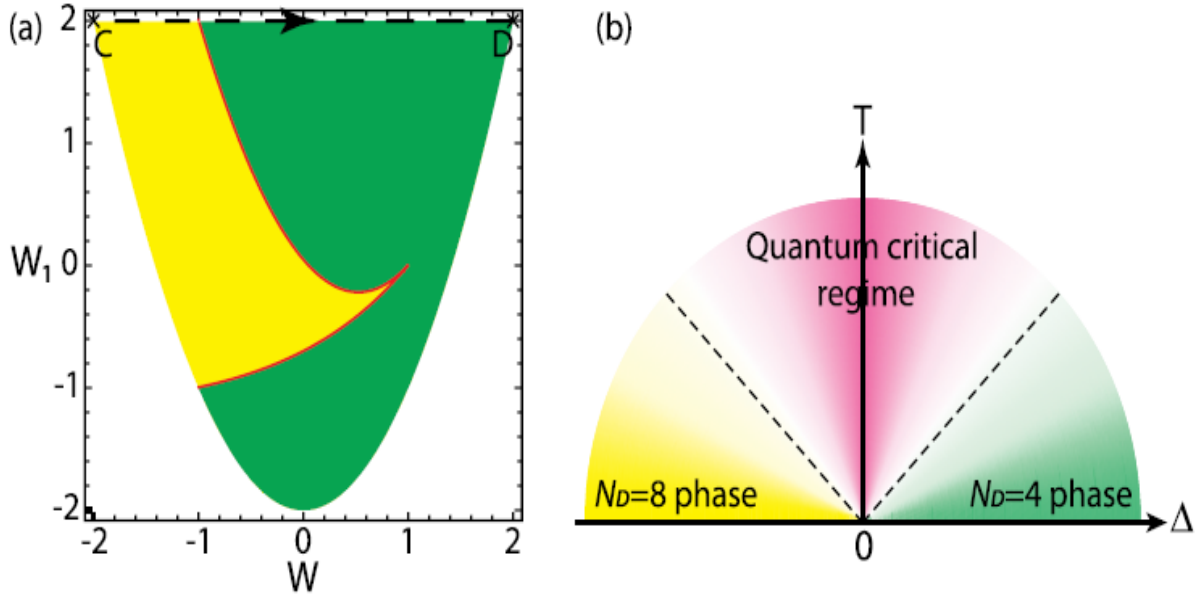

Figure 4 | Finite-T Phase diagram. (a) The gauge-invariant phase diagram in terms of the Wilson loops W and W_1. The yellow (green) regime is $N_D = 8$ ($N_D = 4$). The dashed line corresponds to the one in Fig. 1(b). (b) Finite-T Phase diagram of the topological quantum phase transition as a function of the flux Δ and the temperature T. There is a topological quantum phase transition at $T = 0, \Delta = 0$. The two dashed lines stand for the crossovers at $T \sim |\Delta|$.

2、强关联系统

The interaction between particles are large compared with their kinetic energy.

The growing list of strongly correlated systems include:

- Cuprate and Iron-Based superconductors.

The interactions amongst electrons in localized 3d-shells form an AFM Mott insulator, which develops HTSC when doped.

- Heavy electron compounds.

The localized magnetic moments immersed within the metal give rise to electrons quasiparticles with effective mass ~1000 bare electron mass.

- Fractional quantum Hall system.

The interactions between electrons in the lowest Landau level generate a incompressible state with quasiparticles of fractional charge and statistics.

- Cold atomic gases.

The interactions between the neutral atoms governed by two-body resonances, can be tuned by external magnetic fields.

2、强关联系统：　　高温超导（1986）

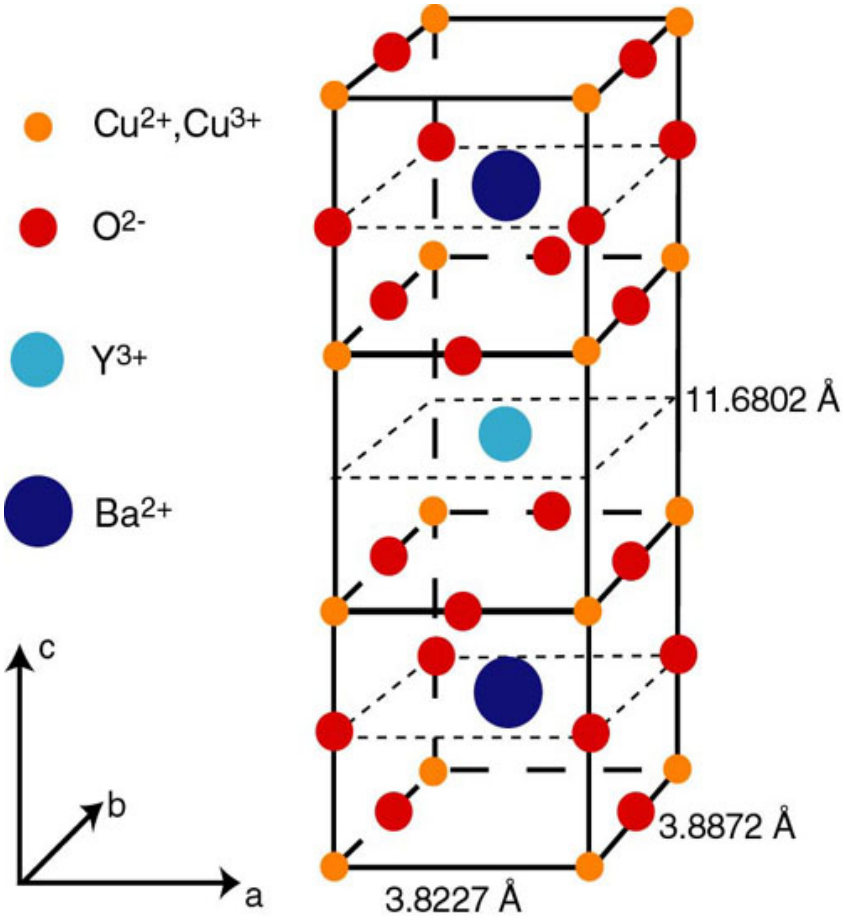

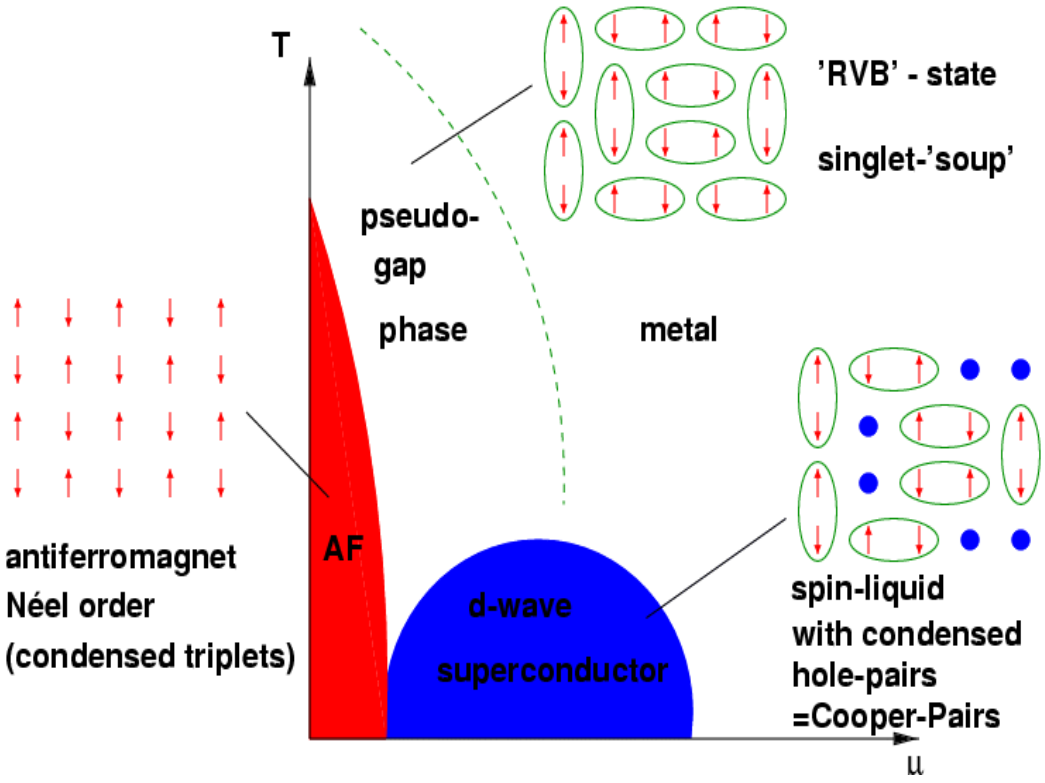

2、强关联系统：　　铁基超导（2008）

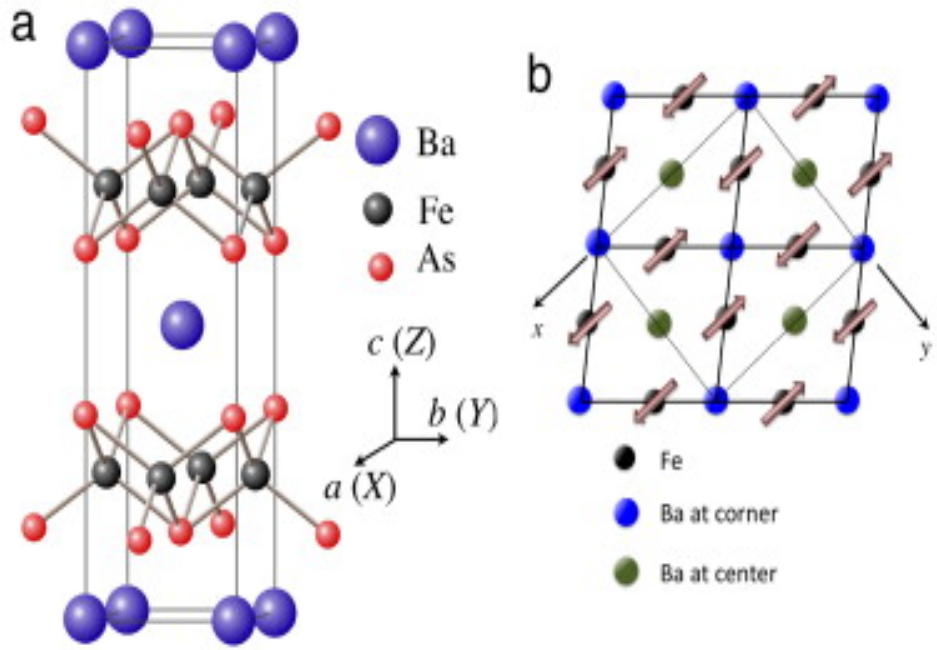

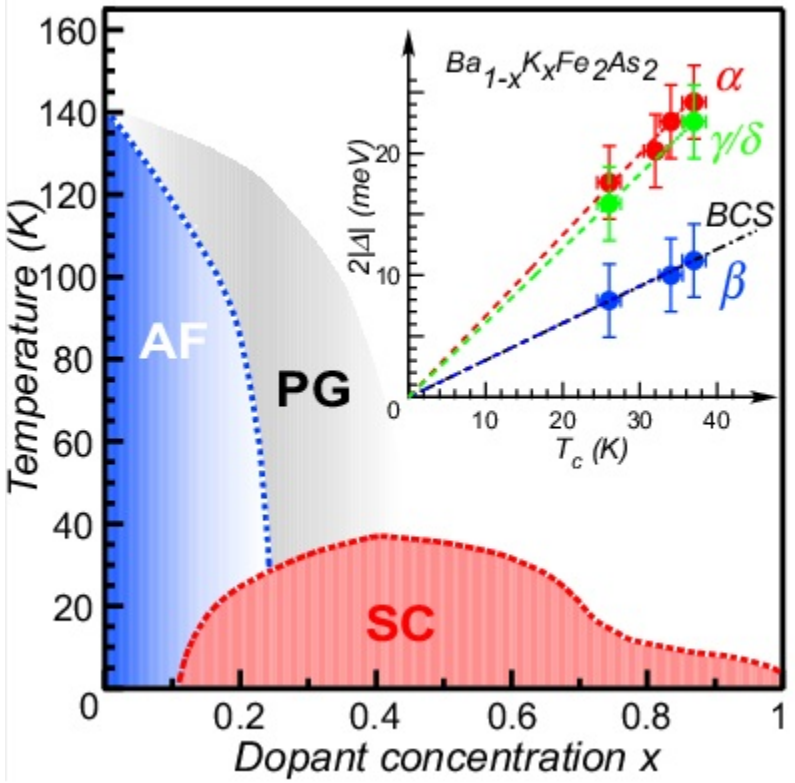

2、强关联系统：　　光晶格冷原子（2002）

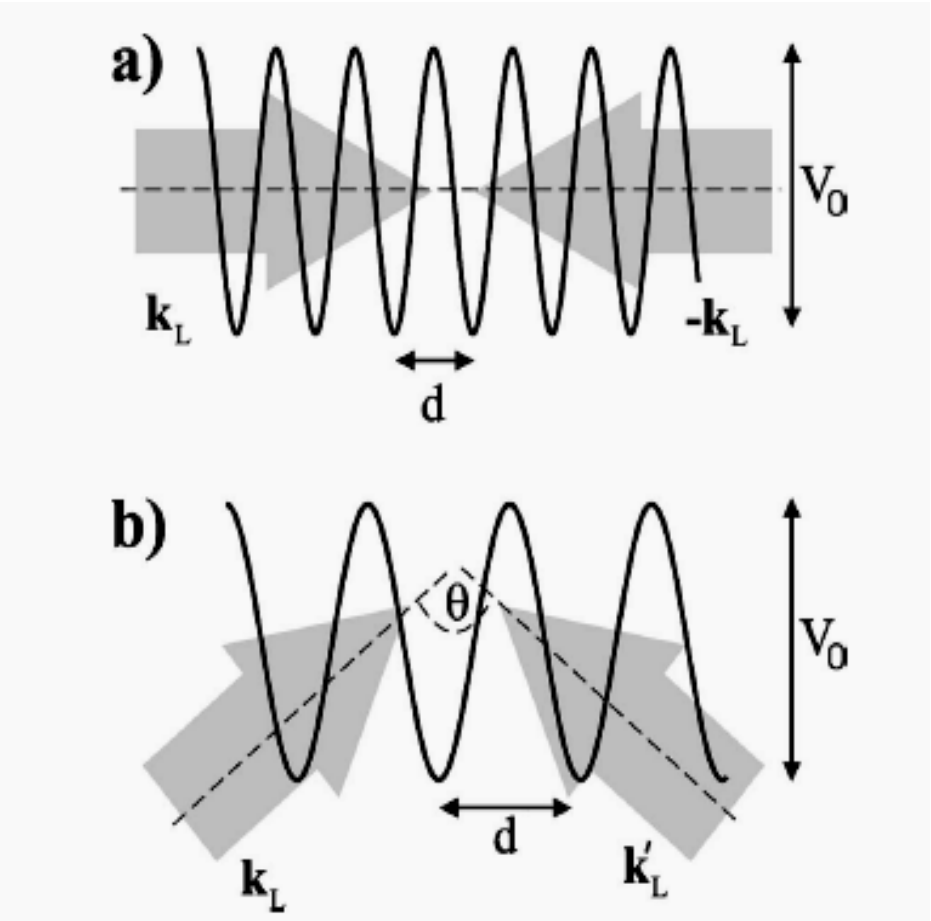

FIG. 1. A one-dimensional optical lattice created from cour terpropagating laser beams (a) and with beams enclosing a angle θ (b). The parameters V_0 (lattice depth) and d (lattic spacing) are defined in the text.

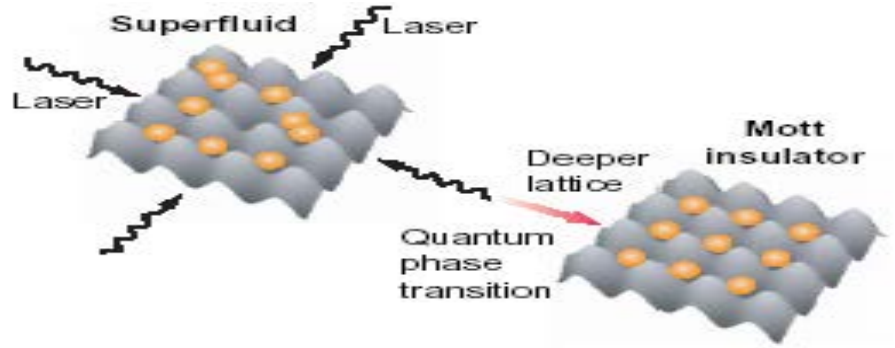

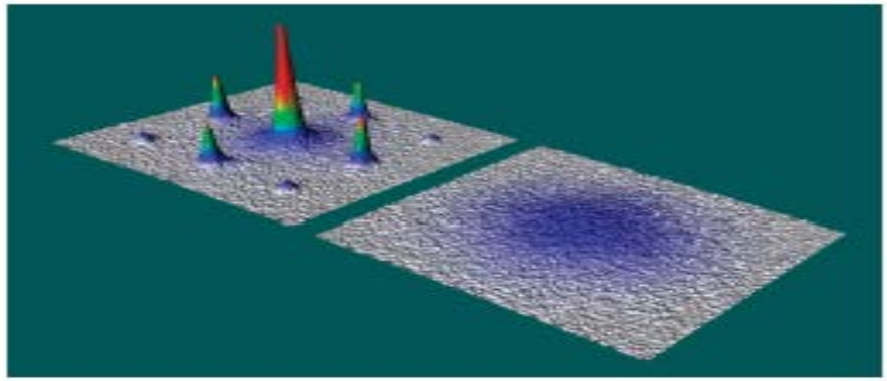

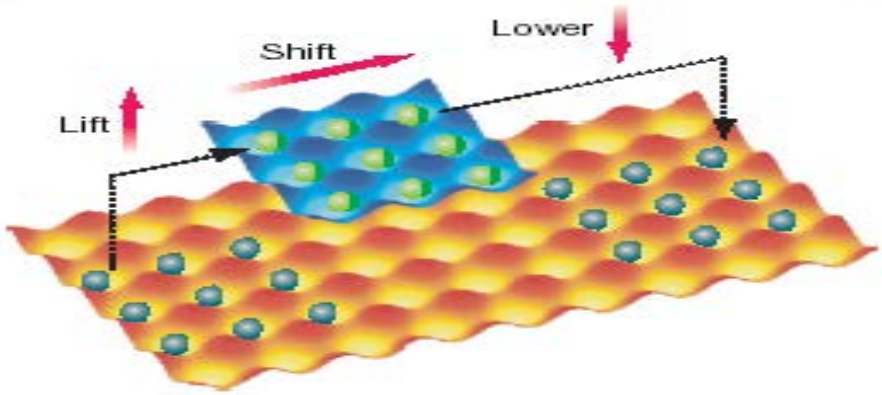

2、强关联系统：　　强关联效应和量子相变

A、调节相互作用

$$H = -t\sum_{\langle i,j\rangle}(b_i^{\dagger}b_j + h.c.) + \frac{U}{2}\sum_i n_i(n_i - 1),$$

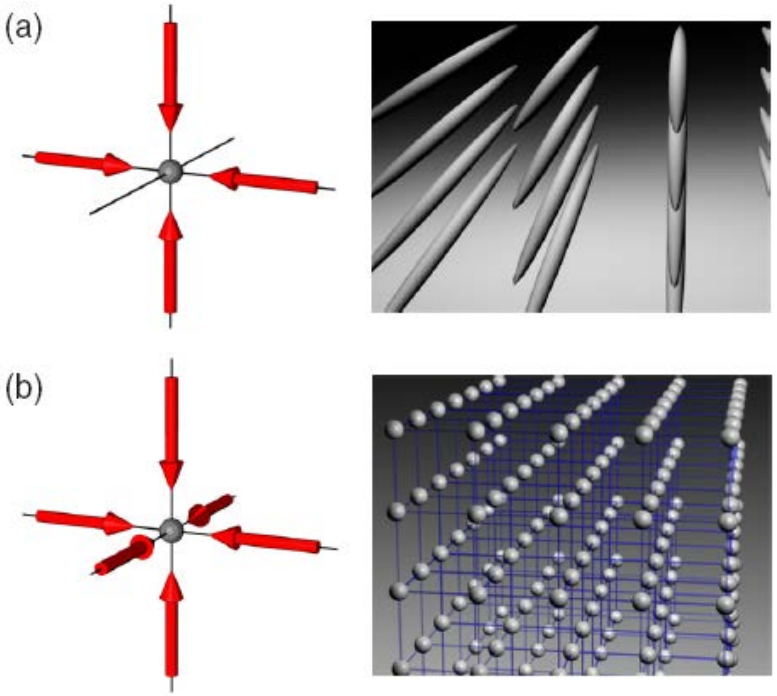

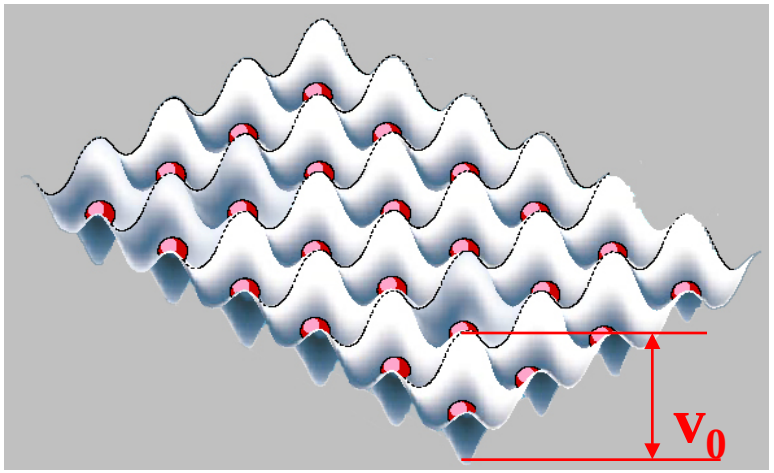

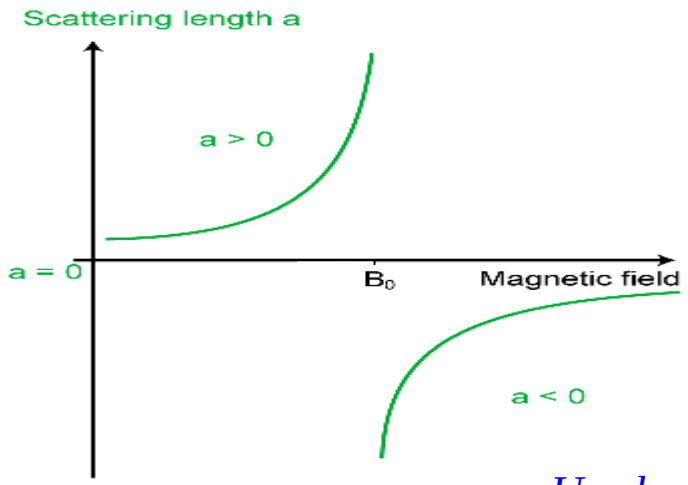

$$U = ka_s E_r \left(\frac{V_0}{E_r}\right)^{3/4}$$

特点：调控相互作用、组份、晶格参数、维度

2、强关联系统：　　强关联效应和量子相变

B、调节维度

一维晶格

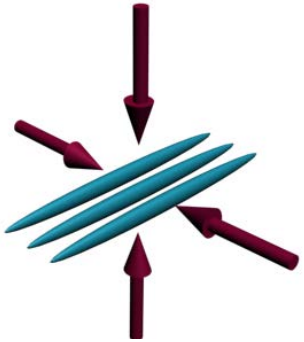

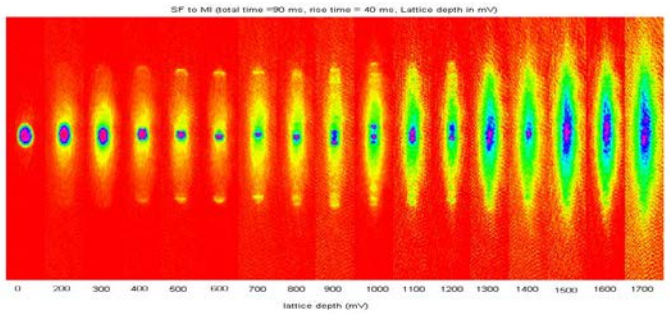

二维晶格

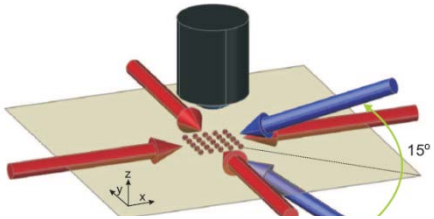

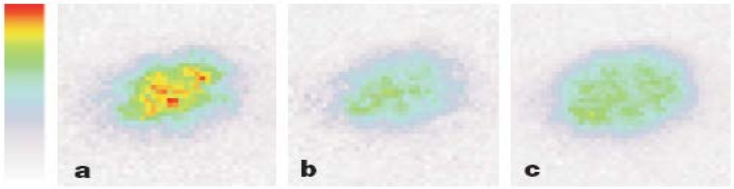

三维晶格

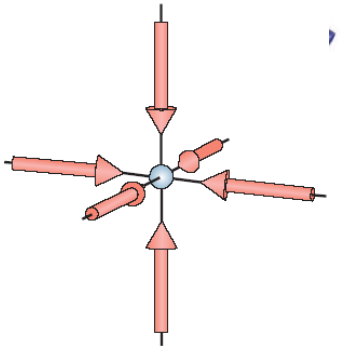

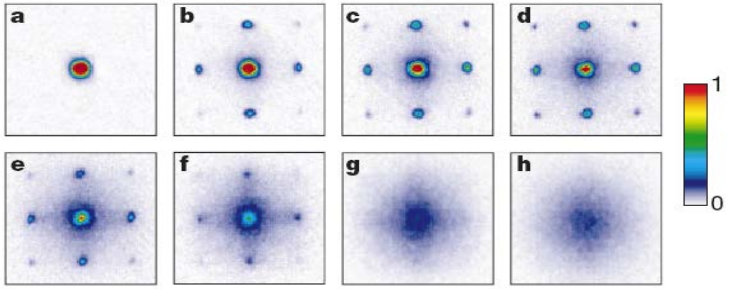

特点：调控维度、相互作用、组份、晶格参数

2、强关联系统：　　强关联效应和量子相变

C、调节组份

(a) 单组份　　**(b)** 双组份　　**(c)** 三组份

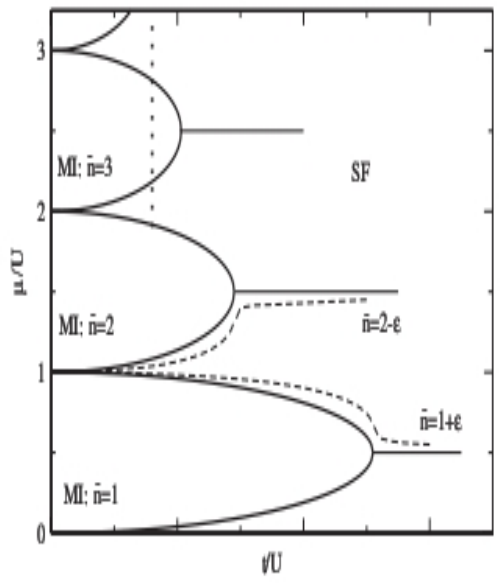

超流-绝缘体相变
(PRA03)

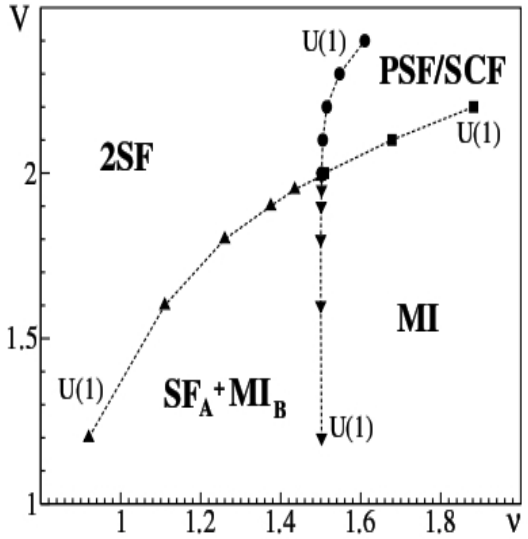

超逆流相（SCF）
(PRL07)

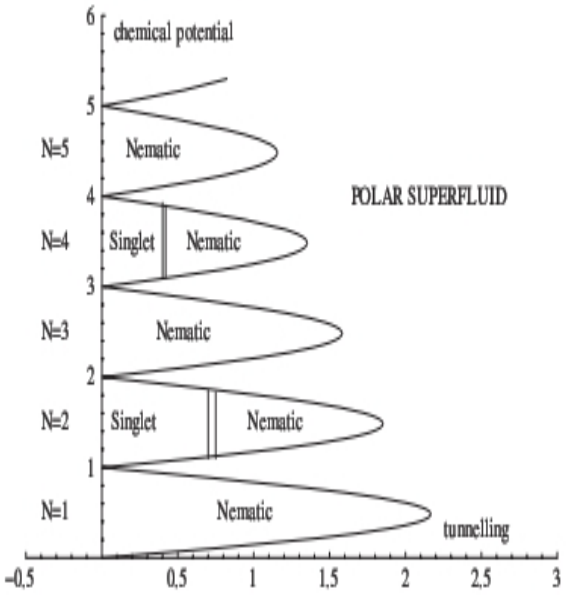

向列相（nematic）
(PRL08)

特点：调控相互作用、组份、晶格参数、维度

2、强关联系统：　　强关联效应和量子相变

D、调控几何结构

三角格子

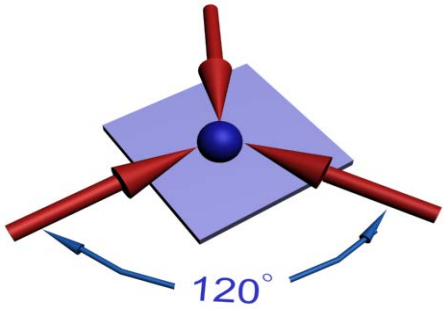

六角格子

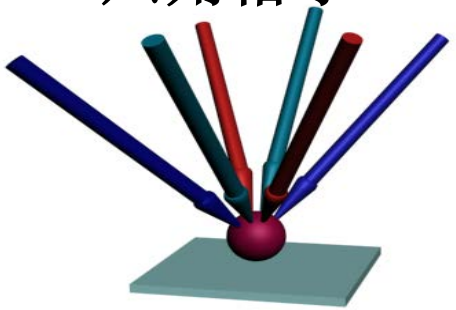

平方格子

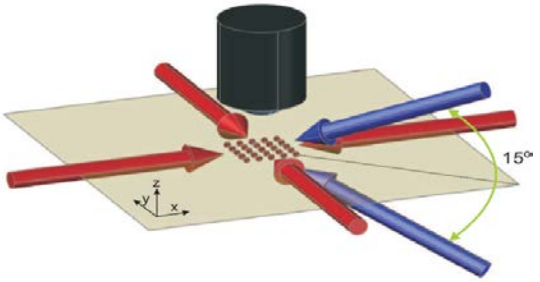

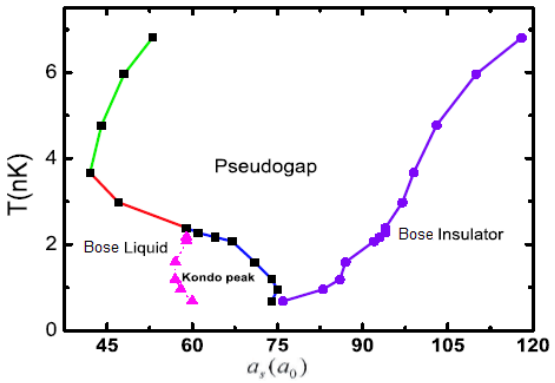

阻挫态

(PRA10)

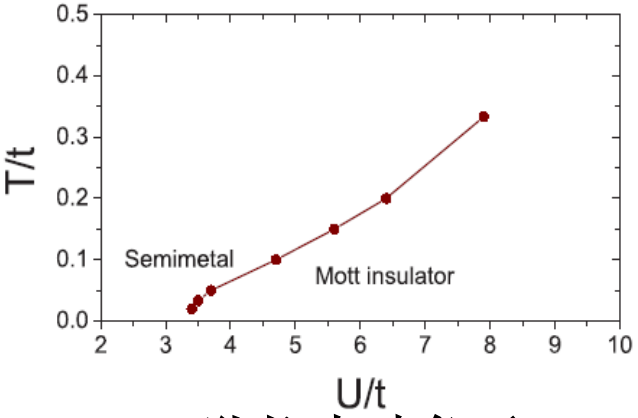

狄拉克玻色子

(PRB10)

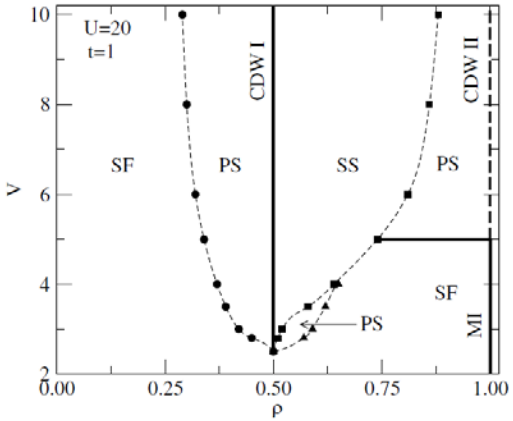

超固体

(PRA10)

特点：调控维度、相互作用、组份、晶格参数

2.1、团簇动力学平均场方法：

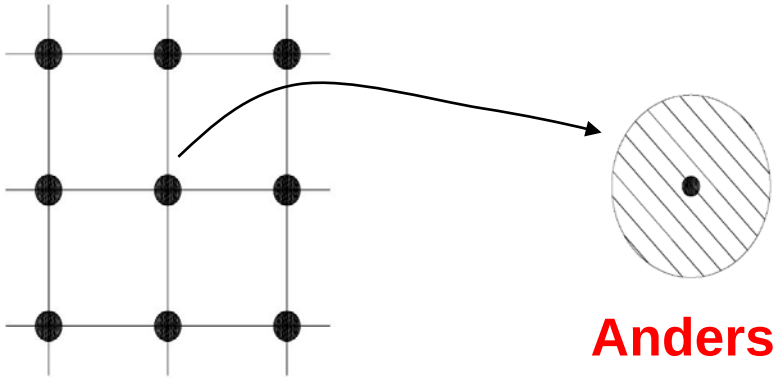

Hubbard Model

Anderson Impurity Model

$$H = -\sum_{<ij>s} t_{ij} C_{is}^{+} C_{js} + \sum_{i} H_i^{on\text{-}site}$$

$$S = \int_0^b dt [\sum_{is} c_{is}^{*}(t)(\frac{\partial}{\partial t} - m) c_{is}(t) - \sum_{<i,j>s} t_{ij} c_{is}^{*}(t) c_{js}(t) + \sum_i H_i^{on\text{-}site}$$

$$H_{imp} = \sum_{ks} [e_k a_{ks}^{+} a_{ks} + V_k (a_{ks}^{+} c_s + c_s^{+} a_{ks})] + H^{on\text{-}site}[c_s^{+}, c_s]$$

$$S_{eff} = \int_0^b dt \int_0^b dt' [\sum_{is} c_{is}^{*}(t)[-g_{0i}^{-1}(t-t')] c_{is}(t')] + \int_0^b dt \sum_i H_i^{on\text{-}site}$$

Weiss 分子场 $$g_0^{-1}(t-t') = -[\frac{\partial}{\partial t} - m - \sum_k V_k^2 (\frac{\partial}{\partial t} + e_k)^{-1}]\delta(t-t') \quad (1)$$

After Fourier transformation: $$g_0^{-1}(iw_n) = iw_n + m - \sum_k \frac{V_k^2}{iw_n - e_k} \quad (2)$$

Dynamical Mean Field Theory (DMFT)

In D=∞ limit, we can get:

$$\Sigma_{ij}(i\omega_n) = \delta_{ij}\Sigma(i\omega_n) \qquad (3)$$

This means that the self-energy is k-independent:

$$\Sigma(k, i\omega_n) = \Sigma(i\omega_n) \qquad (4)$$

So we get:

$$\Sigma_s(k, i\omega_n) = \Sigma_s(i\omega_n) = g_0^{-1}(i\omega_n) - G_s^{-1}(i\omega_n) \qquad (5)$$

In D=∞ limit, we can get:

$$G_s(i\omega_n) = G_{iis}(i\omega_n) = \frac{1}{N}\sum_k G_s(k, i\omega_n)$$

$$= \int_{-\infty}^{+\infty} \frac{D(\varepsilon)}{i\omega_n + \mu - \varepsilon - \Sigma_s(\varepsilon, i\omega_n)} d\varepsilon = \int_{-\infty}^{+\infty} \frac{D(\varepsilon)}{i\omega_n + \mu - \varepsilon - (g_0^{-1}(i\omega_n) - G_s^{-1}(i\omega_n))} d\varepsilon$$

(Dyson Equation) (6)

Dynamical Mean Field Theory (DMFT)

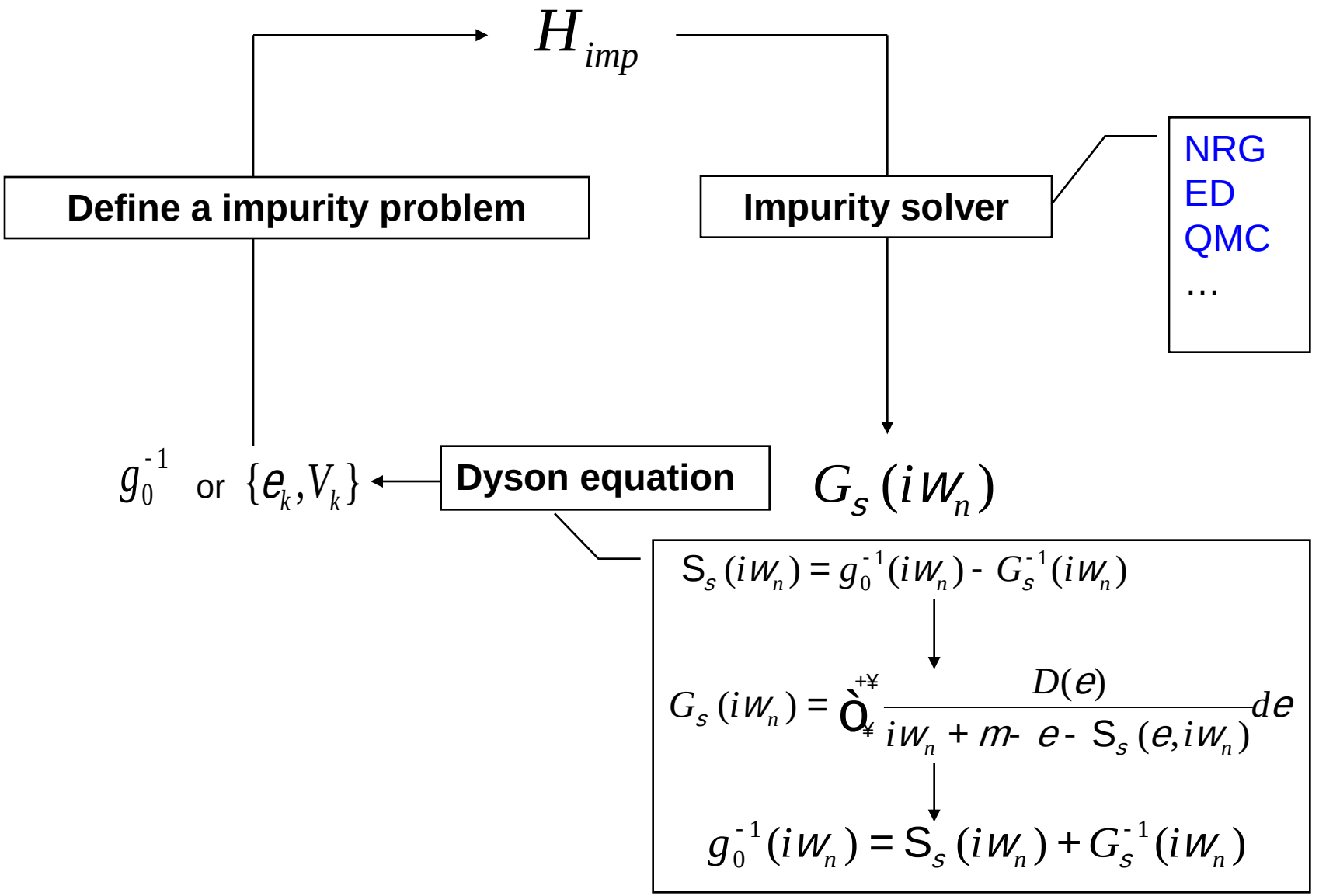

Cluster Dynamical Mean Field Theory (CDMFT)

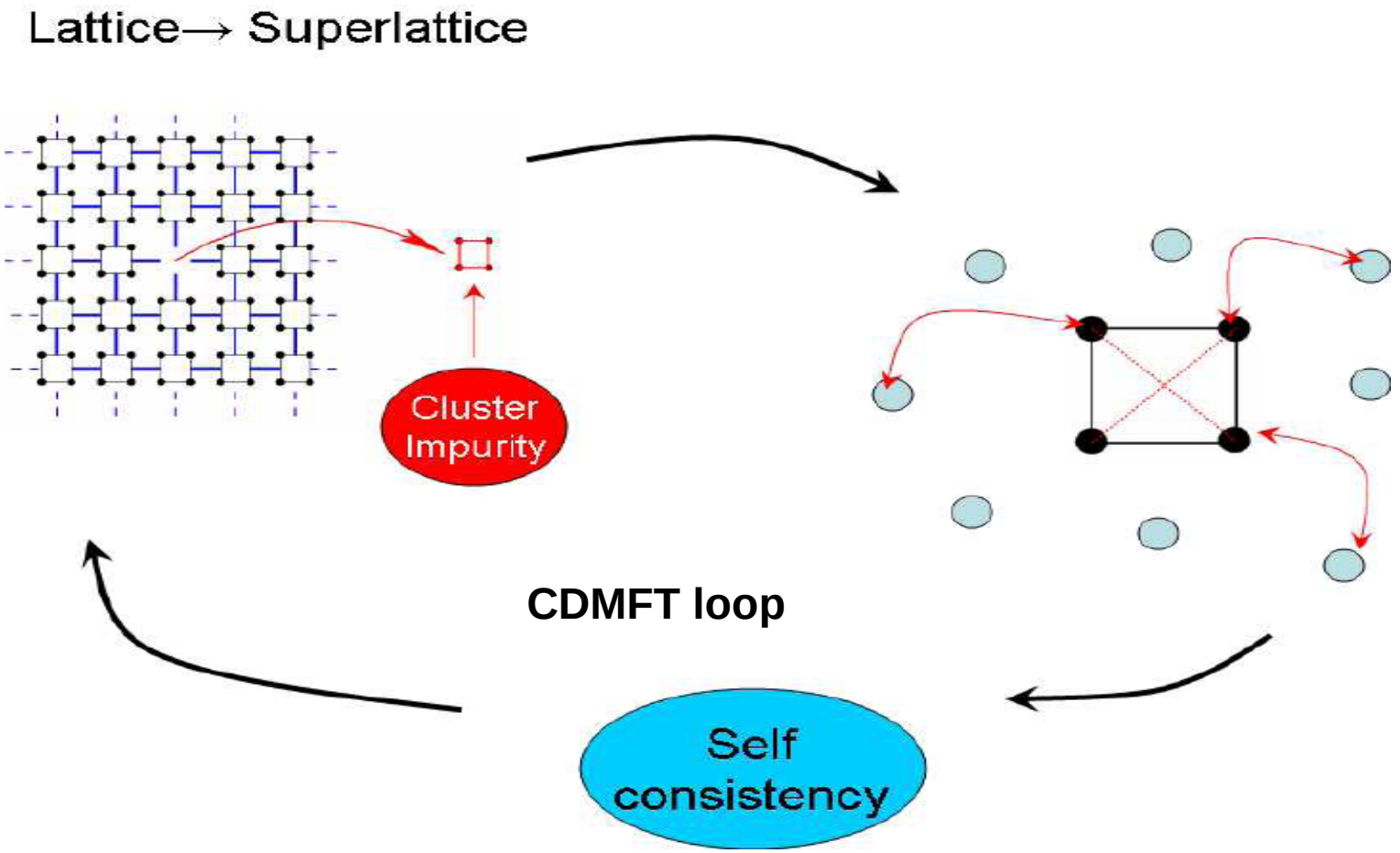

(1) In *CDMFT* approach, many body problem is truncated by introducing a finite basis set of orbitals to truncate self-energy.

(2) It introduces cluster self-energy and lattice self-energy as independent entities.

The CDMFT in the mathematical language

$$\frac{1}{Z_{ef}} e^{-S_{eff}[c^{\dagger}_{m\sigma}, c_{n\sigma}]} \equiv \frac{1}{Z} \int \prod_{(i,j,\sigma)\neq(m,n)} Dc^{\dagger}_{i\sigma} Dc_{j\sigma} e^{-S}$$

$$S_{ef} = \int_0^{\beta} dt \sum_{m n \sigma} c^{\dagger}_{m\sigma}(t) g^{-1}_{m n \sigma}(t) c_{n\sigma} + U \int_0^{\beta} dt \sum_{m} n_{m\uparrow}(t) n_{m\downarrow}(t)$$

$$G_{m n \sigma}(t) = -T_t \left\langle c^{\dagger}_{m\sigma} c_{n\sigma} \right\rangle_{S_{ef}}$$

We construct a super-lattice Green's function assuming the cluster–self-energy Σ_{mn} local as in DMFT (the term local covers a range of size of the cluster-impurity).

$$G(K, i\omega) = \frac{1}{(i\omega + \mu) I + t_K - \Sigma}$$ **K is defined in a Reduced Brillouin Zone**

$$G_{loc}(i\omega_n) = \sum_{K} G(K, i\omega)$$

$$G \equiv G_{loc}(i\omega_n) \; or \; \Sigma_{mn}(i\omega) = g^{-1}_{m n \sigma}(i\omega_n) - G^{loc\,-1}_{m n \sigma}(i\omega_n, \Sigma)$$

Cluster Dynamical Mean Field Theory (DMFT)

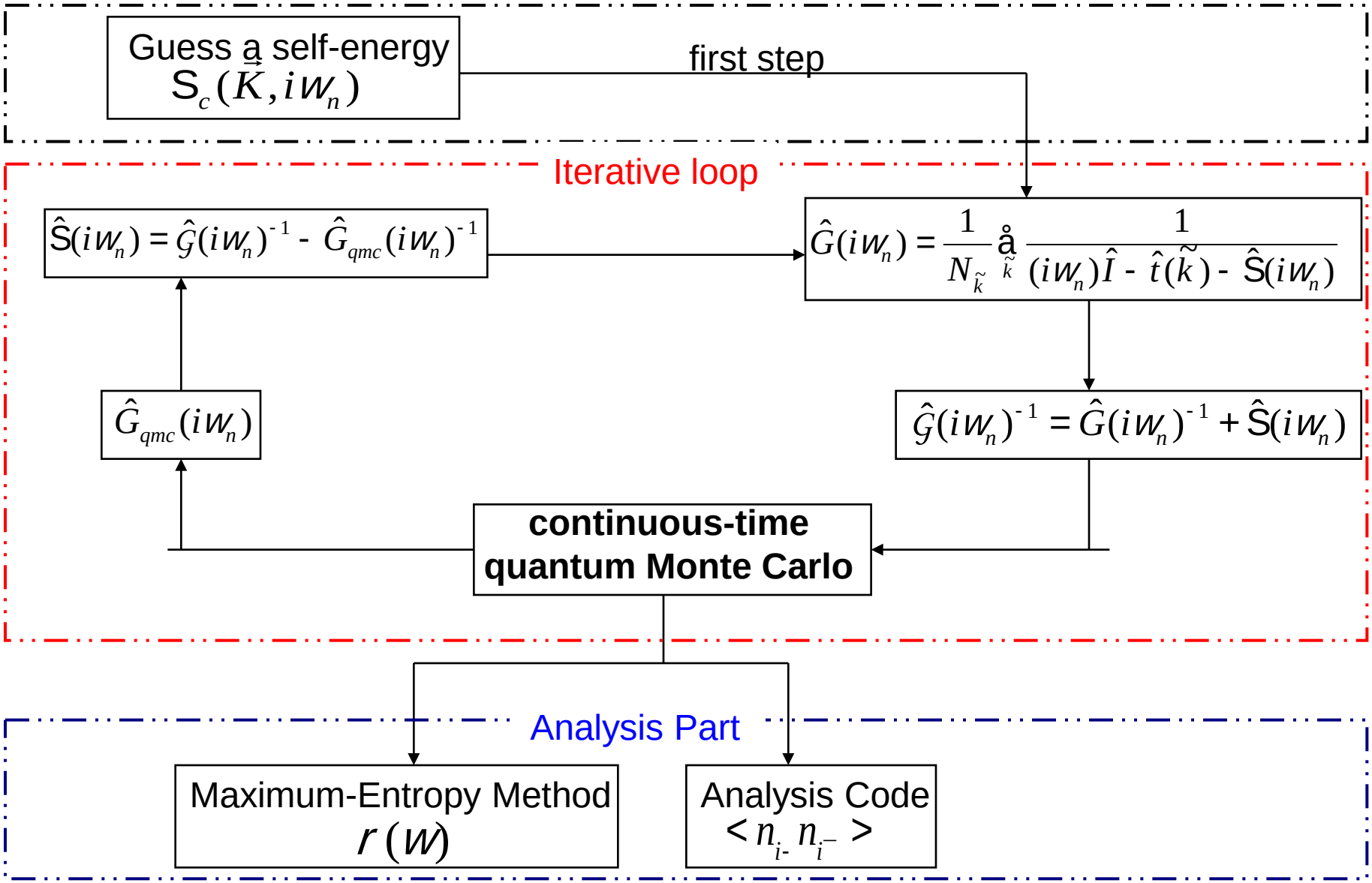

2.2、六角晶格:

W. Wu, Y. H. Chen, H. S. Tao, N. H. Tong, W.M. Liu, Phys. Rev. B 82, 245102 (2010)

(a)

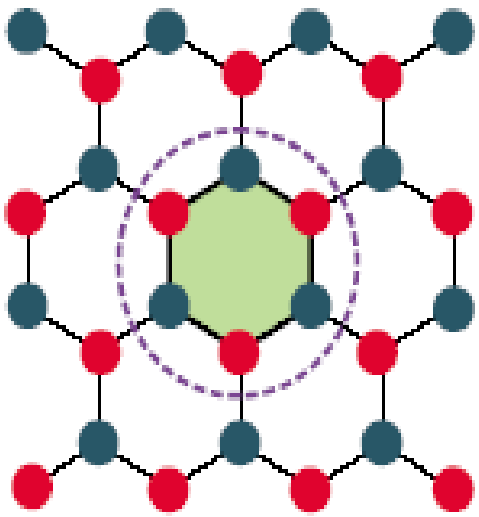

(b)

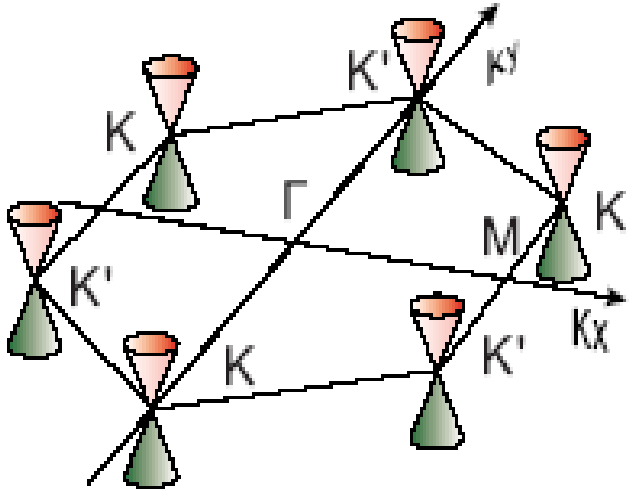

$$H = -t \sum_{<i,j>,s} c_{is}^{+} c_{js} + U \sum_{i} n_{i\uparrow} n_{i\downarrow} + m \sum_{i} c_{is}^{+} c_{is}$$

低能态密度

CDMFT结果：低能态密度不随相互作用强度而变化，这是考虑非局域关联的结果。

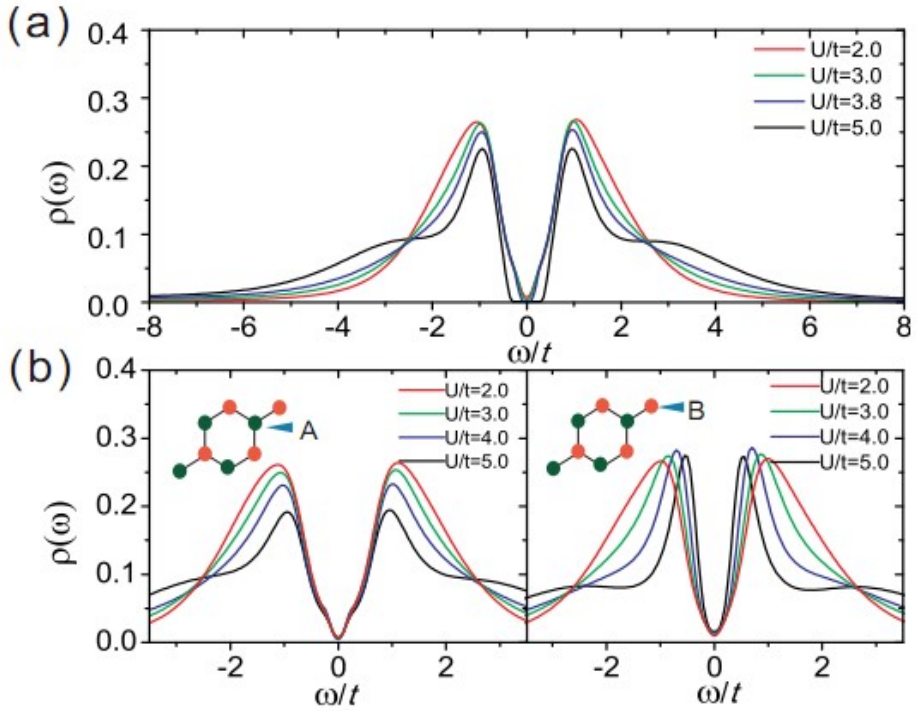

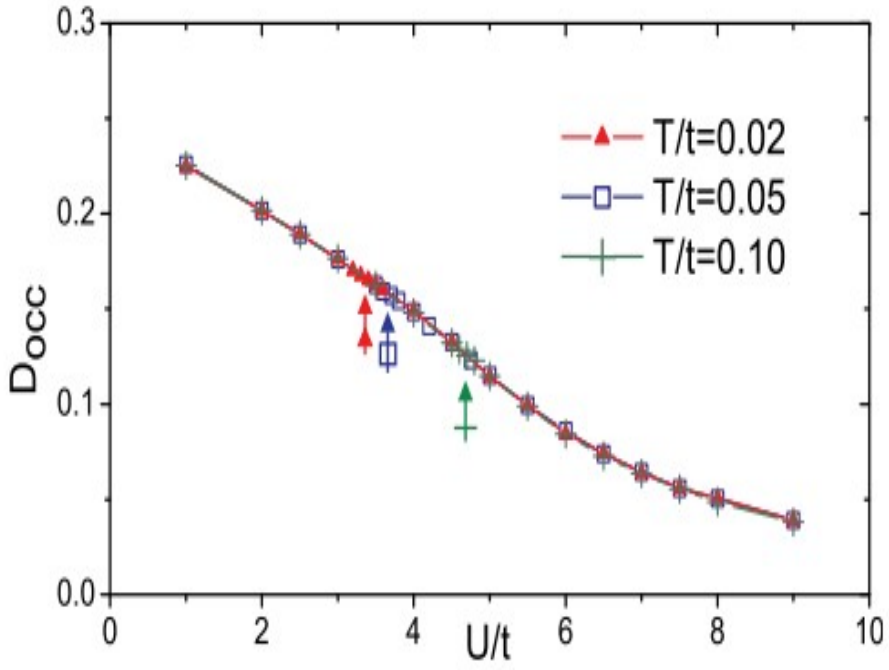

相图

系统存在一个由半金属到非磁绝缘体的连续相变。零温相变 **Uc / t ~ 3.3** 。

单粒子谱函数

相互作用 **Dirac** 费米子**Mott**相变是反铁磁涨落所引起的，如单粒子谱函数所示。

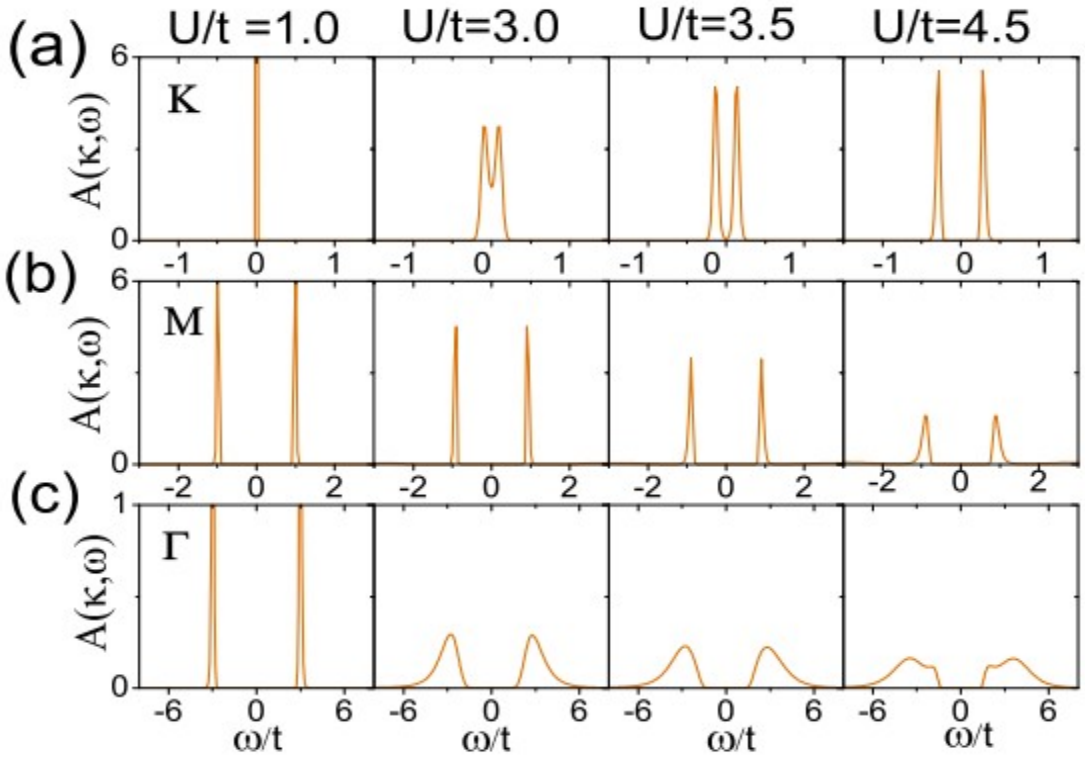

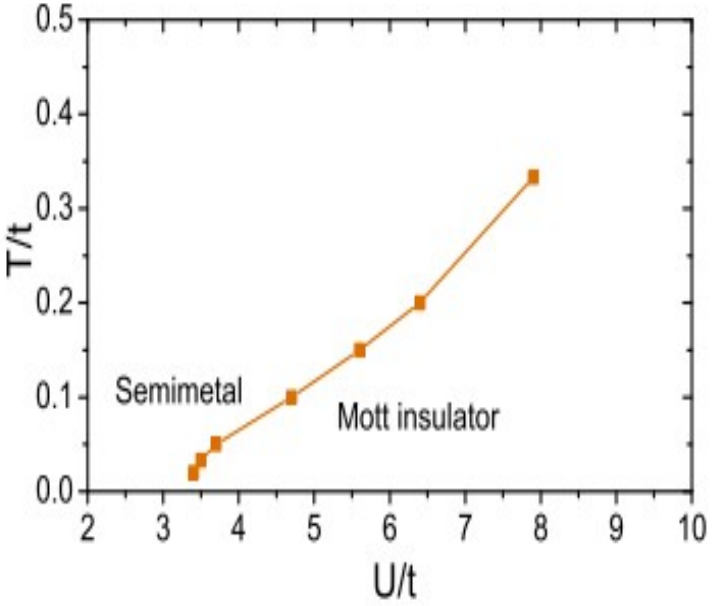

温度相图

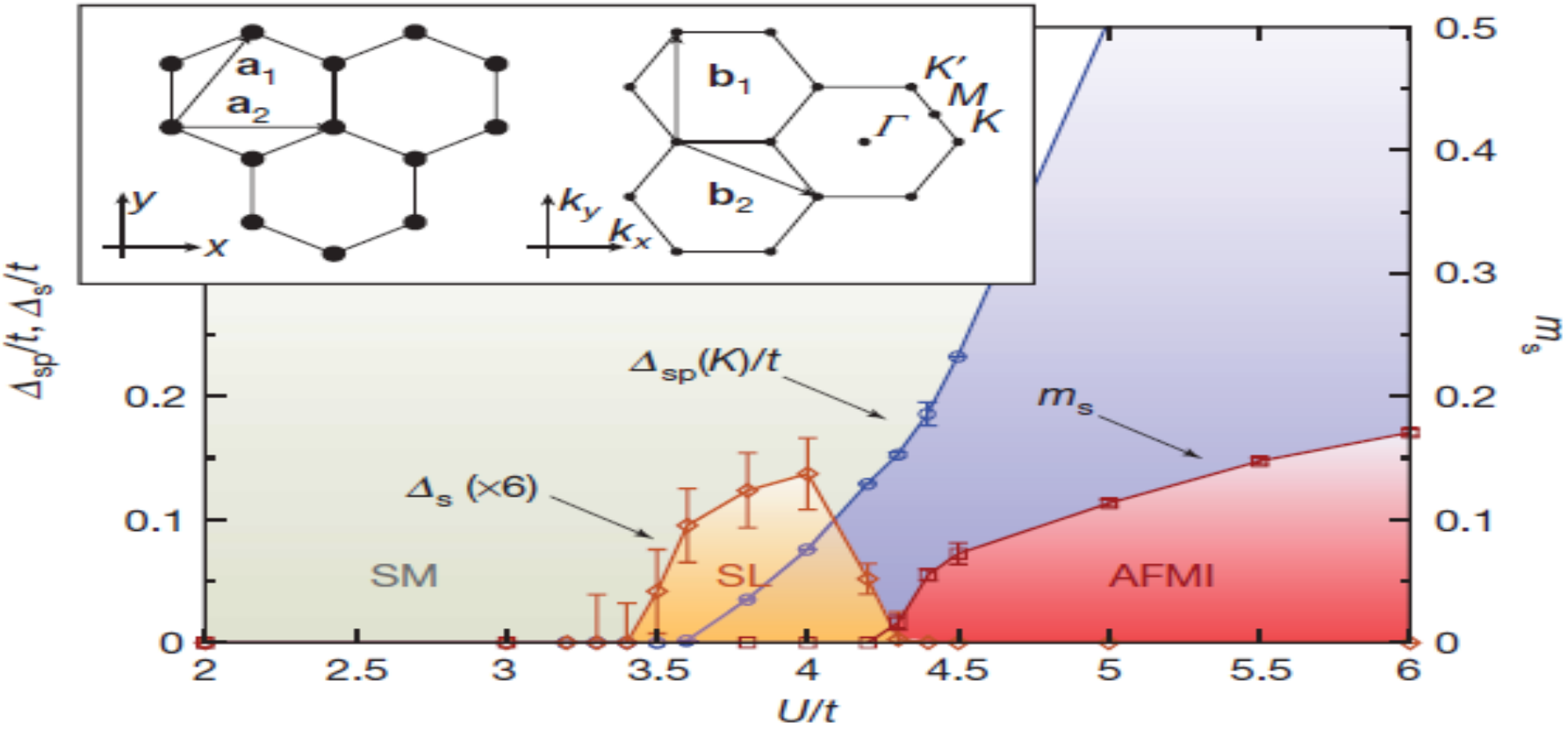

Figure 1 | Phase diagram for the Hubbard model on the honeycomb lattice at half-filling. The semimetal (SM) and the antiferromagnetic Mott insulator (AFMI) are separated by a gapped spin-liquid (SL) phase in an intermediate-coupling regime. $\Delta_{sp}(K)$ denotes the single-particle gap and Δ_s denotes the spin gap; m_s denotes the staggered magnetization, whose saturation value is 1/2. Error bars, s.e.m. Inset, the honeycomb lattice with primitive vectors $\mathbf{a}_1$ and $\mathbf{a}_2$, and the reciprocal lattice with primitive vectors $\mathbf{b}_1$ and $\mathbf{b}_2$. Open and filled sites respectively indicate two different sublattices. The Dirac points K and K' and the M and Γ points are marked.

Z. Y. Meng, T. C. Lang, S. Wessel, F. F. Assaad, A. Muramatsu, Nature 464, 847 (2010)

量子自旋霍尔效应

W. Wu, S. Rachel, W. M. Liu, K. Le Hur, Phys. Rev. B 85, 205102 (2012)

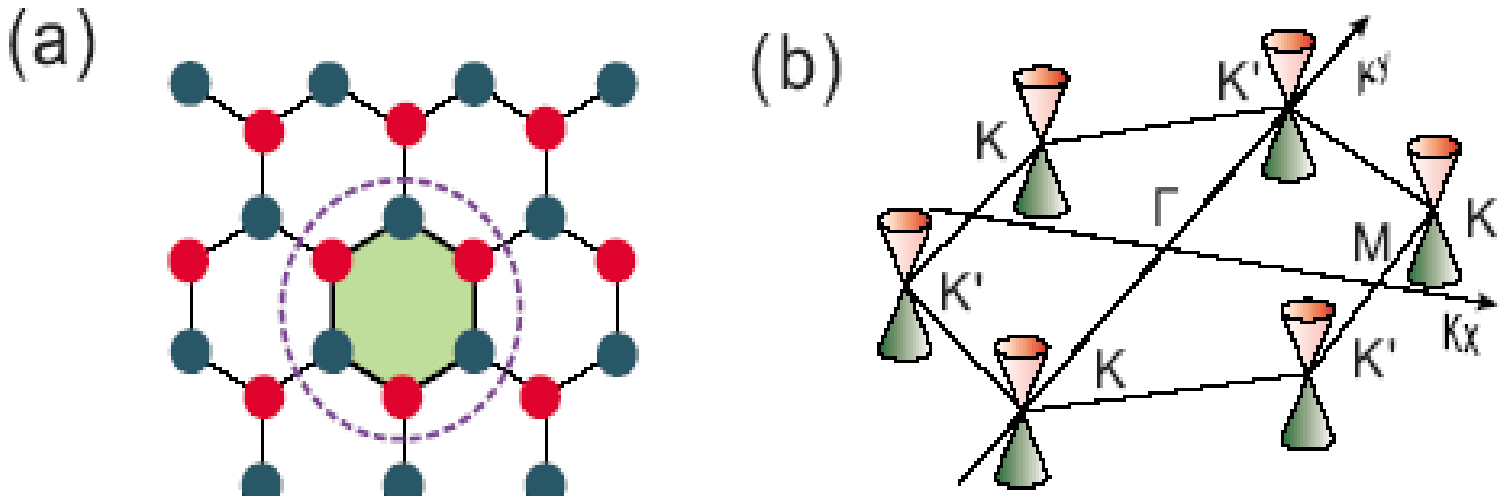

$$H = -t \sum_{\langle ij \rangle \sigma} c^{\dagger}_{i\sigma} c_{j\sigma} + i\lambda \sum_{\ll ij \gg \alpha\beta} v_{ij} c^{\dagger}_{i\alpha} \sigma^{z}_{\alpha\beta} c_{j\beta} + U \sum_{i} n_{i\uparrow} n_{i\downarrow}$$

(a) Illustration of honeycomb lattice. The dashed line sketches the six-site cluster scheme. (b) The first Brillouin zone of honeycomb lattice. The linear low-energy dispersion relation displays conical shapes near Fermi level.

相互作用体系的量子自旋霍尔效应

- 问题的起源: 量子霍尔效应导致电场下二维材料中存在无耗散的边缘电流。

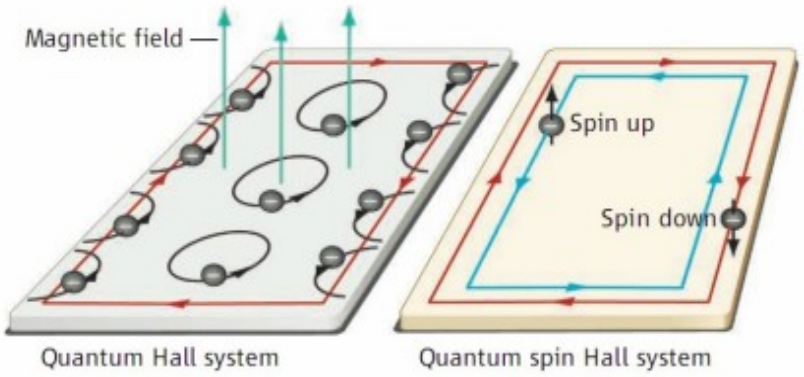

霍尔电导的大小只与费米面下朗道能级的个数相关, 与杂质等非本征因素无关。

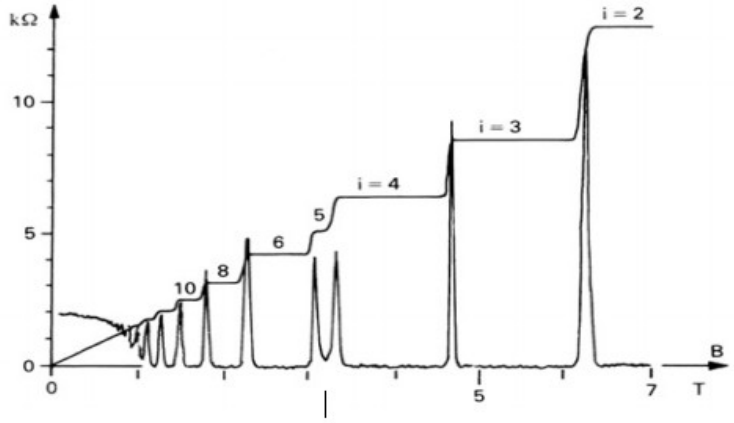

相互作用体系的量子自旋霍尔效应

- 没有磁场 — 即没有朗道能级的量子霍尔效应

  量子反常霍尔效应， 量子自旋霍尔效应 等

- 量子自旋霍尔效应：**Kane-Mele 模型**

$$H = t\sum_{\langle ij\rangle} c_i^\dagger c_j + i\lambda_{so}\sum_{\ll ij\gg} v_{ij} c_i^\dagger \sigma^z c_j + i\lambda_R \sum_{\langle ij\rangle} c_i^\dagger (\vec{\sigma}\times\vec{d_{ij}})_z c_j + \lambda_v \sum_i \xi_i c_i^\dagger c_i$$

- 相图：

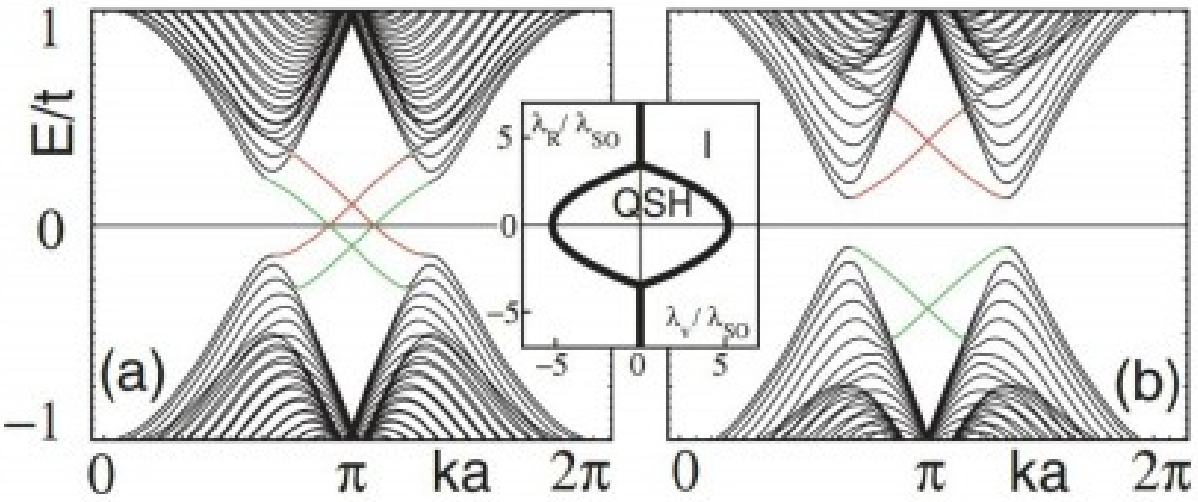

相互作用体系的量子自旋霍尔效应

- 模型： **Kane – Mele – Hubbard 模型**

$$H = -t \sum_{\langle ij \rangle \sigma} c^{\dagger}_{i\sigma} c_{j\sigma} + i\lambda \sum_{\ll ij \gg \alpha\beta} v_{ij} c^{\dagger}_{i\alpha} \sigma^{z}_{\alpha\beta} c_{j\beta} + U \sum_{i} n_{i\uparrow} n_{i\downarrow}$$

U=0 时，体能隙：

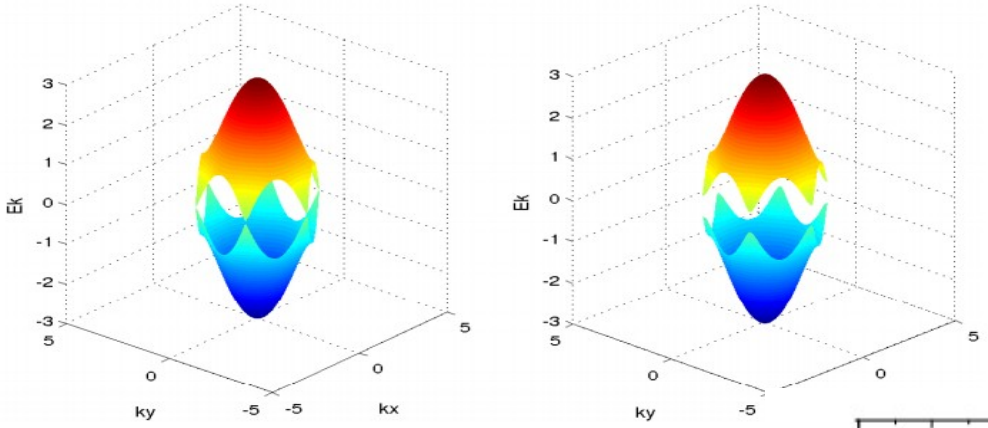

U = 0 时，边缘态

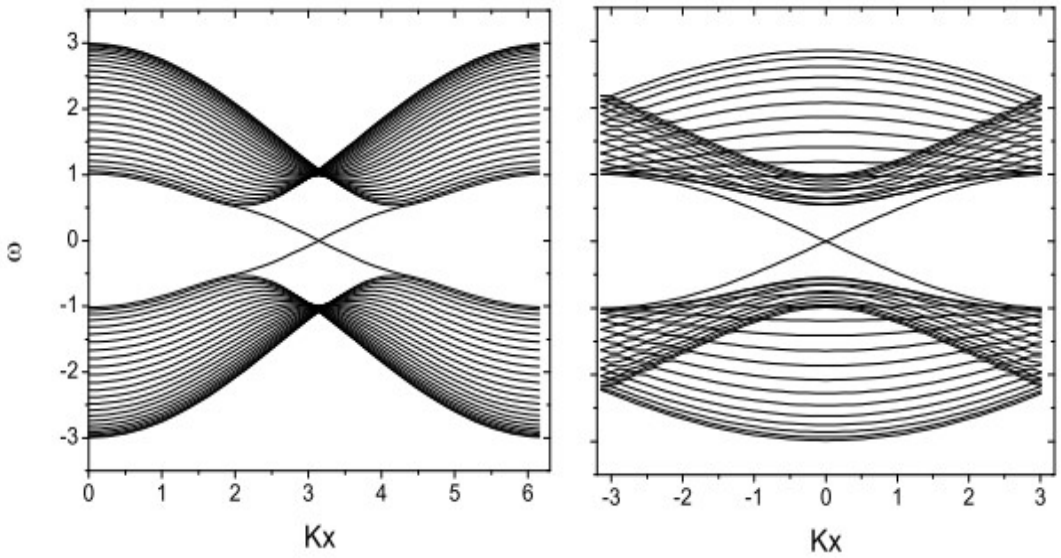

相互作用体系的量子自旋霍尔效应

- 大U极限，自旋-轨道耦合引起易磁化方向的改变。

$$\widetilde{H} = \frac{4\lambda^2}{U}(-S_i^x S_j^x - S_i^y S_j^y + S_i^z S_j^z)$$

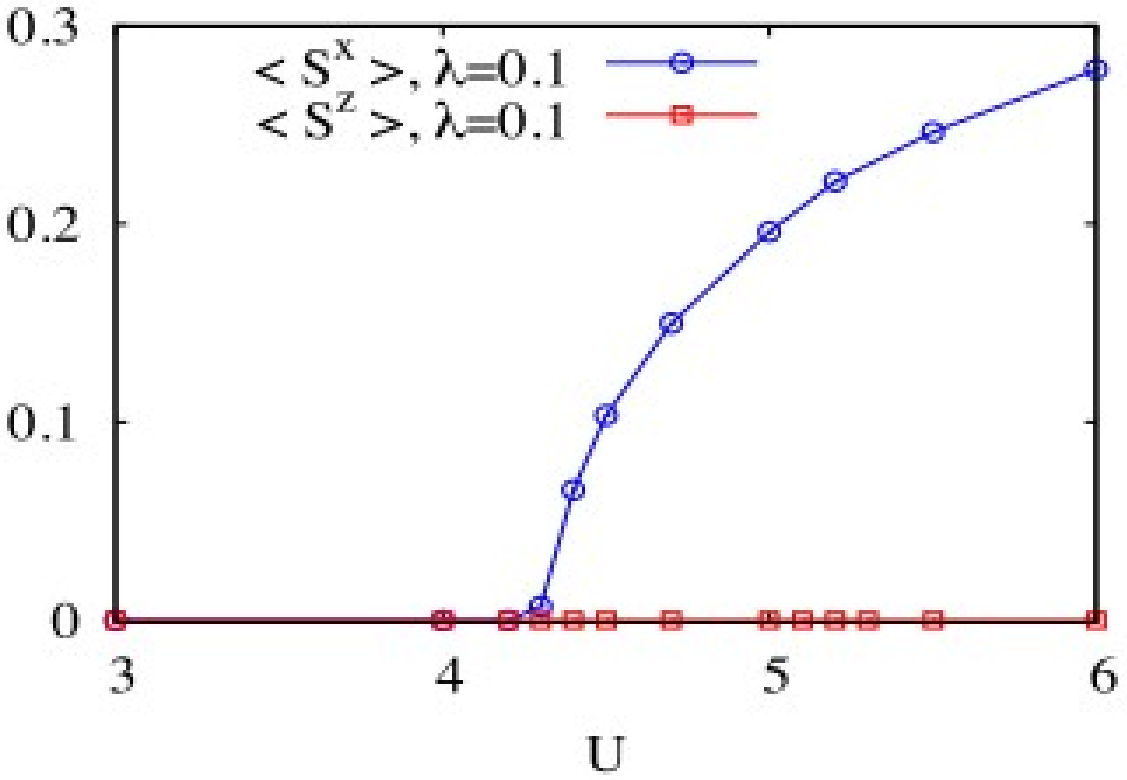

相互作用体系的量子自旋霍尔效应

- 中等强度的耦合—相图.

SDW：反铁磁绝缘体,　　**SL**：自旋液体

SM：半金属　　**TBI/QSH**：拓扑绝缘体

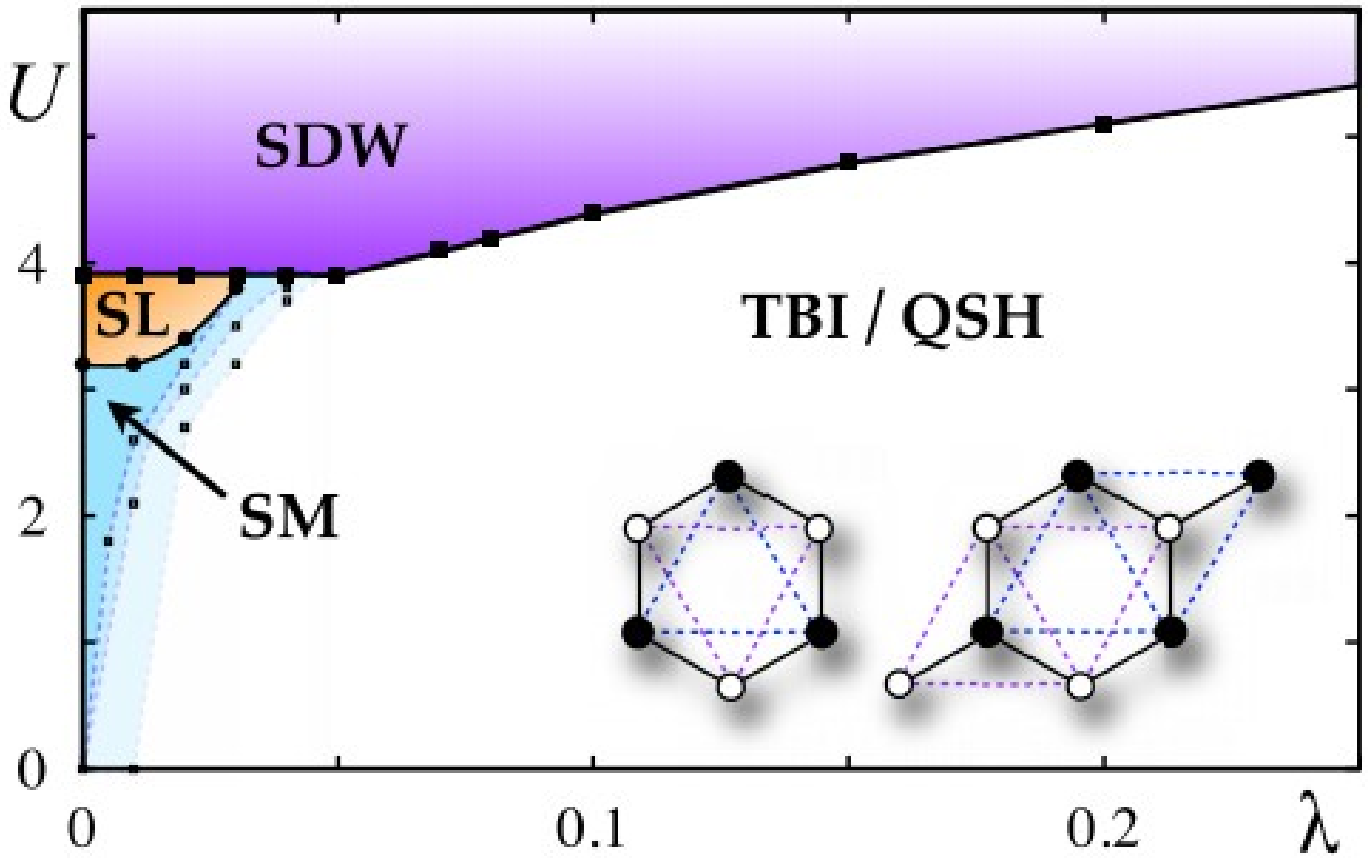

shown (from right to left) for temperatures *T* = 0.025, 0.0125, and 0.005.

量子自旋霍尔效应

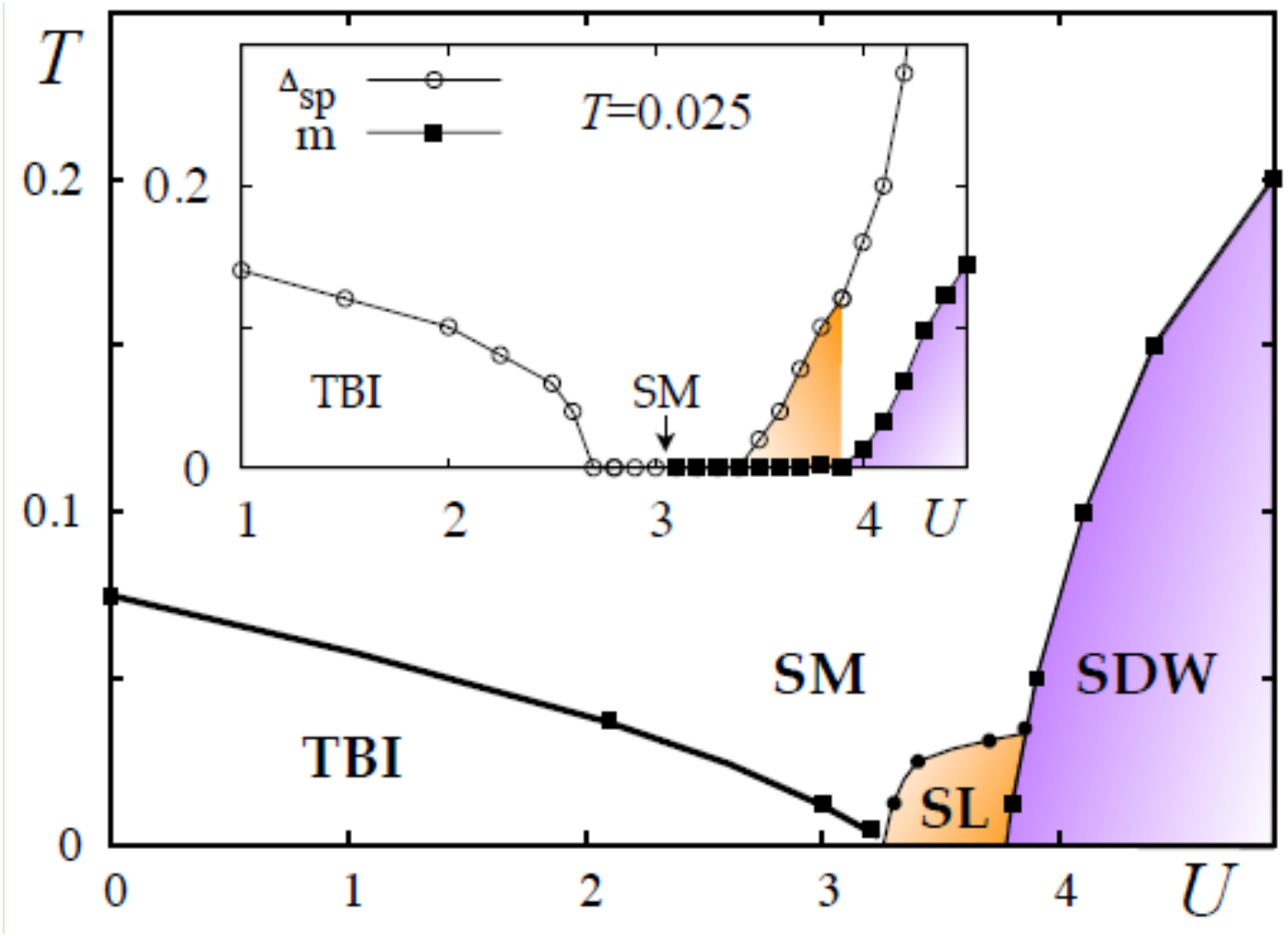

Temperature dependence of phase diagram at SOCλ=0.02. Inset: Single-particle gap Δsp and magnetization m vs. U is shown forλ=0.02 and T=0.025.

拓扑绝缘体

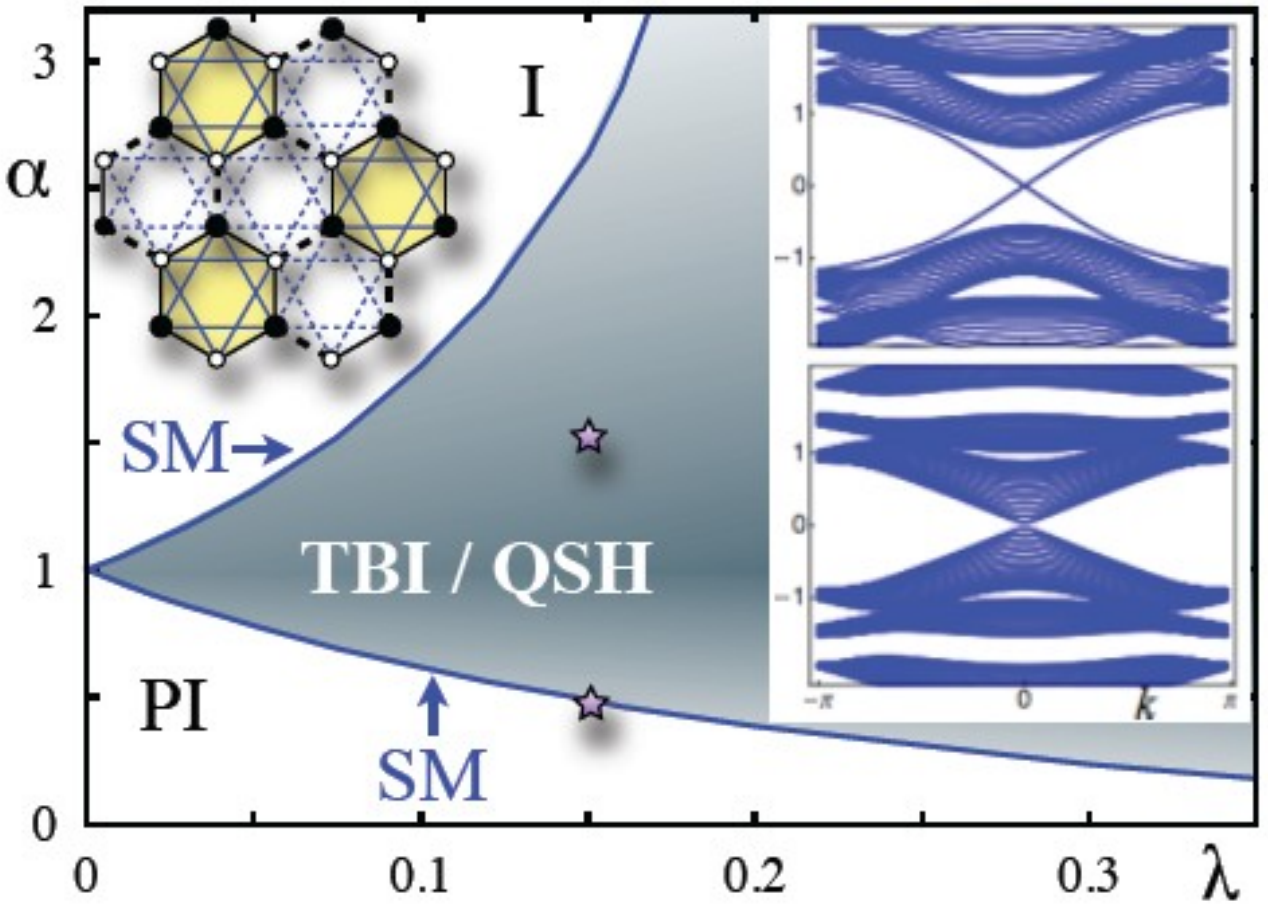

α-λ phase diagram of plaquette honeycomb model at U=0. Theα=1 line corresponds to KM model. Spectra for armchair ribbons (L=96) are shown atλ=0.15,α=1.5 (top, QSH phase) andα=0.48 (bottom, entrance of PI phase). Blue lines correspond to SM.

相互作用体系的量子自旋霍尔效应

边缘态的研究

方法: **real space CDMFT**

相互作用使得边缘态模糊，并重整化**Plasmon**速度。

$$v = \sqrt{v_f{}^2 - g^2},$$

$$K = \sqrt{(v_f - g)/(v_f + g)}.$$

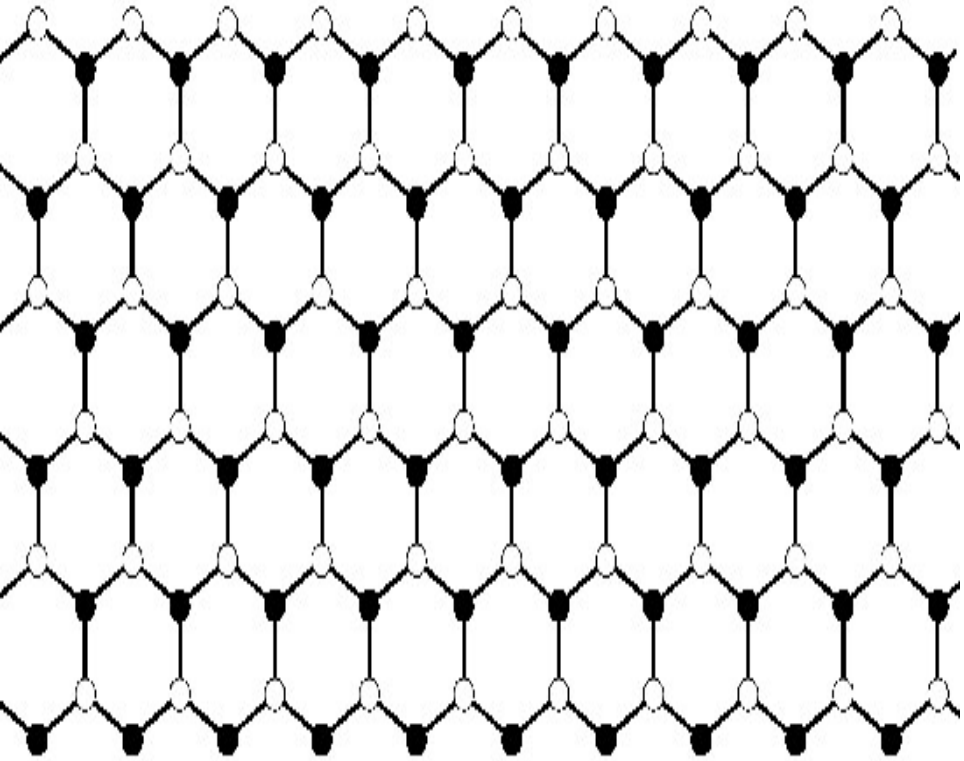

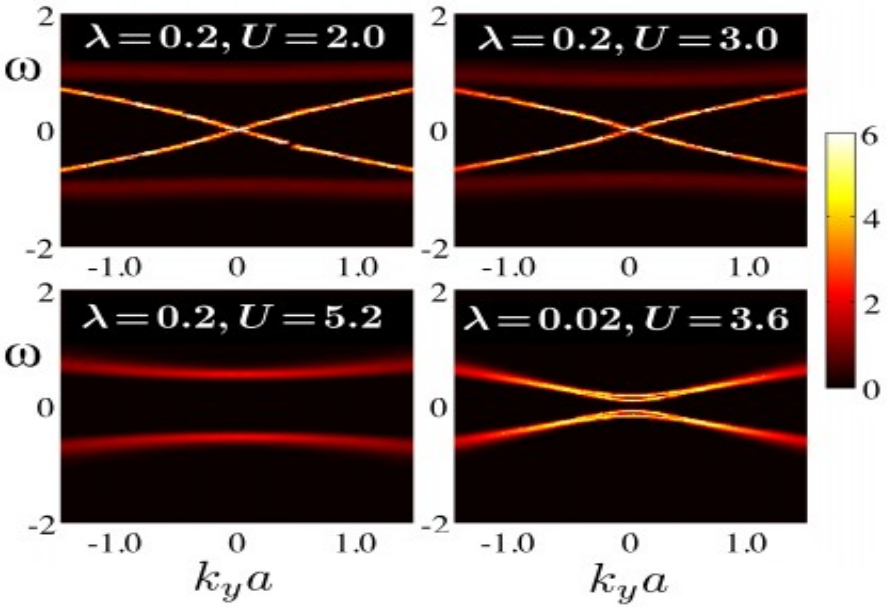

相互作用体系的量子自旋霍尔效应

- 当体的磁相变发生时，边缘态被破坏。

$$H=\int dx\frac{v}{2}[\frac{1}{K}(\partial_x\phi)^2+K(\partial_x\theta)^2]-\frac{Umsin\sqrt{4\pi}\phi}{(\pi a)^2}$$

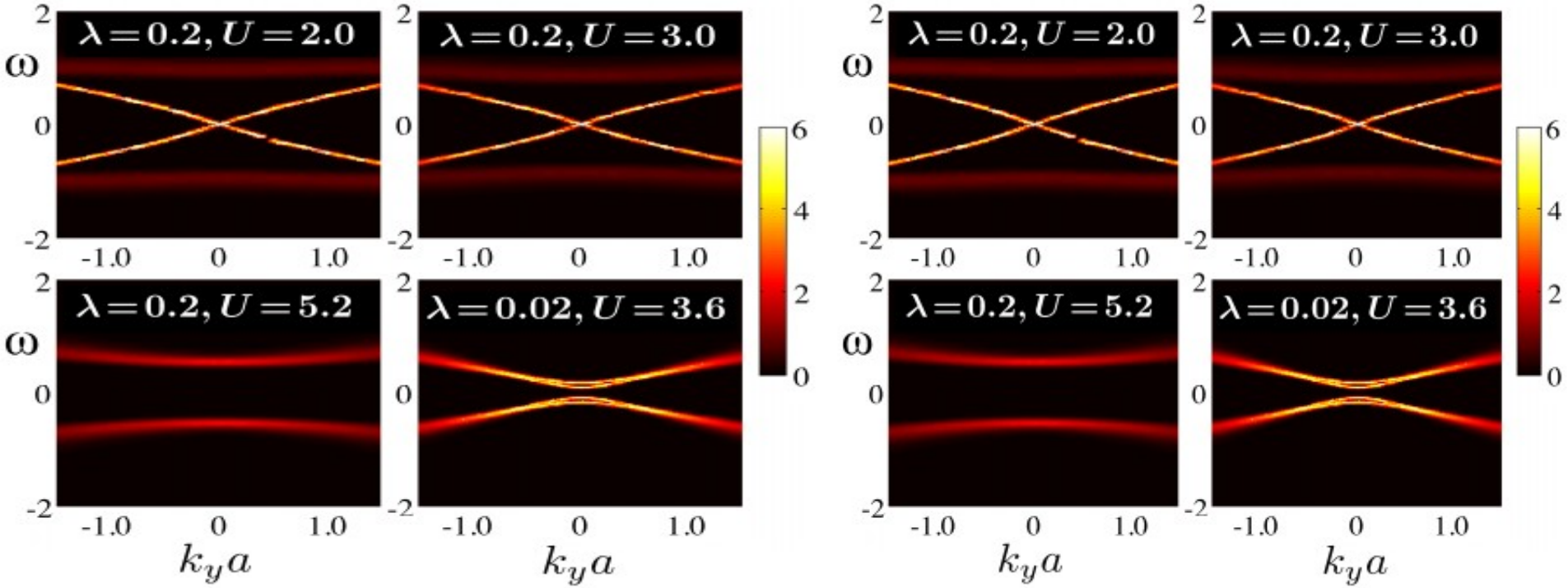

- 在量子自旋液体区域，有体能隙，边缘态不能存在。

相互作用体系的量子自旋霍尔效应

边缘态在实空间中的重新分布

边缘电子自由度受限，在有相互作用情况下其局域性较中央区域更强，导致边缘态更容易被散射回中央。

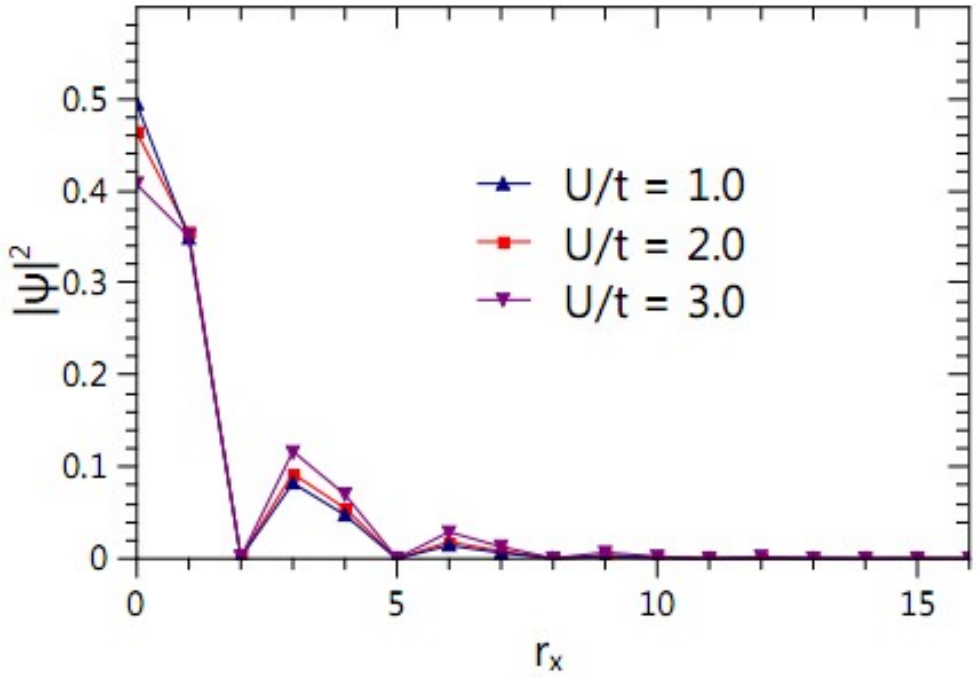

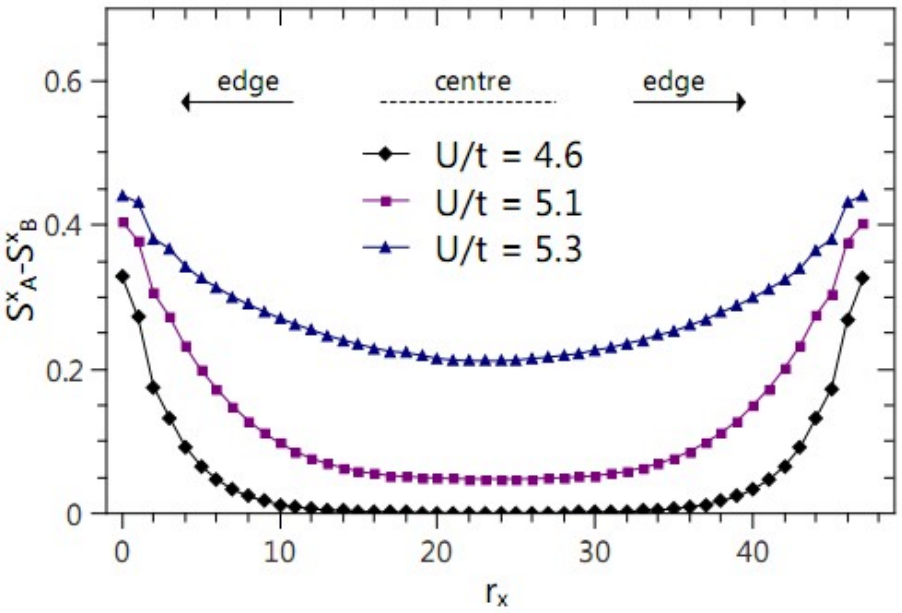

CDMFT的弱点：过高估计边缘磁性

拓扑量子相变

F.D. Sun, X.L. Yu, J. Ye, H. Fan, W.M. Liu, Scientific Reports 3, 2119 (2013)

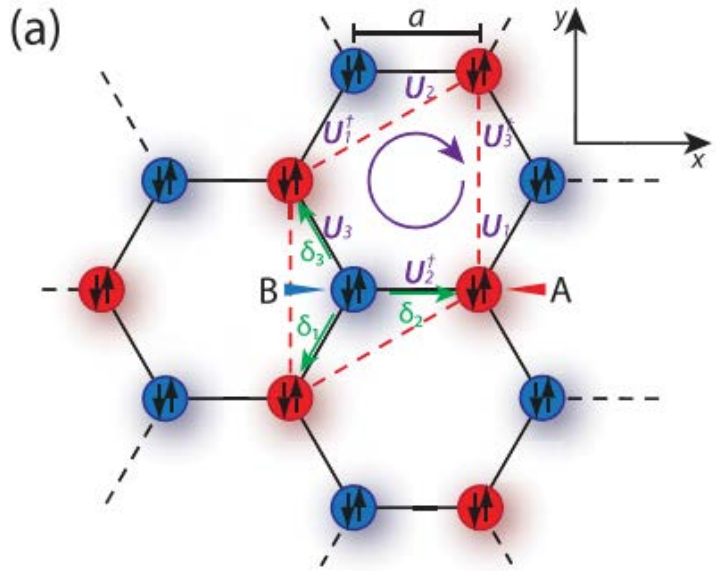

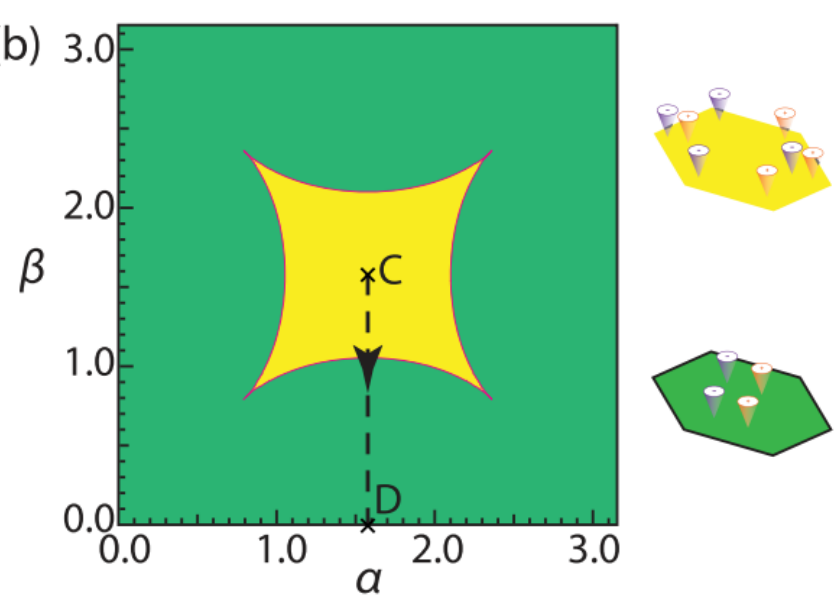

$$\mathcal{H}_0 = -t \sum_{\langle i,j \rangle} c_A^\dagger(i\sigma) U_{ij}^{\sigma\sigma'} c_B(j\sigma') + h.c.,$$

Figure 1 | Lattice geometry and phase diagram. (a) The honeycomb lattice consists of sublattice *A* (red dots) and sublattice *B* (blue dots). The up and down arrows represent the spin degrees of freedom. *a* is the lattice constant. The non-Abelian gauge potentials $U_{1,2,3}$ with directions are displayed on the three links inside the unit cell. (b) The phase diagram of our system as a function of gauge parameters α and β. The yellow (green) region has $N_D = 8$ ($N_D = 4$) Dirac points shown in the insets. The center *C* point is the π flux Abelian point. The 4 edges of the square belong to the gauge equivalent trivial Abelian point. We investigate the topological quantum phase transition from *C* point to *D* point along the dashed line.

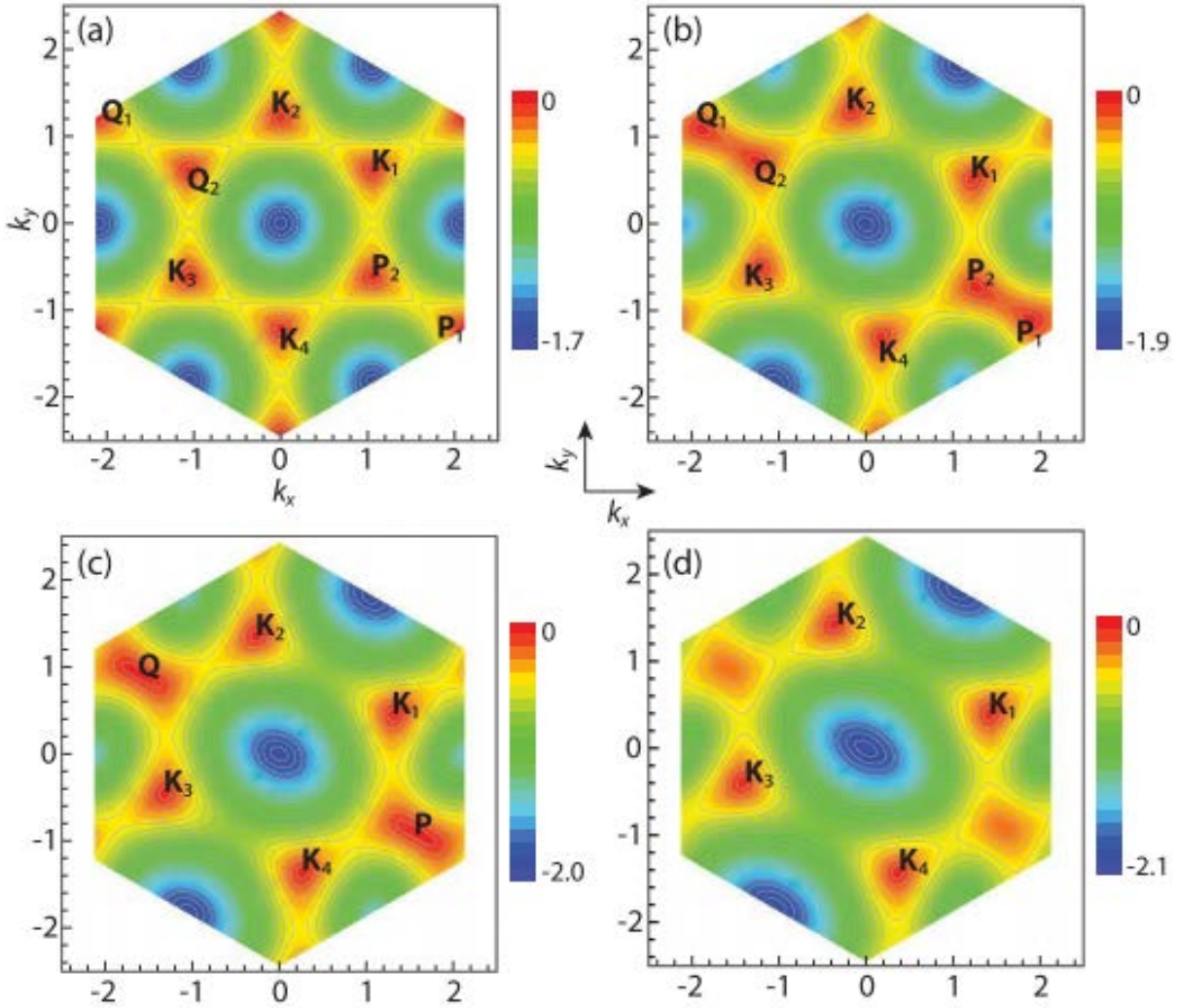

Figure 2 | Topologies of different Fermi surface. The different Fermi surface topologies of the ϵ_{1-} in the 1st Brillouin zone along the dashed line in the Fig. 1(b). (a) The π flux Abelian point $\alpha = \pi/2$, $\beta = \pi/2$ inside the $N_D = 8$ phase, (b) The $\alpha = \pi/2$, $\beta = 2\pi/5$ inside the $N_D = 8$ phase, (c) The TQPT at $\alpha = \pi/2$, $\beta_c = \pi/3$. The two emerging points are located at $\mathbf{P} = \left(\frac{\pi}{2}, -\frac{\pi}{2\sqrt{3}}\right)$ and its time-reversal partner $\mathbf{Q} = -\mathbf{P}$. The four Dirac points are locatedvat $\mathbf{K}_1 = \left(\frac{5\pi}{12}, \frac{\pi}{4\sqrt{3}}\right) = -\mathbf{K}_3$, $\mathbf{K}_2 = \left(-\frac{\pi}{12}, \frac{\sqrt{3}\pi}{4}\right) = -\mathbf{K}_4$. (d) The $\alpha = \pi/2$, $\beta = \pi/4$ inside the $N_D = 4$ phase.

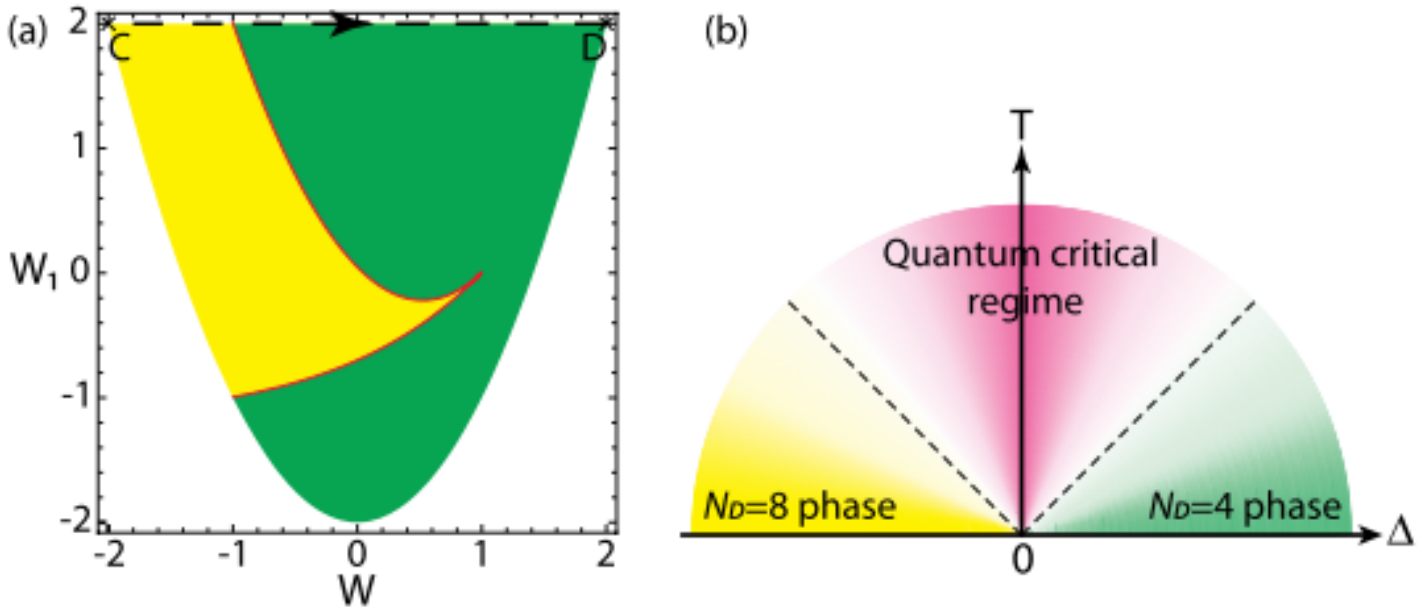

Figure 4 | Finite-T Phase diagram. (a) The gauge-invariant phase diagram in terms of the Wilson loops W and W_1. The yellow (green) regime is $N_D = 8$ ($N_D = 4$). The dashed line corresponds to the one in Fig. 1(b). (b) Finite-T Phase diagram of the topological quantum phase transition as a function of the flux Δ and the temperature T. There is a topological quantum phase transition at $T = 0$, $\Delta = 0$. The two dashed lines stand for the crossovers at $T \sim |\Delta|$.

层间反铁磁体

H.S. Tao, Y.H. Chen, H.F. Lin, H.D. Liu, W.M. Liu, Sci. Rep. 4, 5367 (2014)

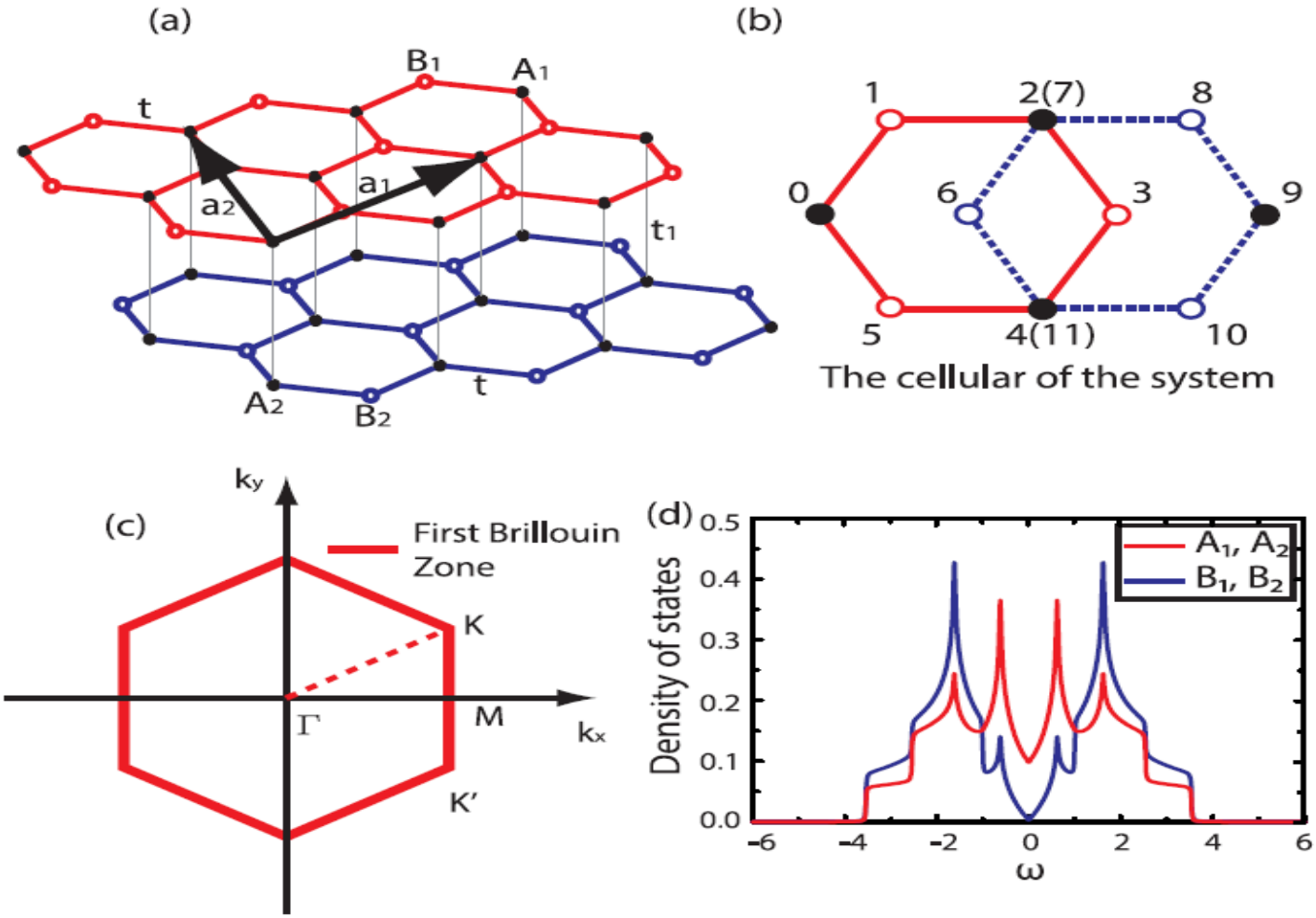

$$H = -t \sum_{\langle ij\rangle\sigma\alpha} (c^{\dagger}_{i\sigma\alpha} c_{j\sigma\alpha} + h.c.) + U \sum_{i\alpha} n_{i\uparrow\alpha} n_{i\downarrow\alpha} - t_1 \sum_{i\sigma\alpha} c^{\dagger}_{i\sigma\alpha} c_{i\sigma(1-\alpha)} - \mu \sum_{i\sigma\alpha} n_{i\sigma\alpha},$$

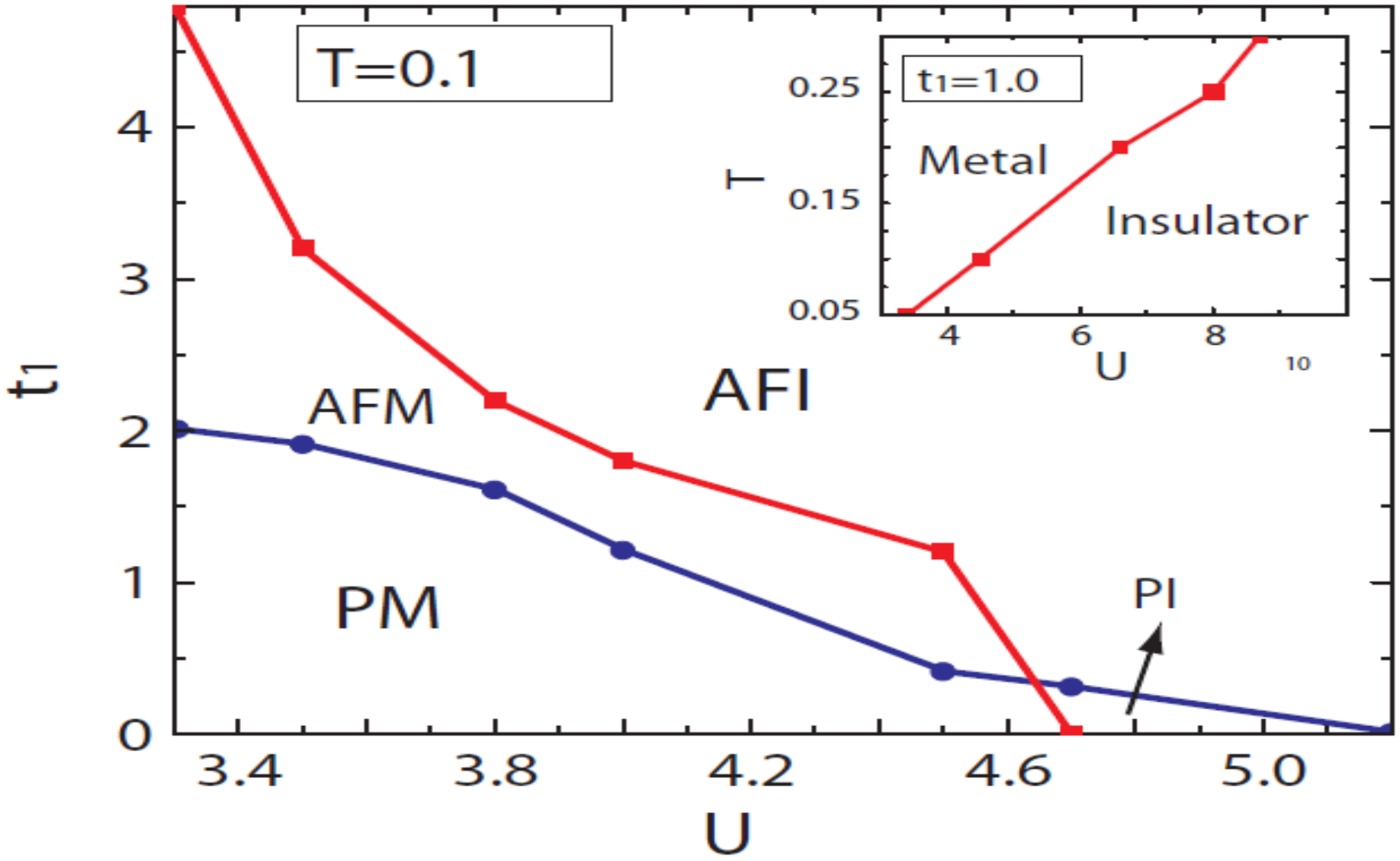

Fig. 2 Metal-insulator phase diagram as a function of inter-layer hopping t1 and interaction U at T=0.1

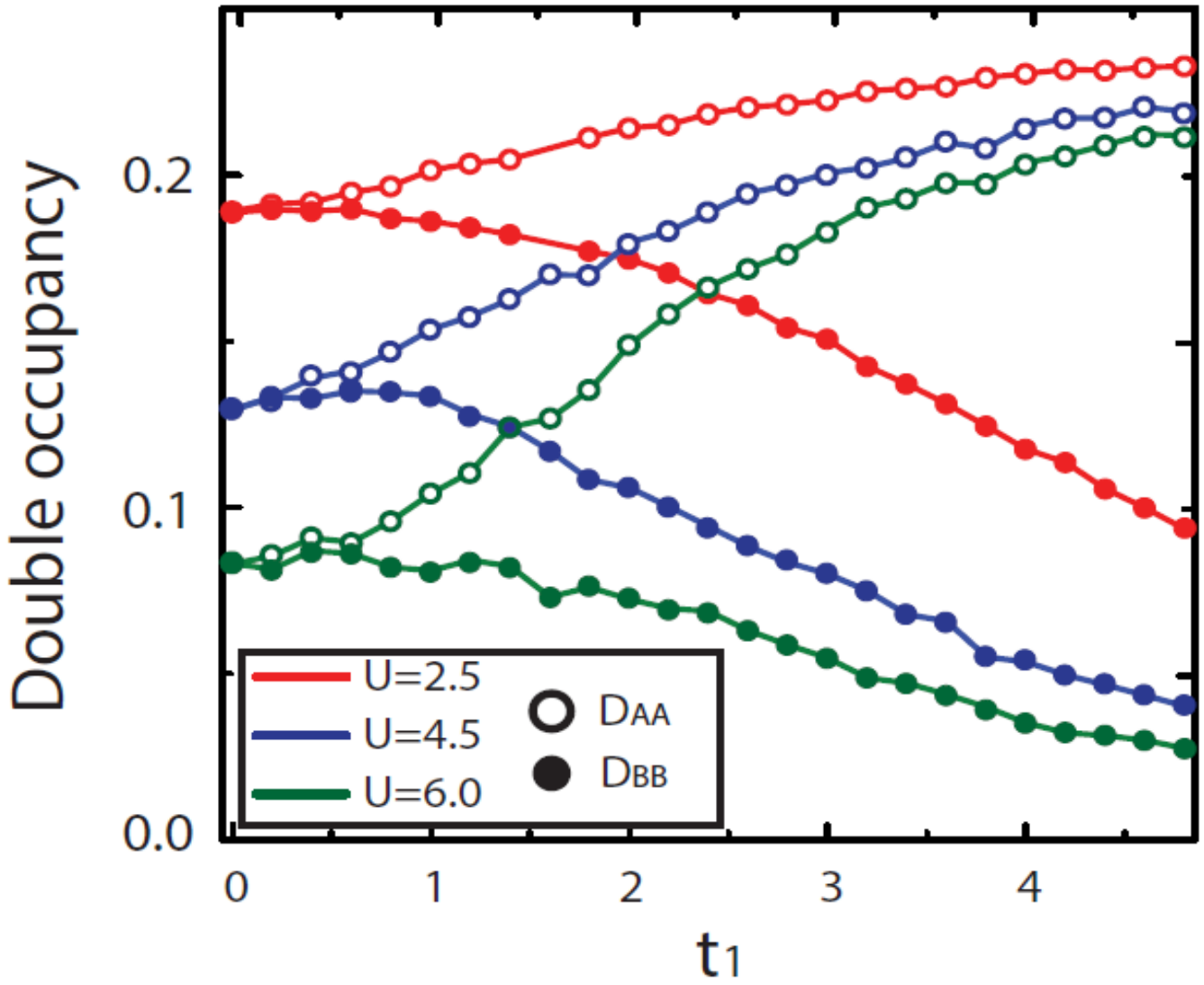

Fig. 3 The evolution of double occupancy D_{occ} as a function of inter-layer hopping t_1 for different interaction U at temperature T=0.1. The dimer sites tend to be double occupied however non-dimer sites tend to be single occupied, with increasing t_1.

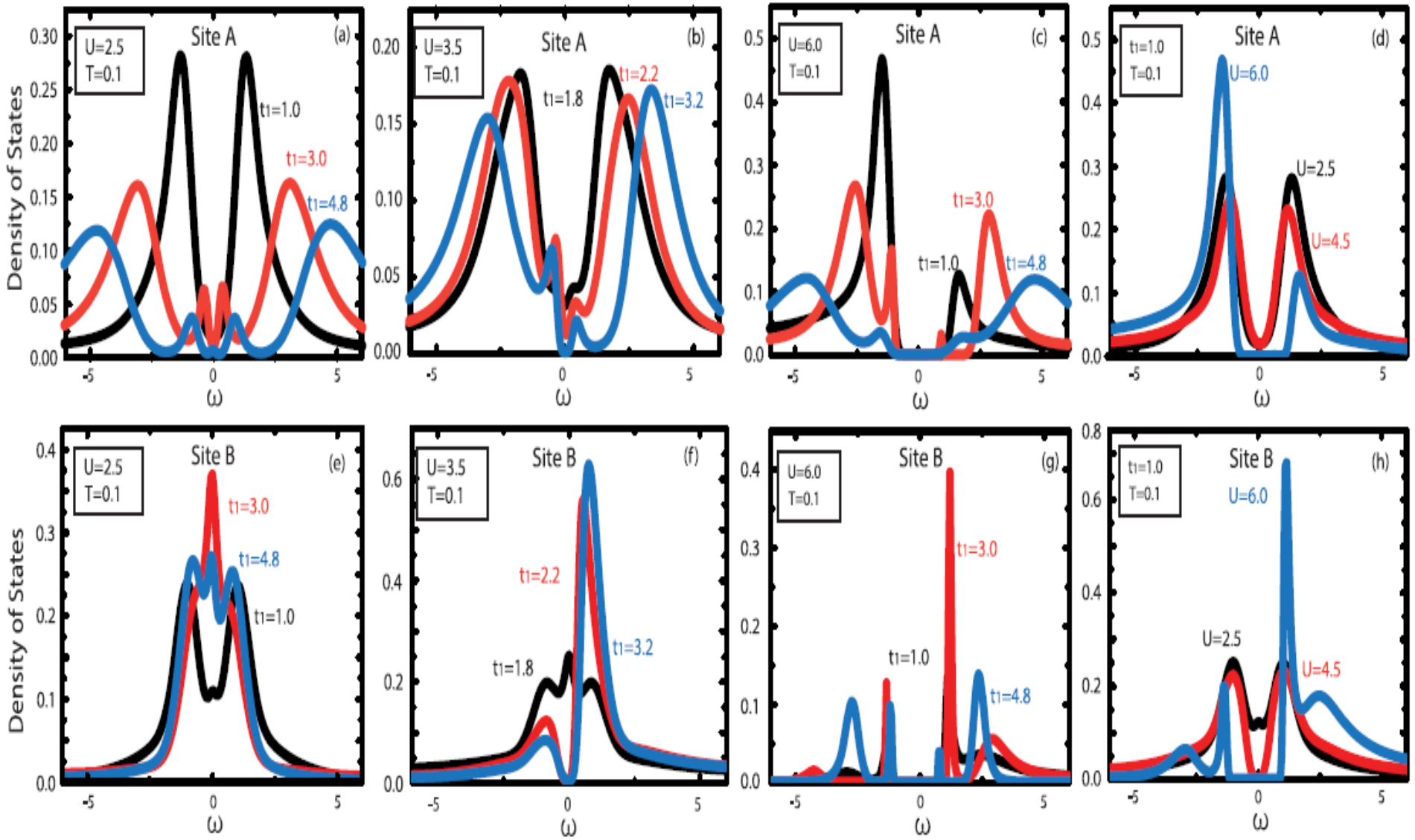

Fig. 4 The density of states as a function of frequency v for different inter-layer hopping t1 at temperature T=0.1. (a), (e): The metallic phase at U=2.5 for A sites and B sites. (b): For A sites, as we increase t1, system undergoes a phase transition from etal (at U=3.5 and t1=1.8) to insulator (at t1=3.2). (f): For B sites, same tendency occurs and the critical point is at about t1=3.2. (c), (g): The insulating phase at U=6.0. (d), (h): The density of states as a function of v for different U with fixed t1.

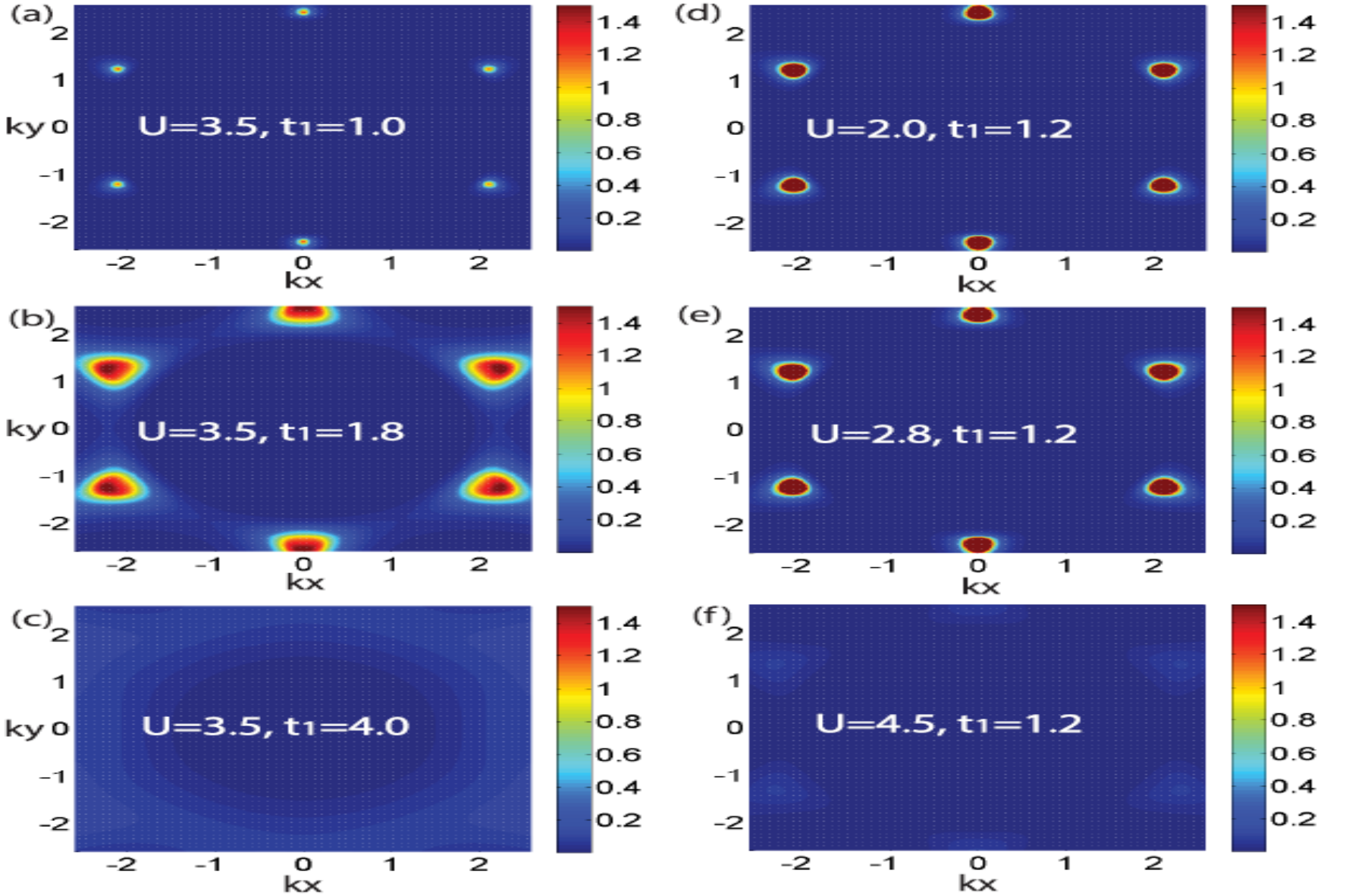

Fig. 5 The evolution of spectral function A(k, ω=0) near Fermi surface for different inter-layer hopping t1 at T=0.1 and U=3.5: (a) t1=1.0, (b) t1=1.8, (c) t1=4.0. The A(k,ω=50) when T=0.1 and t1=1.2 for different interaction U: (d) U=2.0, (e) U=2.8, (f) U=4.5.

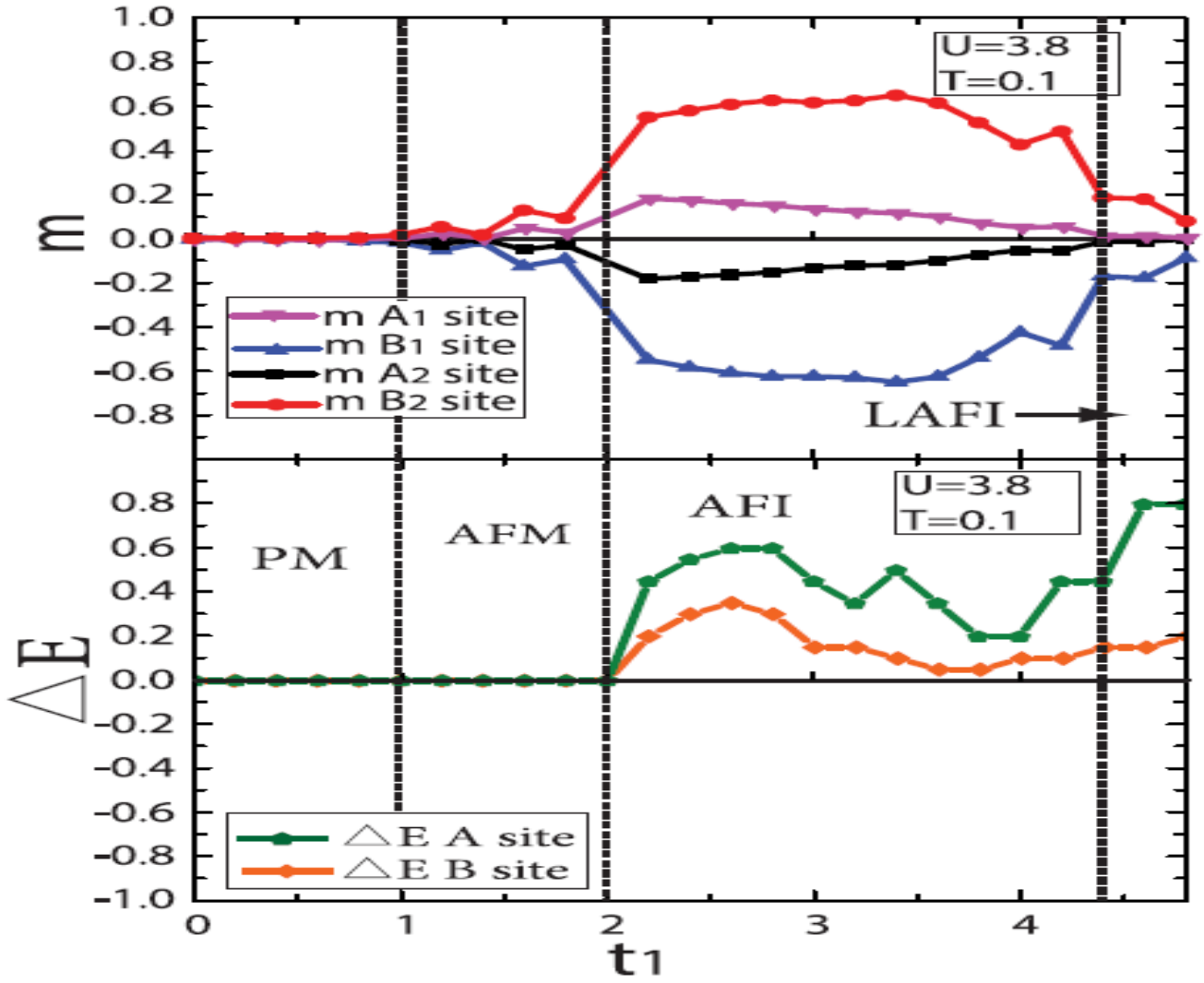

Fig. 6 The evolution of magnetic order parameter m at T=0.1 and U=3.8. For t1=1.0, magnetic parameter m is nonzero and has opposite sign between A1/A2 sites and B1/ B2 sites. The system goes into anti-ferromagnetic phase. At large t1 magnetization of A1/A2 sites are more easily decreasing to zero while B1/B2 sites are still nonzero. The system is layer anti-ferromagnetic phase. Single particle excitation gap DE denoted by dark green solid line and orange solid line, divide phase into PM, AFM, AFI and LAFI.

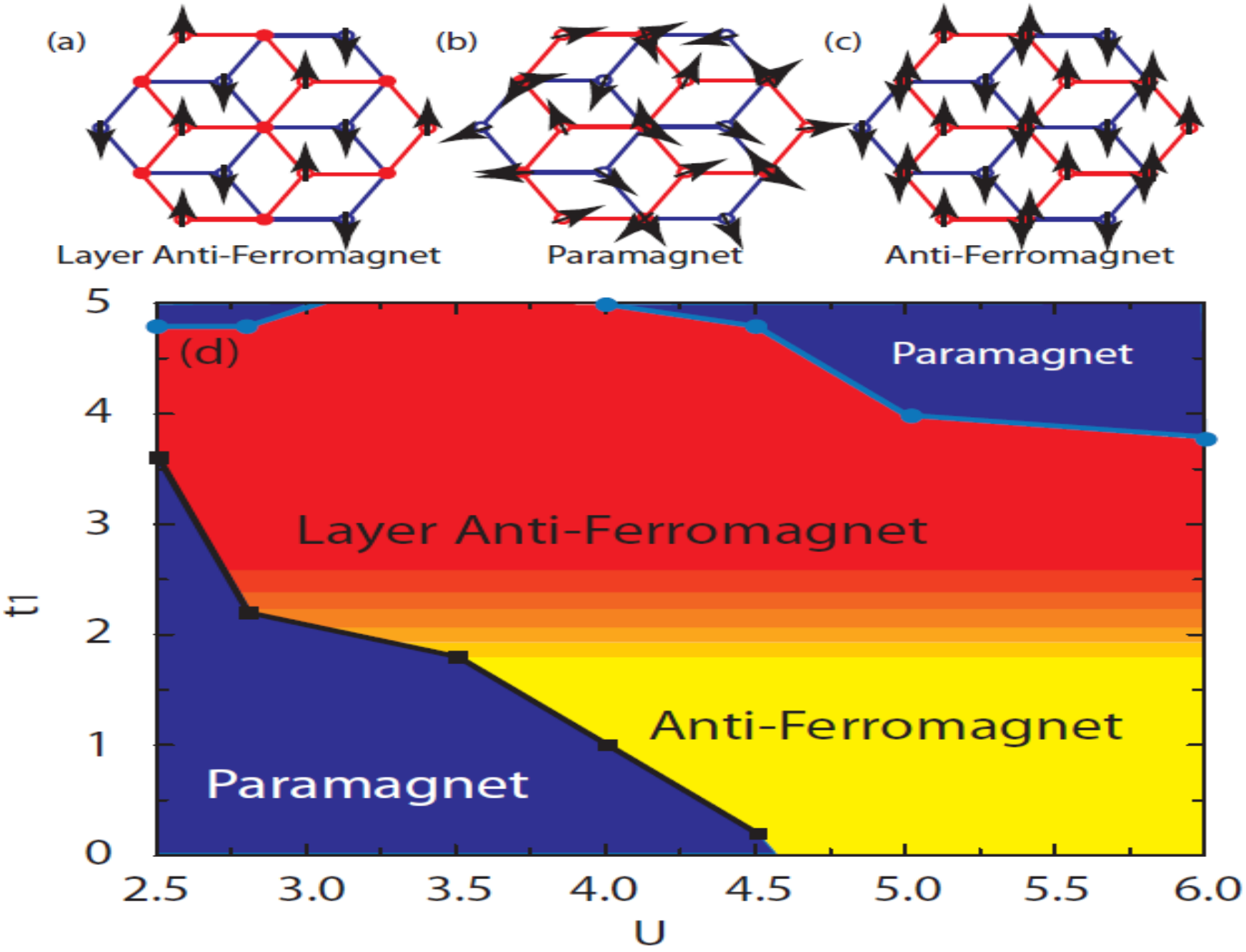

Fig. 7 Phase diagram of magnetic phase transition

2.3、三角晶格:

Y. H. Chen, W. Wu, H. S. Tao, W.M. Liu, Phys. Rev. A 82, 043625 (2010)

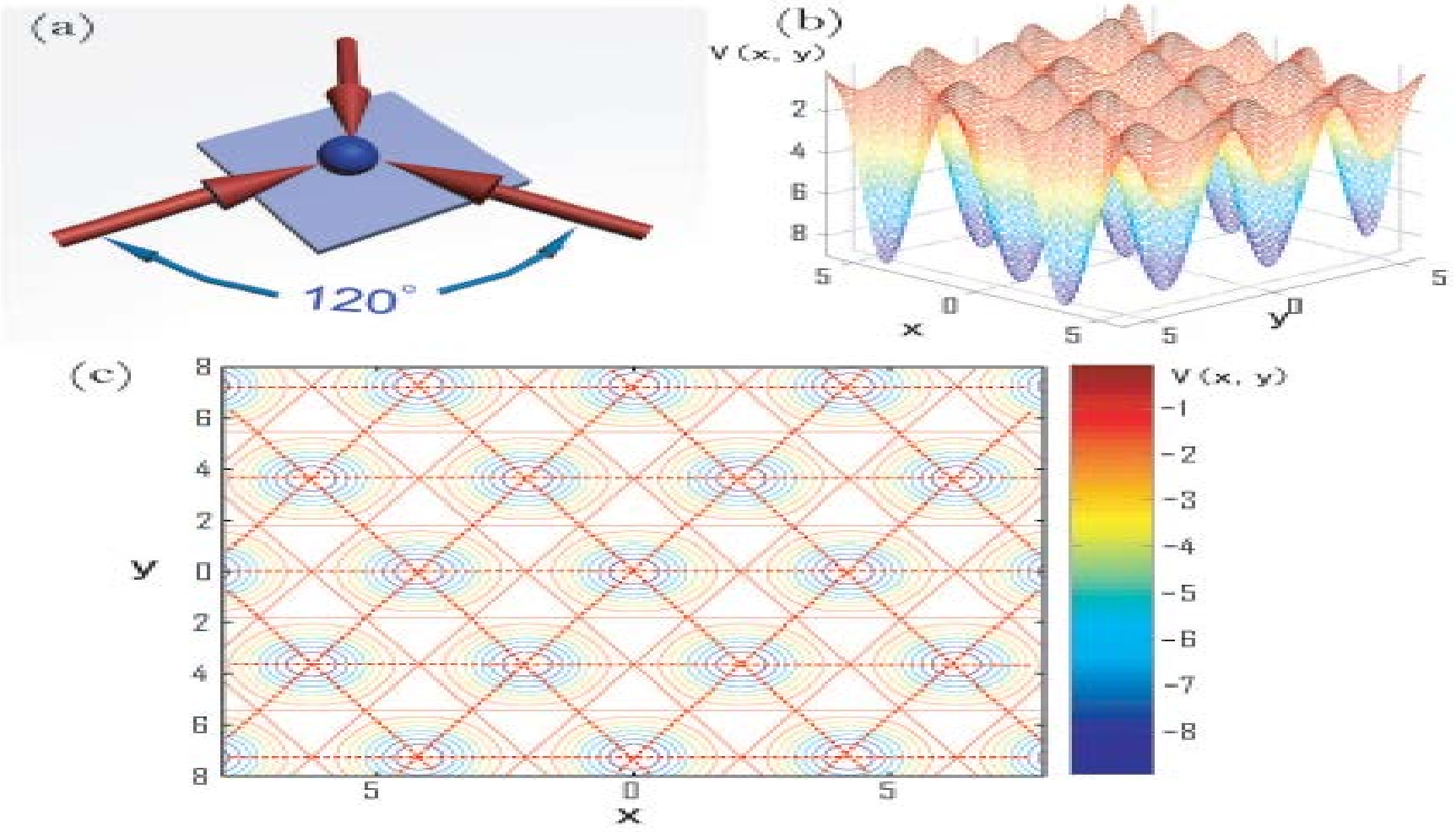

FIG. 1: Triangular optical lattice

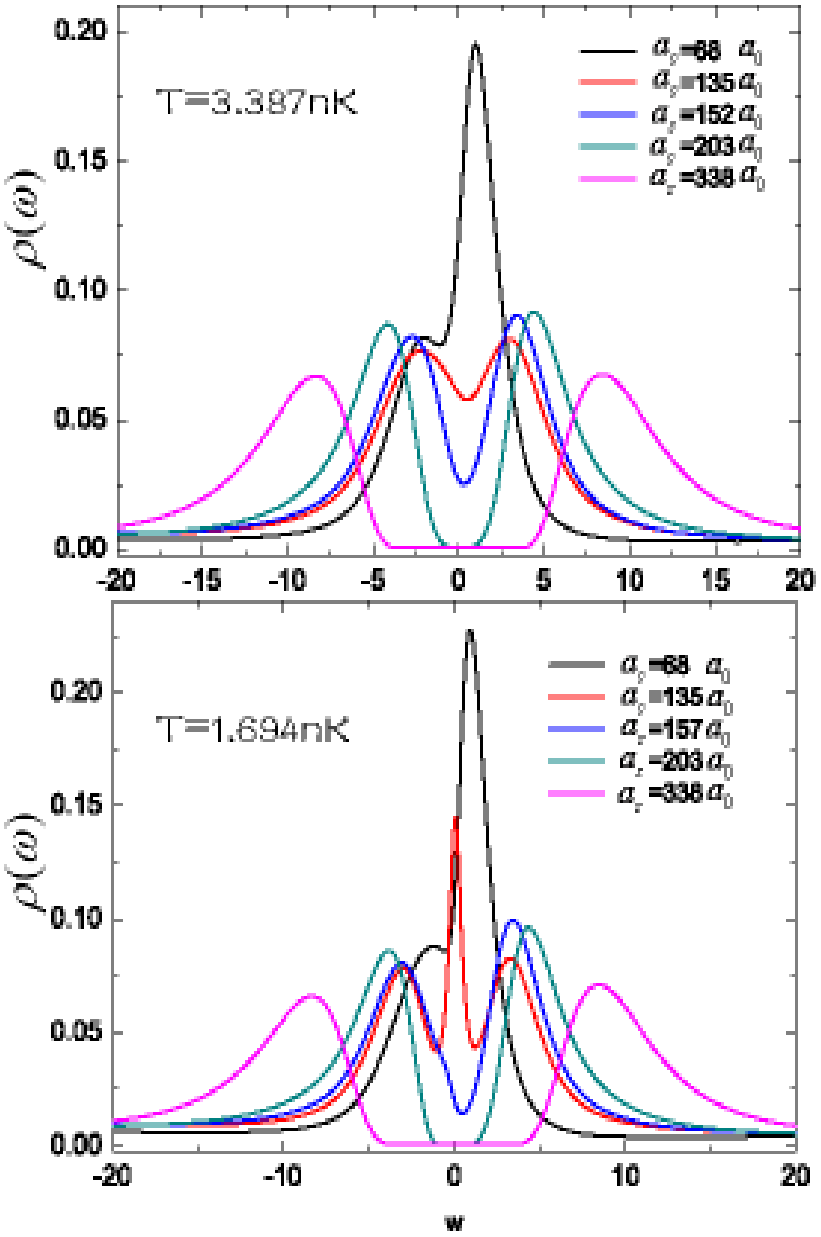

Fig.3 Density of states

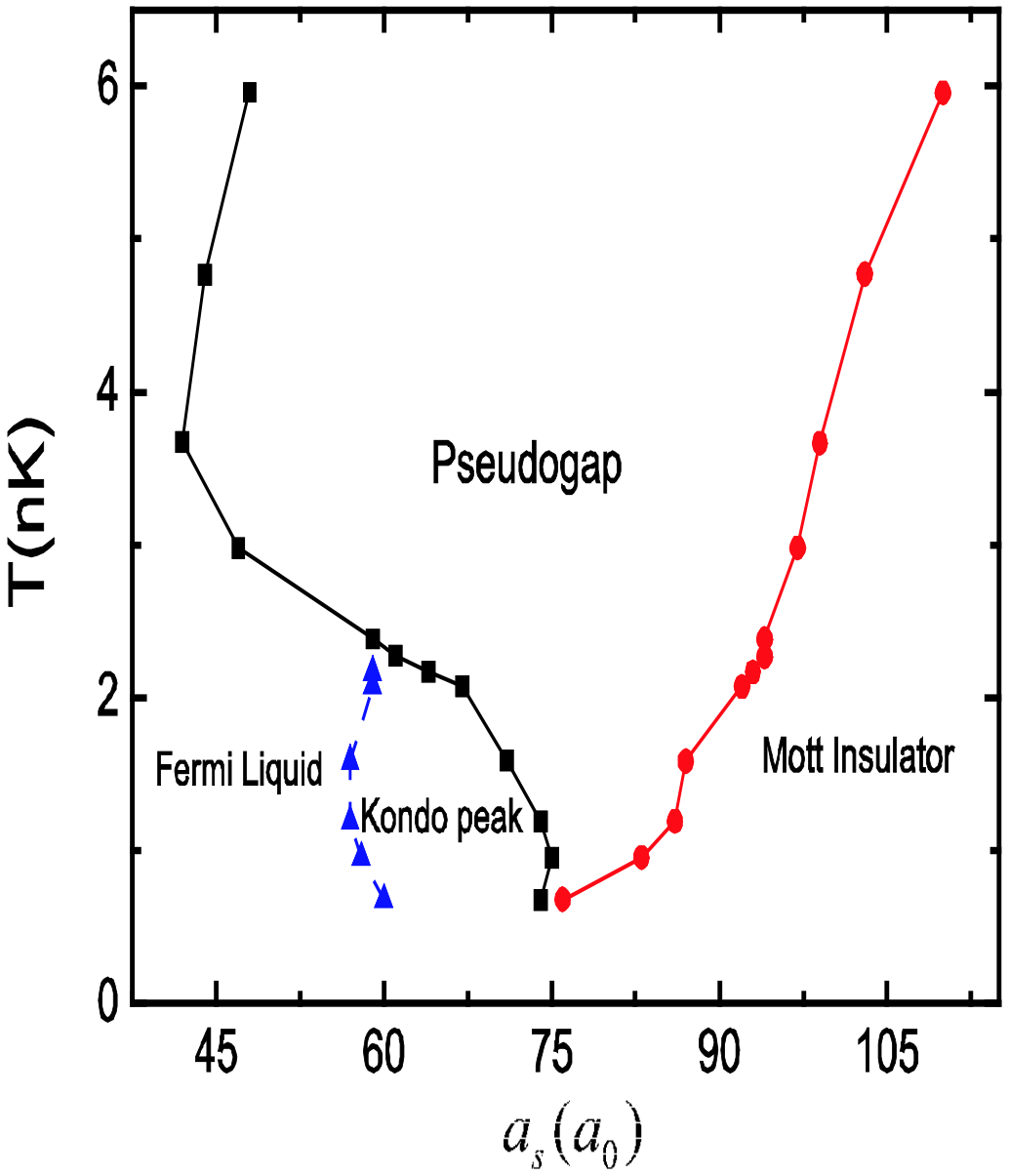

Fig.4 Phase diagram

三角 kagome 晶格

Y.H. Chen, H.S. Tao, D.X. Yao, W.M. Liu, Phys. Rev. Lett. 108, 246402 (2012)

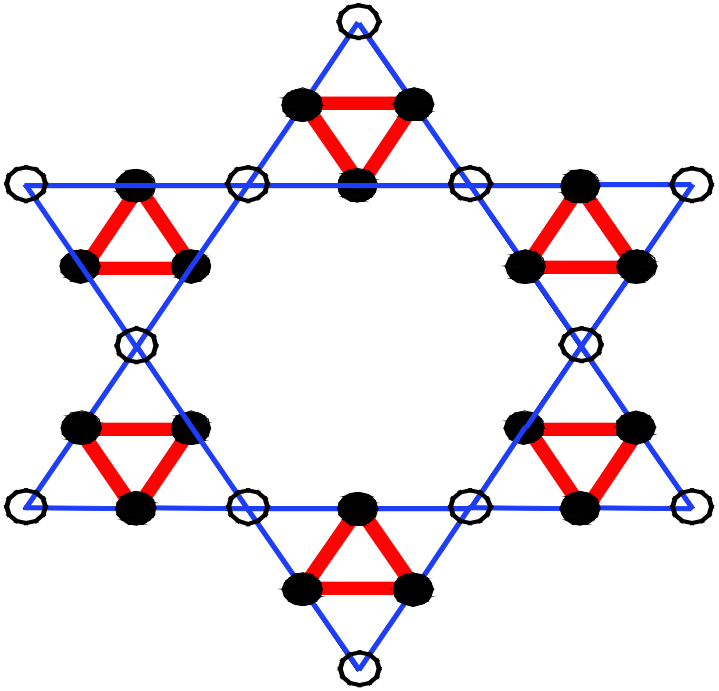

$$H = -\sum_{\langle ij\rangle s} t_{ij} c_{is}^{\dagger} c_{js} + U \sum_{i} n_{i\uparrow} n_{i\downarrow} + m \sum_{is} n_{is}$$

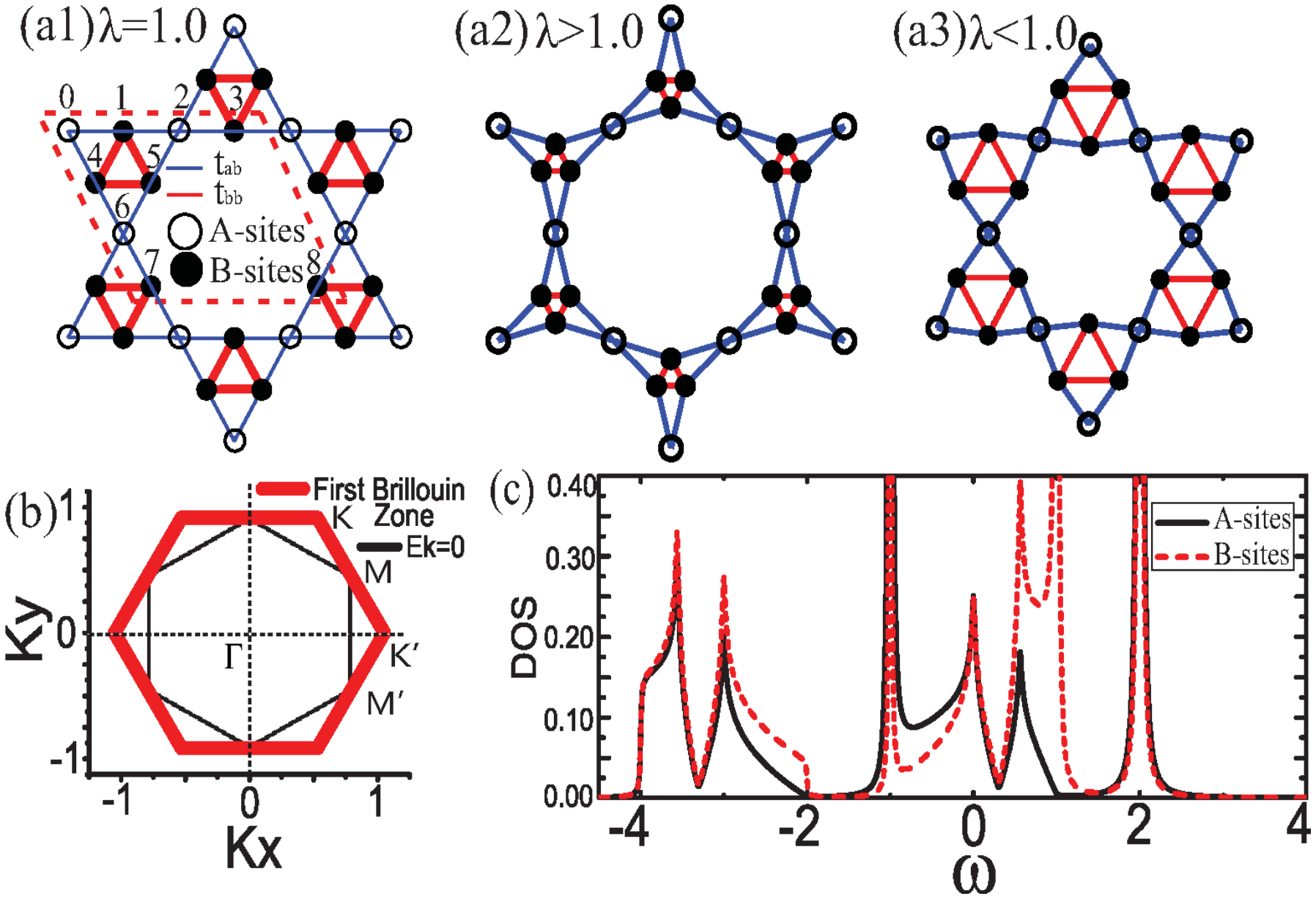

图1 三角 kagome 格子示意图。（a）具有不同非均匀性因子λ的三角 kagome 格子示意图，λ=1 时系统是均匀的。（b）三角kagome在 λ=1, U=0 情况下的第一布里渊区与费米面。(c）三角 kagome 在λ=1, U=0 情况下的态密度。

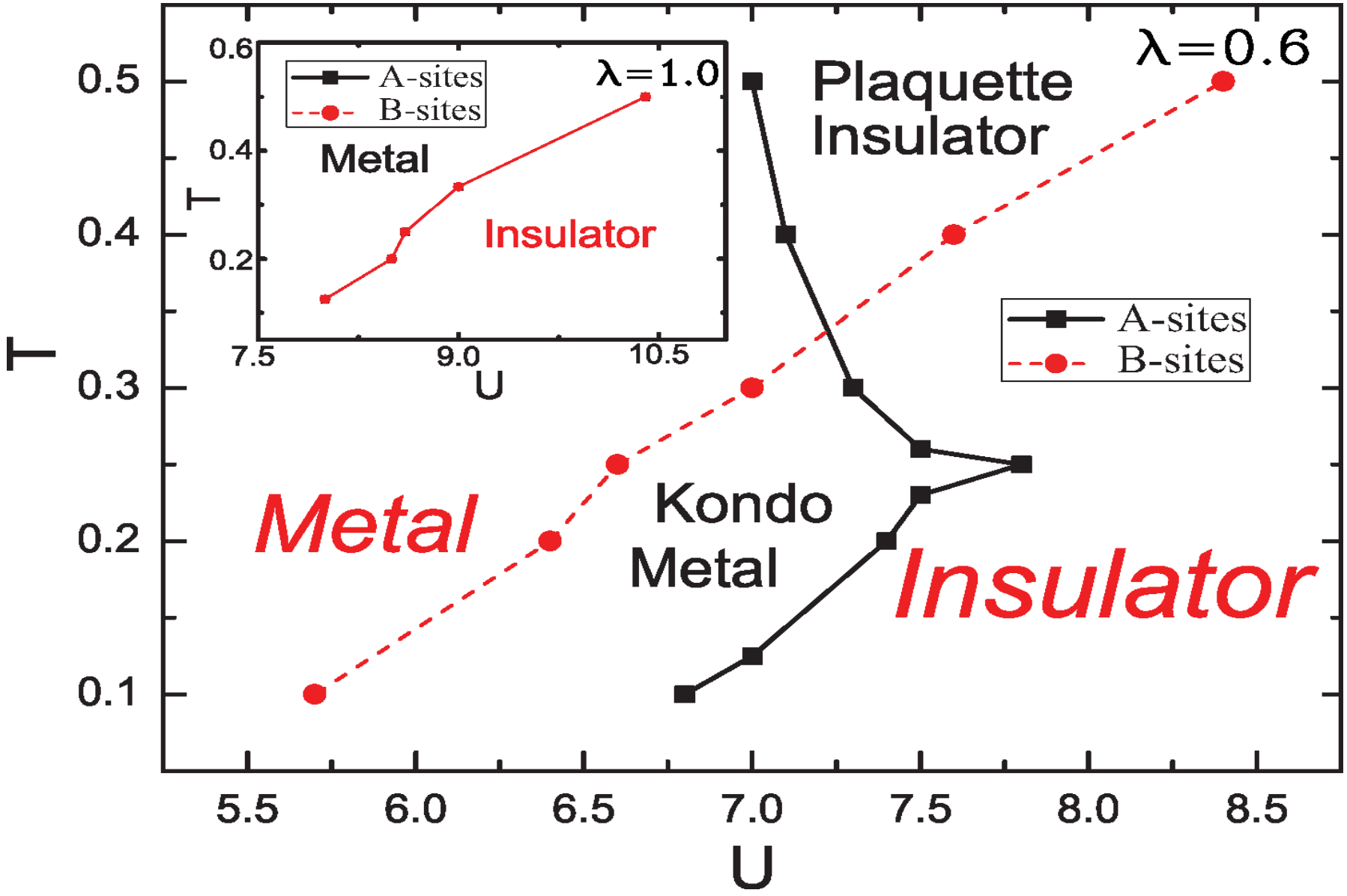

图2 当λ=0.6 时，三角 kagome 格子的相图。非均匀性λ使得三角 kagome 格子的相变线发生变化。A 子格和B 子格的相变点发生分离，形成两种新的相：片绝缘体（Plaquette Insulator）和Kondo金属（Kondo Metal）。

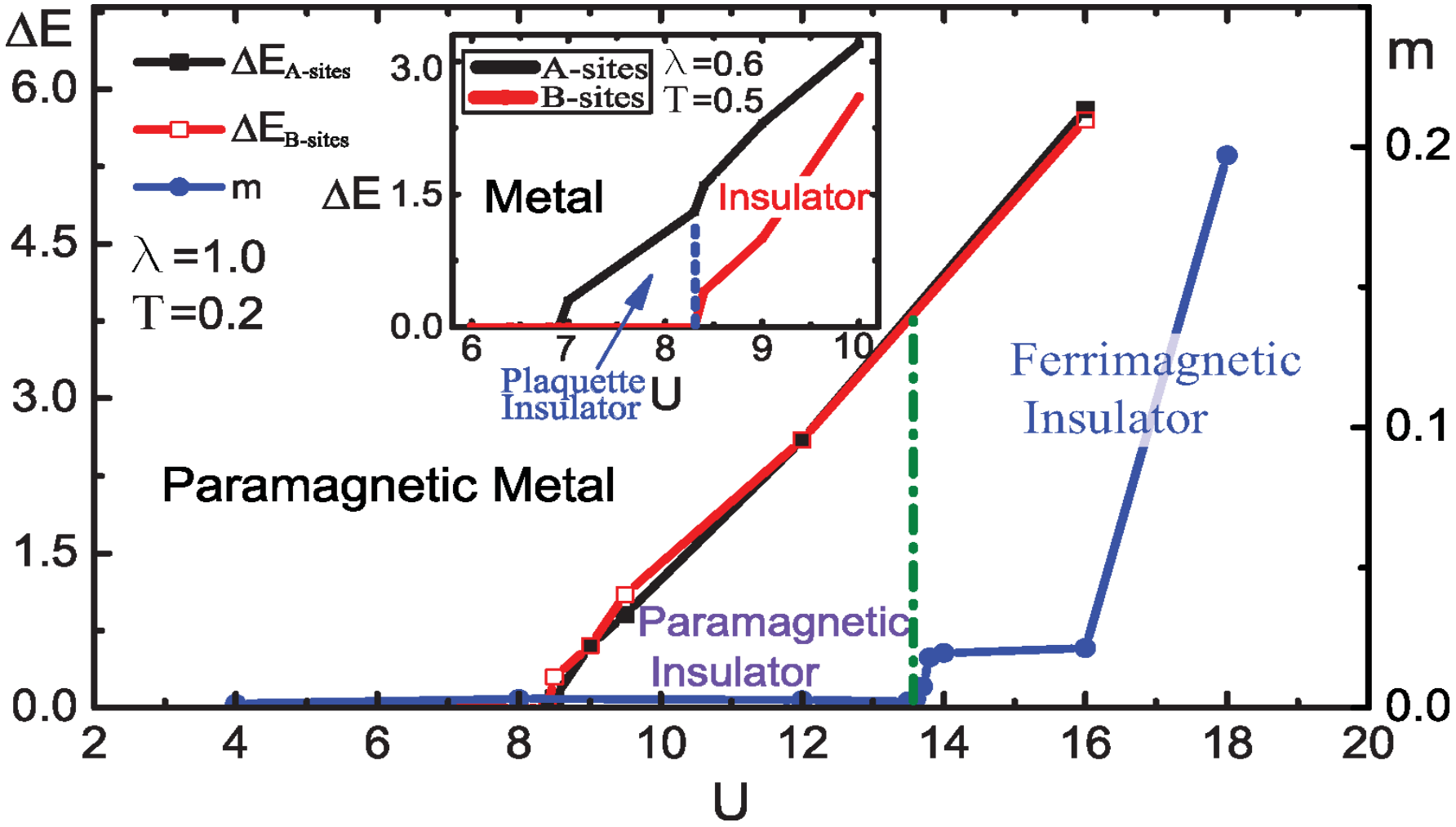

FIG. 6: The evolution of single particle gap ΔE and ferrimagnetic order parameter m at $\lambda = 1$ and $T = 0.2$. A paramagnetic metallic phase is found when U is weak with $\Delta E = 0$ and $m = 0$. As U increases, a gap is opened and no magnetic order is formed with $\Delta E \neq 0$ and $m = 0$. This paramagnetic insulating state can be a short range RVB spin liquid. An obvious magnetic order is formed when U is strong enough with $\Delta E \neq 0$ and $m \neq 0$. The inset picture shows the evolution of ΔE at $\lambda = 0.6$ and $T = 0.5$. A plaquette insulator is found when the A-sites are insulating and the B-sites are metallic.

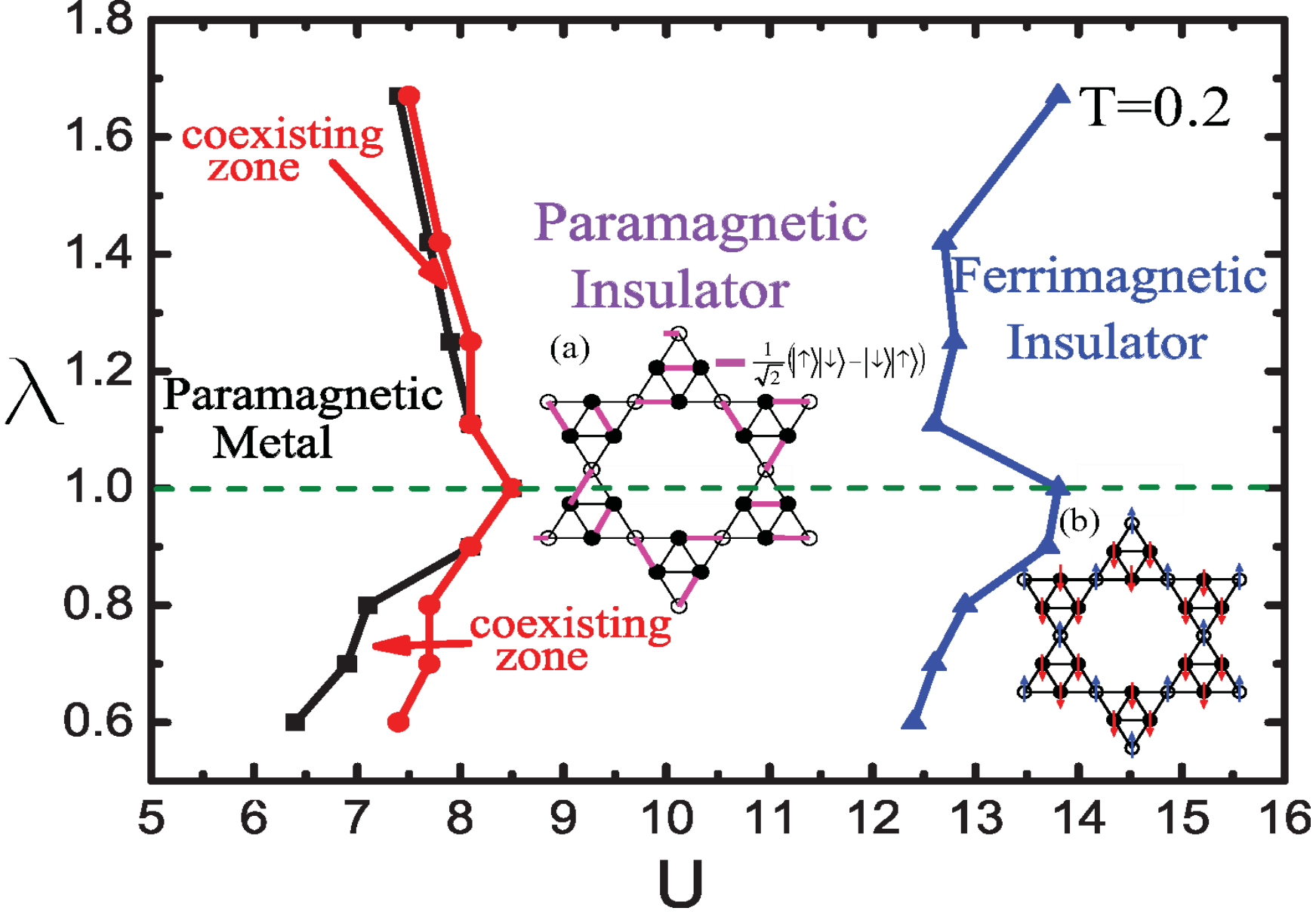

图7 三角 **kagome** 格子随相互作用 **U** 和非均匀性因子 **λ** 变化的相图。插入图（**a**）：顺磁绝缘体中可能存在的共价键分布示意图。 插入图（**b**）：亚铁磁绝缘体的自旋分布示意图。

2.4、Shastry-Sutherland 晶格

H.D. Liu, Y.H. Chen, H.F. Lin, H.S. Tao, W.M. Liu, Scientific Reports 4, 4829 (2014)

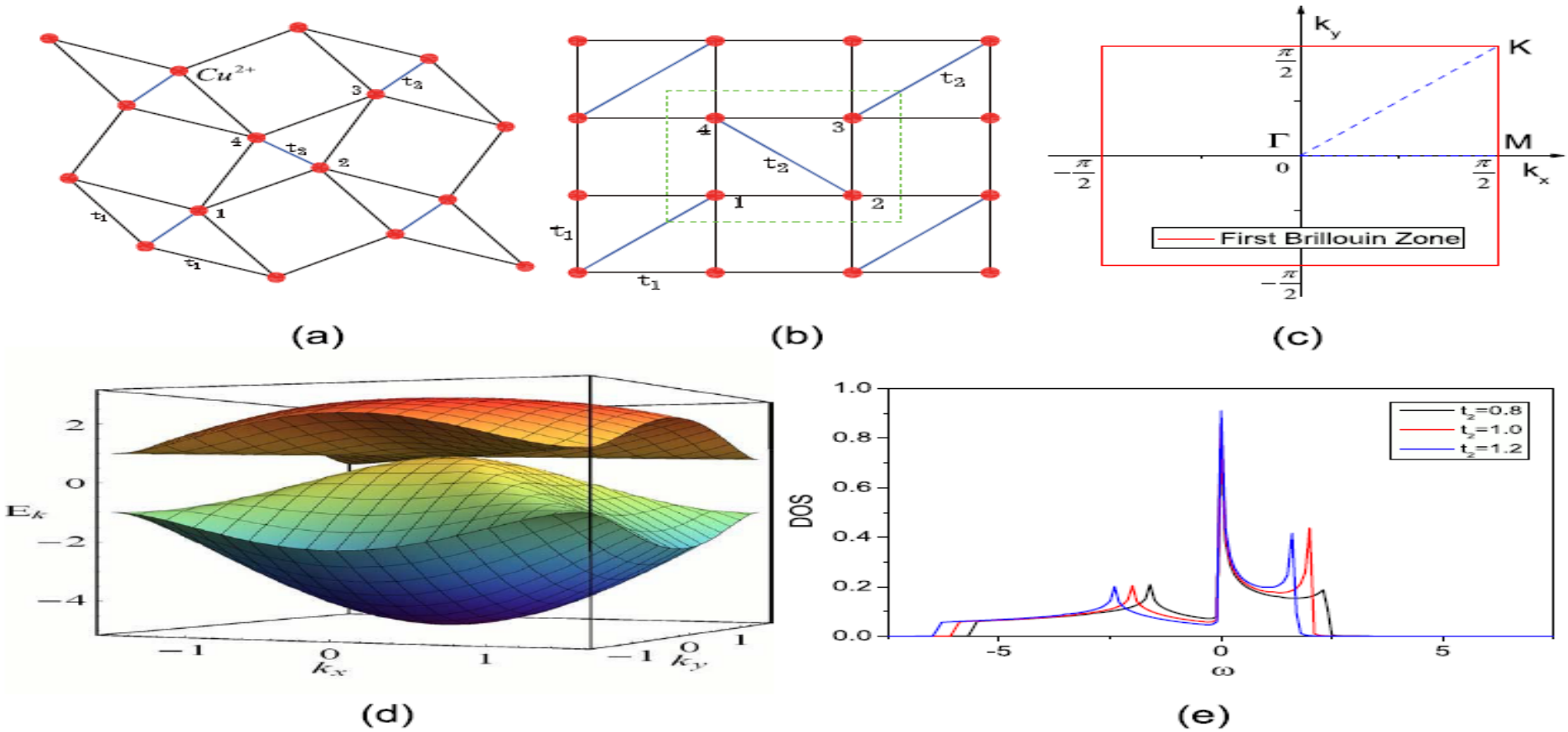

$$H = -t_1 \sum_{\langle ij\rangle_1,\sigma} c^{+}_{i\sigma} c_{j\sigma} - t_2 \sum_{\langle ij\rangle_2,\sigma} c^{+}_{i\sigma} c_{j\sigma} + U \sum_{i} n_{i\uparrow} n_{i\downarrow},$$

FIG. 1 (a) Two dimensional lattice structure of Cu^{2+} in $SrCu_2(BO_3)_2$; (b) Sketch of Shastry-Sutherland lattice, which is topologically equivalent to (a).

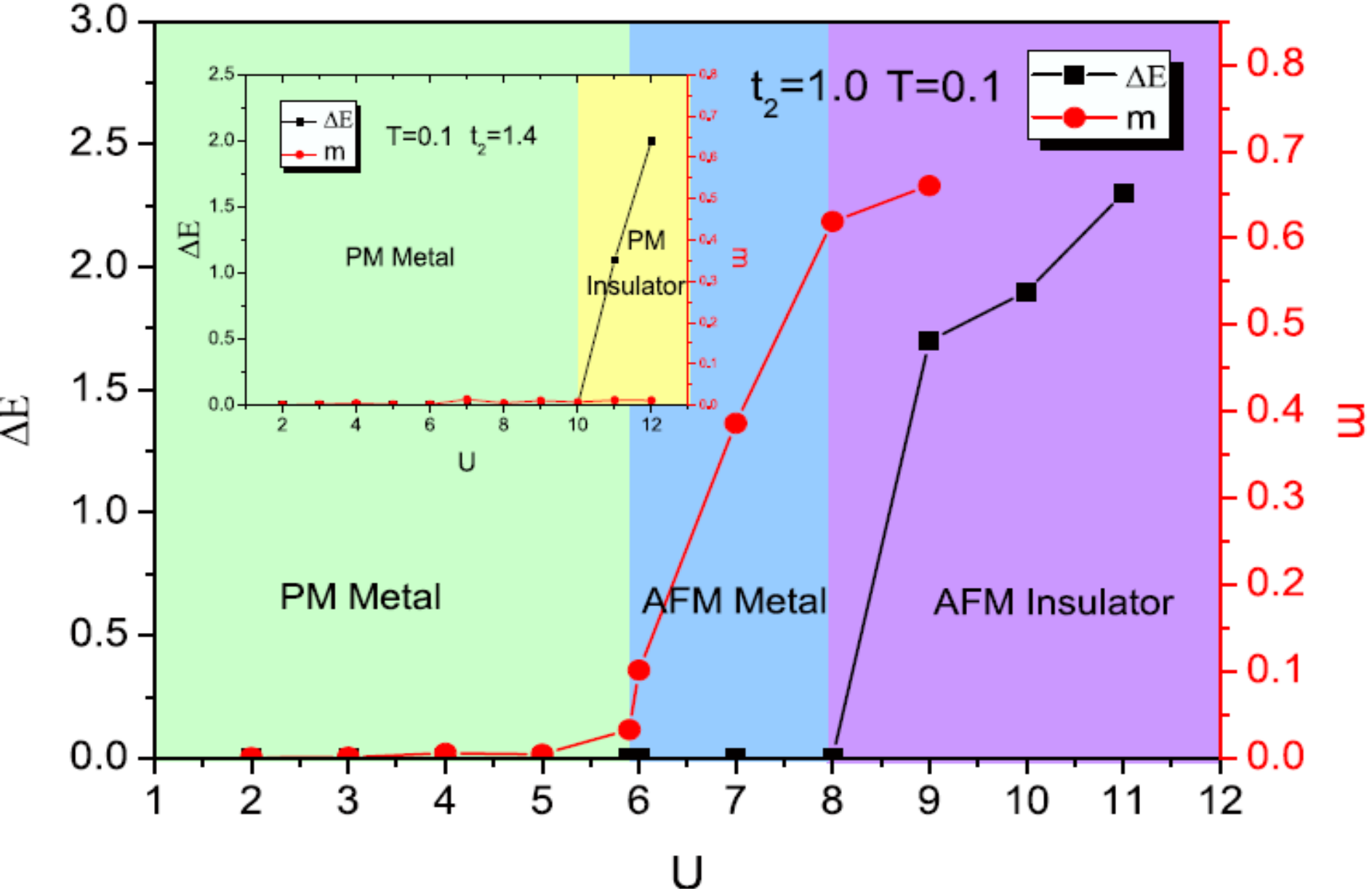

Fig. 5 Evolution of the staggered magnetic order parameter m and the single particle gap △E as a function of U.

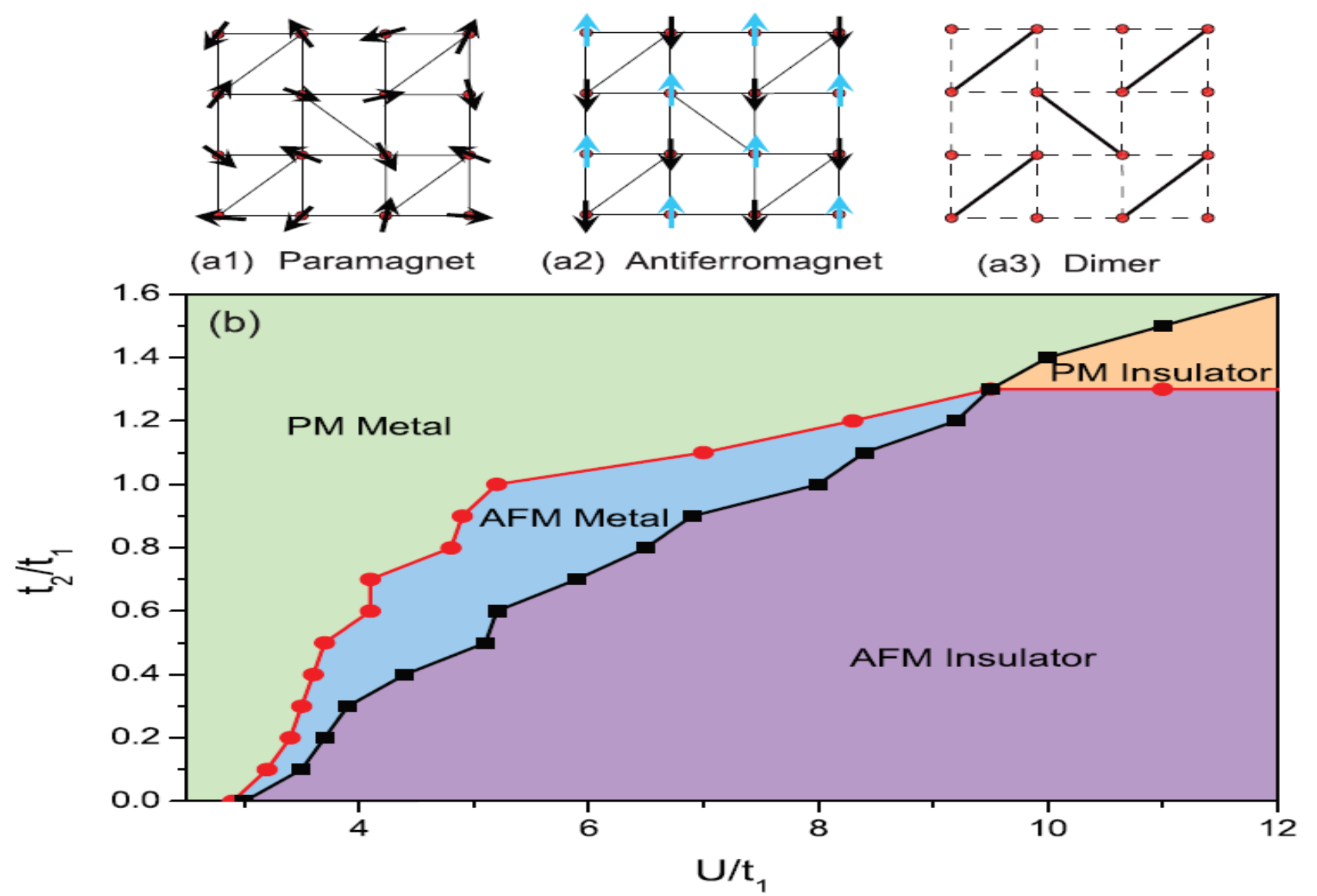

Fig. 6 t_2-U phase diagram at T=0.1

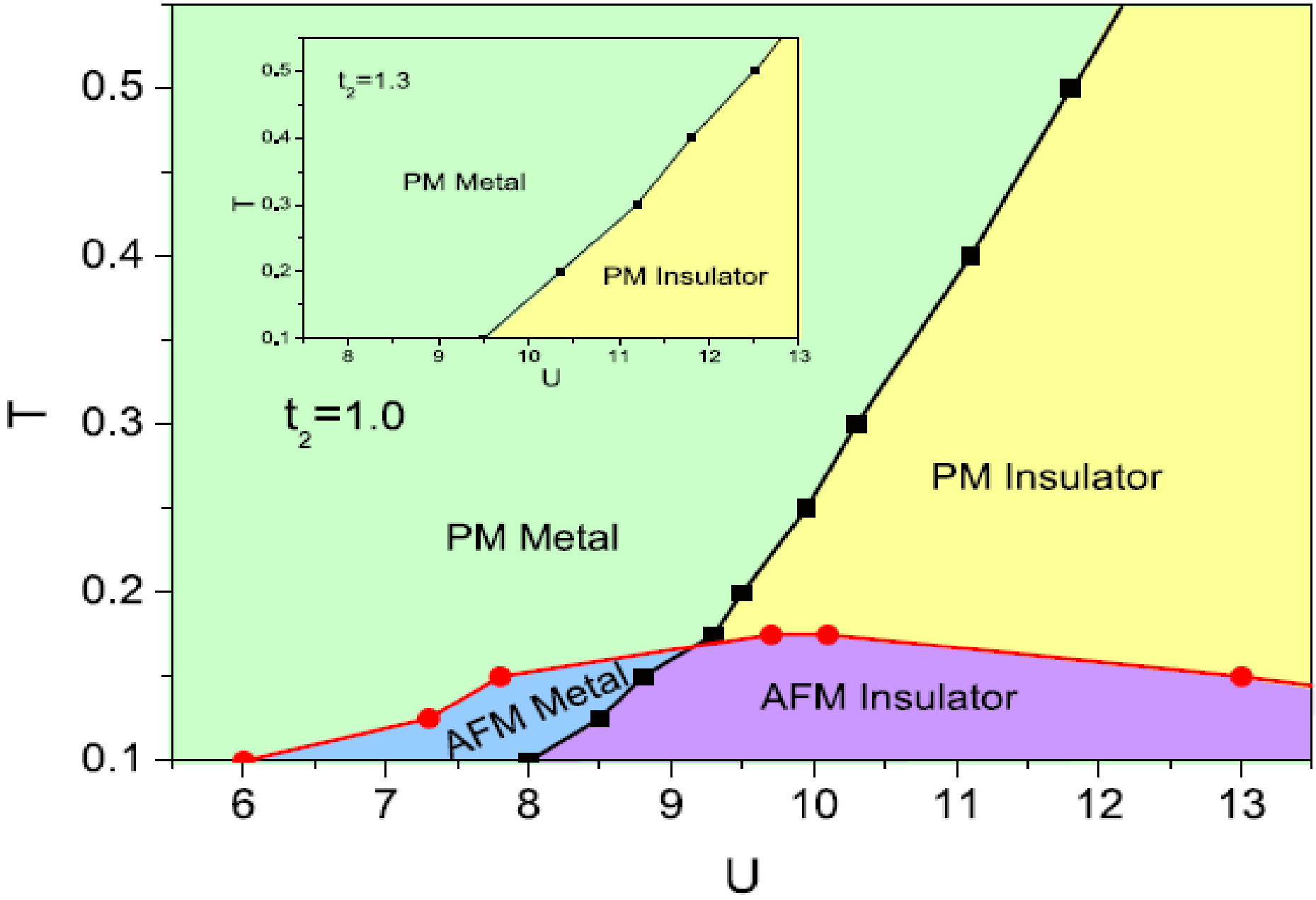

Fig. 7 Phase diagram of interacting fermions

3、自旋-轨道耦合系统

Example: 2D surfaces in 3D

A closed surface is characterized by its genus, g = # holes

g=0 g=1




g is an integer topological invariant that can be expressed in terms of the gaussian curvature κ that characterizes the local radii of curvature

$$\kappa = \frac{1}{r_1 r_2}$$

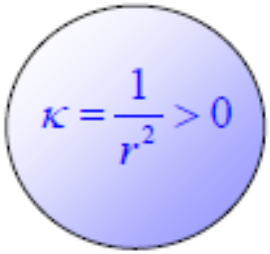

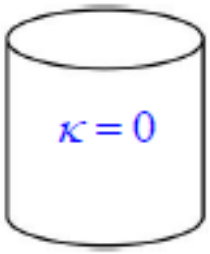

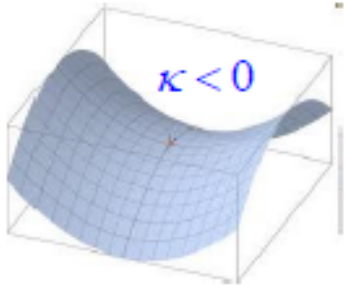

Gauss Bonnet Theorem : $\int_S \kappa dA = 4\pi(1-g)$

See Kane's talk on Summer School lectures on Topological Insulators and Superconductors

3、自旋-轨道耦合系统

Berry phase (1984)

$$e^{-i\Delta\varphi_{12}} = \frac{\langle\Psi_0(\kappa_1)|\Psi_0(\kappa_2)\rangle}{|\langle\Psi_0(\kappa_1)|\Psi_0(\kappa_2)\rangle|};$$

$$\Delta\varphi_{12} = -\,\mathrm{Im}\,\log\langle\Psi_0(\kappa_1)|\Psi_0(\kappa_2)\rangle\,.$$

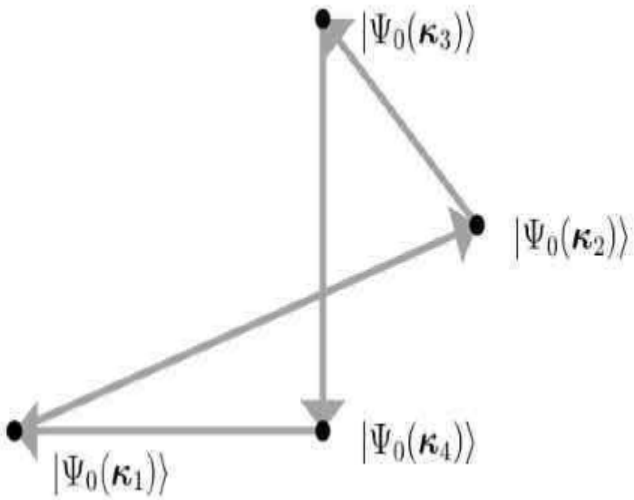

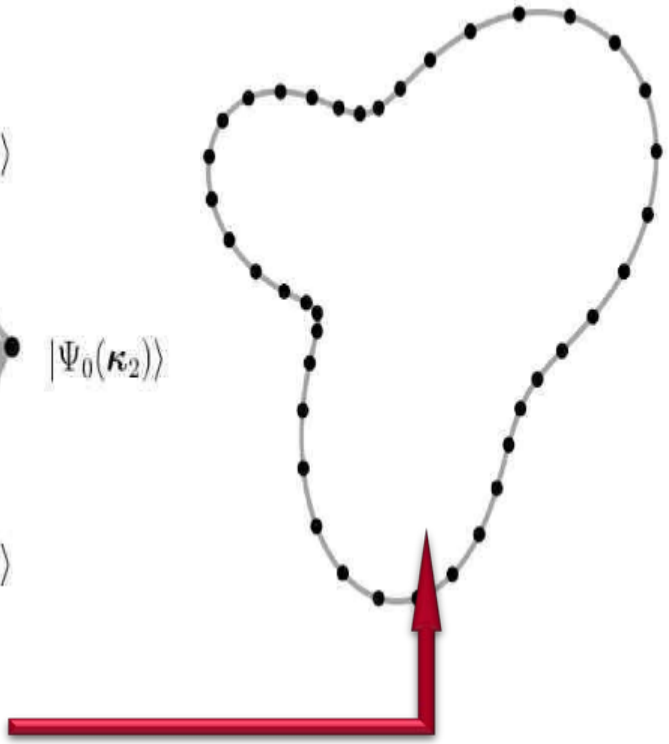

$$\gamma = \Delta\varphi_{12} + \Delta\varphi_{23} + \Delta\varphi_{34} + \Delta\varphi_{41}$$

$$= -\,\mathrm{Im}\,\log\langle\psi(\xi_1)|\psi(\xi_2)\rangle\langle\psi(\xi_2)|\psi(\xi_3)\rangle\langle\psi(\xi_3)|\psi(\xi_4)\rangle\langle\psi(\xi_4)|\psi(\xi_1)\rangle$$

discrete case

continuum case

$$\gamma = \sum_{s=1}^{M}\Delta\varphi_{s,s+1} \longrightarrow \oint_C \mathcal{A}(\xi)\cdot d\xi$$

Gauge invariant!

Observable!

3、自旋-轨道耦合系统

Chern number

Wave function single valued along the path
(choose a gauge!)

+

Closed path (closed surface)

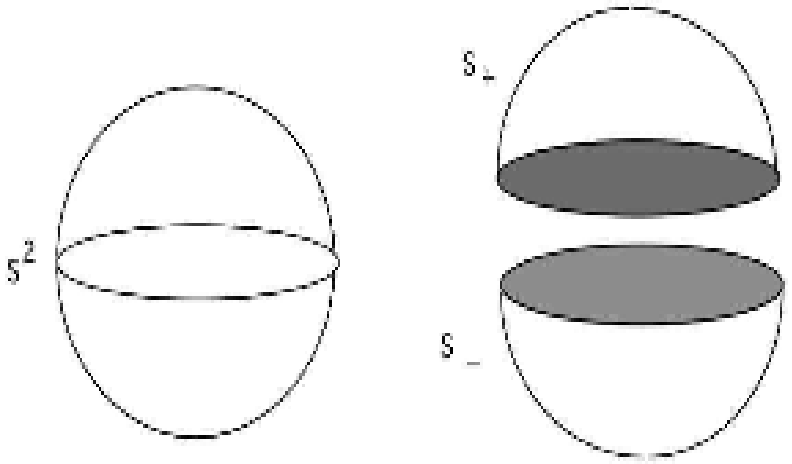

$$\gamma_n = \oint_C d\boldsymbol{R} \cdot \mathcal{A}_n(\boldsymbol{R}).$$

$$\zeta(\boldsymbol{R}(0)) - \zeta(\boldsymbol{R}(T)) = 2\pi \times \text{integer}.$$

$$\sigma_{xy} = n\frac{e^2}{h}.$$

$$\int_{S^2} \boldsymbol{\Omega}(\boldsymbol{\xi}) \cdot \mathbf{n}\, d\sigma = \int_{S_+} \boldsymbol{\Omega}(\boldsymbol{\xi}) \cdot \mathbf{n}\, d\sigma + \int_{S_-} \boldsymbol{\Omega}(\boldsymbol{\xi}) \cdot \mathbf{n}\, d\sigma.$$

$$\int_{S^2} \boldsymbol{\Omega}(\boldsymbol{\xi}) \cdot \mathbf{n}\, d\sigma = \oint_C \boldsymbol{\mathcal{A}}_+(\boldsymbol{\xi}) \cdot d\boldsymbol{\xi} - \oint_C \boldsymbol{\mathcal{A}}_-(\boldsymbol{\xi}) \cdot d\boldsymbol{\xi}$$

$$\sigma_{xy} = \frac{e^2}{\hbar} \int_{\mathrm{BZ}} \frac{d^2k}{(2\pi)^2} \Omega_{k_x k_y},$$

Quantum distance, Quantum adiabatic approximation and the non-Abelian quantum geometric tensor

$$\left|\Psi\left(\lambda^{\mu}\right)\right\rangle$$

Ground-state (GS)

$$\lambda^{\mu}\left(\mu=\mu_1,\cdots,\mu_n\right)\in M$$

Parameters manifold

$$\left|\Upsilon\left(l^{m}\right)\right\rangle=\sum_{i=1}^{g}C_i\left(l^{m}\right)\left|y_i\left(l^{m}\right)\right\rangle \qquad \left|\Upsilon\left(l^{m+dm}\right)\right\rangle=\sum_{i=1}^{g}C_i\left(l^{m+dm}\right)\left|y_i\left(l^{m+dm}\right)\right\rangle$$

GS over l^{m} and l^{m+dm} in a g-dimensional degenerated Hilber space

An intuitional definition for the distance :

$$dS^2=\left\|\Upsilon\left(l^{m+dm}\right)-\Upsilon\left(l^{m}\right)\right\|^2=\sum_{u,m}^{g}\left\langle\partial_m\Upsilon\,dl^{m}\middle|\partial_u\Upsilon\,dl^{u}\right\rangle$$

3.1、第一性原理计算方法：

$$H\Phi(\{R\},\{r\}) = E\Phi(\{R\},\{r\})$$

$$H = -\sum_i \frac{\hbar^2}{2m}\nabla_i^2 - \sum_I \frac{\hbar^2}{2M_I}\nabla_I^2 + \frac{1}{2}\sum_{i,j}\frac{e^2}{|r_i - r_j|} - \sum_{I,i}\frac{Z_I e^2}{|R_I - r_i|} + \frac{1}{2}\sum_{I,J}\frac{Z_I Z_J e^2}{|R_I - R_J|}$$

$$\left(-\frac{\hbar^2}{2m}\nabla^2 + V(r) + e^2\sum_i \int dr' \frac{|\varphi_{i'}(r')|^2}{|r'-r|}\right)\varphi_i(r) - e^2\sum_{i\neq i'}\int dr' \frac{\varphi^+_{i'}(r')\varphi_i(r')}{|r'-r|}\varphi_{i'}(r) = E_i\varphi_i(r)$$

Born-Oppenheimer 近似

$$\psi(\mathbf{q}) = \frac{1}{\sqrt{N!}}\begin{vmatrix} \varphi_1(q_1) & \varphi_1(q_2) & \cdots & \varphi_1(q_N) \\ \varphi_2(q_1) & \varphi_2(q_2) & \cdots & \varphi_2(q_N) \\ \vdots & \vdots & \ddots & \vdots \\ \varphi_N(q_1) & \varphi_N(q_2) & \cdots & \varphi_N(q_N) \end{vmatrix}$$

$$\Psi(r,R) = \chi(R)\psi(r,R)$$

$$\left(-\frac{\hbar^2}{2me}\sum_i \nabla^2 + \frac{1}{2\sum_{i\neq j}\frac{e^2}{|r_i - r_j|} + \sum_i V(r_i)}\right)\psi(r) = E\psi(r)$$

$$\psi(r) = \varphi_1(r_1)\varphi_2(r_2)\varphi_3(r_3)\ldots\varphi_N(r_N)$$

$$\left(-\frac{\hbar^2}{2m}\nabla^2 + V(r) + e^2\sum_i \int dr' \frac{|\varphi_{i'}(r')|^2}{|r'-r|}\right)\varphi_i(r) = E_i\varphi_i(r)$$

Hartree 近似

SE Hard problem to solve Schrödinger equation

“Easy” problem to Solve DFT **DFT**

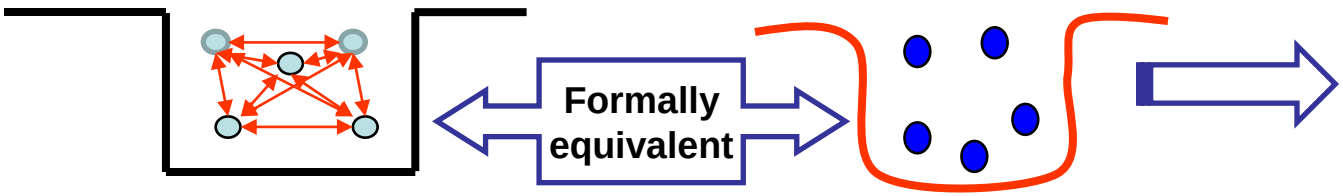

Properties of the system

Electron

Interaction

External potential

Non-interacting electron (KS particle)

Effective potential

Density Functional Theory (1964)

$$H = H_{int} + V_{ext}$$

$$V_{ext} = \sum_i V(\mathbf{r}_i)$$

$$H_{int} = T + V_{ee} = -\frac{\hbar^2}{2m_e}\sum_i \nabla_i^2 + \frac{1}{2}\sum_{i\neq j}\frac{e^2}{|\mathbf{r}_i - \mathbf{r}_j|}$$

$V_{ext}(r) \leftrightarrow \rho_0(r)$ Hohenberg-Kohn定理

$$\rho(\mathbf{r}) = D(V_{ext}); V_{ext}(\mathbf{r}) = G(\rho)$$

$$E(\rho, V) = \langle\psi(\rho)|T + V_{ee} + V_{ext}|\psi(\rho)\rangle = T(\rho) + V_{ee}(\rho) + \int d^3\mathbf{r} V_{ext}(\mathbf{r})\rho(\mathbf{r})$$

$$= T(\rho) + \frac{1}{2}\int d^3\mathbf{r}d^3\mathbf{r}'\frac{\rho(\mathbf{r})\rho(\mathbf{r}')}{|\mathbf{r} - \mathbf{r}'|} + E_{xc}(\rho) + \int d^3\mathbf{r} V_{ext}(\mathbf{r})\rho(\mathbf{r})$$

$|T_0(\rho) - T(\rho)| \longrightarrow E_{xc}(\rho)$

$$\equiv F(\rho) + \int d^3\mathbf{r} V_{ext}(\mathbf{r})\rho(\mathbf{r})$$

$$\rho(\mathbf{r}) = \sum_i |\varphi_i(\mathbf{r})|^2$$

$$T_0(\rho) = \sum_i \int d^3\mathbf{r}\varphi_i^*(\mathbf{r})(-\nabla^2)\varphi_i(\mathbf{r})$$

Make variation in $\varphi_i(r)$ Kohn-Sham Equation

$$\left(-\frac{\hbar}{2m}\nabla^2 + V_{ext}(\mathbf{r}) + e^2\int d^3\mathbf{r}'\frac{\rho(\mathbf{r}')}{|\mathbf{r}' - \mathbf{r}|} + \frac{\delta E_{xc}(\rho)}{\delta\rho}\right)\varphi_i(\mathbf{r}) = E_i\varphi_i(\mathbf{r})$$

Effective potential

$$V_{eff}(r) = \underbrace{v(r) + \int \frac{n(r')}{|r-r'|} dr'}_{f(r)} + \underbrace{\frac{dE_{xc}[n]}{dn}}_{V_{xc}(r)}$$

$V_{xc}(r)$ ⇐ LDA, GGA, etc

General form:

$E_{xc}[\rho] = \int \rho(\mathbf{r}) \varepsilon_{xc}[\rho, \mathbf{r}] d\mathbf{r}$

ε_{xc} at **r** depends on the shape of ρ *everywhere*

Local Density Approximation (LDA)

$\Rightarrow E_{xc}[\rho] = \int \rho(\mathbf{r}) \varepsilon_{xc}(\rho(\mathbf{r})) d\mathbf{r}$

ε_{xc} at **r** only depends on the density at **r** (exact for hom. el. gas)

Generalized Gradient Approximation (GGA)

$\Rightarrow E_{xc}[\rho] = \int \rho(\mathbf{r}) \varepsilon_{xc}(\rho(\mathbf{r}), \nabla\rho(\mathbf{r}), \ldots) d\mathbf{r}$

ε_{xc} at **r** depends on the density and its gradient (+ higher terms) at **r**

etc

LDA+U

$$E_{DFT+U}[\{N(r)\}] = E_{DFT}[\{n(r)\}] + E_{Hab}[\{n^{I\sigma}\}] - E_{dc}[\{n^{I\sigma}\}]$$

LDA/GGA functional — *Hubbard correction* — *Subtract "double counting"*

First approximation:

Ignore exchange type terms

Average over atomic orbitals

$$V_{m_1 m_2 m_3 m_4} \rightarrow U^I \delta_{m_1 m_4} \delta_{m_2 m_3}$$

$$U^I = \frac{1}{(2l+1)^2} \sum_{m_1 m_2} \int d^3r' |\Phi^I_{m_1}(r)|^2 |\Phi^I_{m_2}(r')|^2 V_{ee}(r-r')$$

Apply

$$E_{Hub}[\{n^{I\sigma}\}] = \sum_{I,\sigma} \frac{U^I}{2} \left\{ (n^{I\sigma})^2 + n^{I\sigma} n^{I-\sigma} - Tr[n^{I\sigma} n^{I\sigma}] \right\}$$

$$n^{I\sigma} = Tr[n^{I\sigma}] \qquad n^I = \sum_\sigma Tr[n^{I\sigma}]$$

Apply

$$E_{dc}[\{n^{I\sigma}\}] = \sum_I \frac{U^I}{2} n^I (n^I - 1)$$

Collecting the contributions:

$$E_{DFT+U}[\{n(r)\}] = E_{DFT}[\{n(r)\}] + \sum_{I,\sigma} Tr[n^{I\sigma}(1 - n^{I\sigma})]$$

LDA+U energy functional :

$$E_{local}^{LDA+U} = E^{LDA} - UN(N-1)/2 + \frac{1}{2}U\sum_{i\neq j} n_i n_j$$

LDA+U potential :

$$V_i(\vec{r}) = \frac{\delta E}{\delta n_i(\vec{r})} = V^{LDA}(\vec{r}) + U(\frac{1}{2} - n_i)$$

LDA+U eigenvalue :

$$\varepsilon_i = \frac{\partial E}{\partial n_i} = \varepsilon^{LDA} + U(\frac{1}{2} - n_i)$$

For occupied state n_i=1,

$$\varepsilon_i = \varepsilon^{LDA} - U/2$$

For unccupied state n_i=0,

$$\varepsilon_i = \varepsilon^{LDA} + U/2$$

$$\Rightarrow \Delta\varepsilon_i = U$$

The SCF Loop

How to solve the Kohn-Sham eqns. For a set of fixed nuclear (ionic position)

V_{ion} known /constructed

Initial guess

$n_{in}(r)$

Calculate $V_H(n)\&V_{xc}(n)$

$$V_{eff}(r) = V(r) + V_H(r) + V_{xc}(r)$$

$$H\psi_i(r) = \left[-\frac{1}{2\nabla^2} + V_{eff}(r)\right]\psi_i(r) = \varepsilon_i\psi_i(r)$$

Calculate new $n(r) = \sum_i |\psi_i(r)|^2$

Self-consistent?

NO

Generate new *n(r)*

Yes

Problem solved! Can now calculate energy, force, etc

3.2、单层砷： Arsenene

M. Yang, W.M. Liu, arXiv: 1501.04350

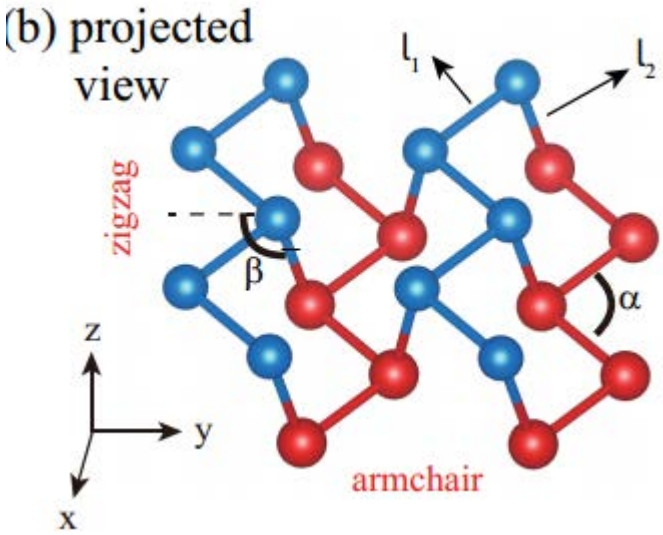

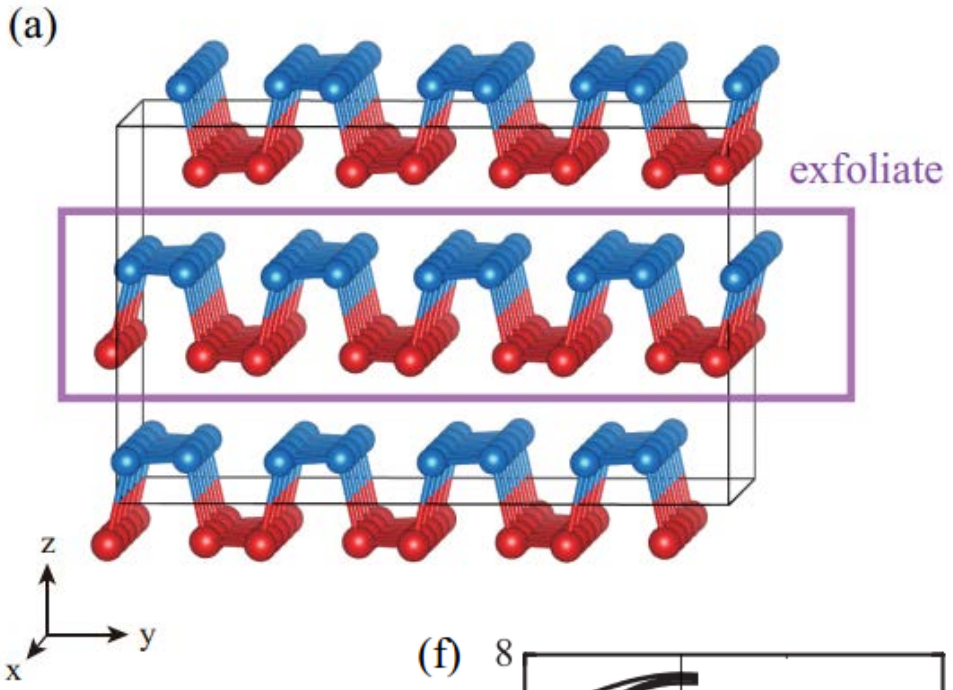

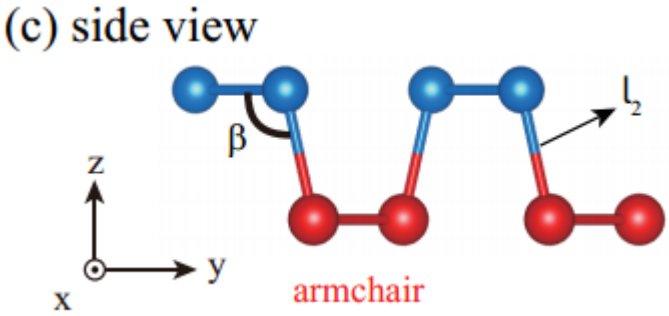

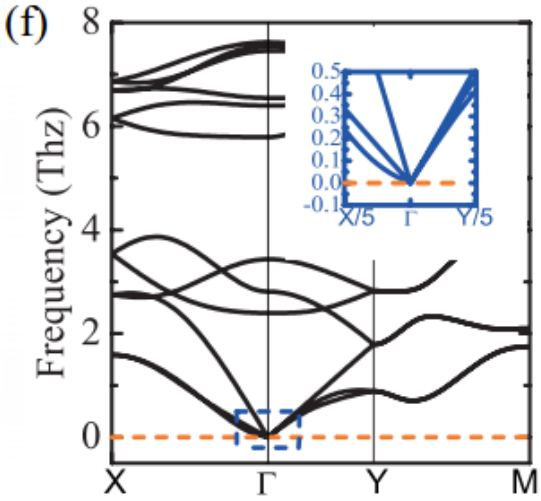

Quantum topological phase transition

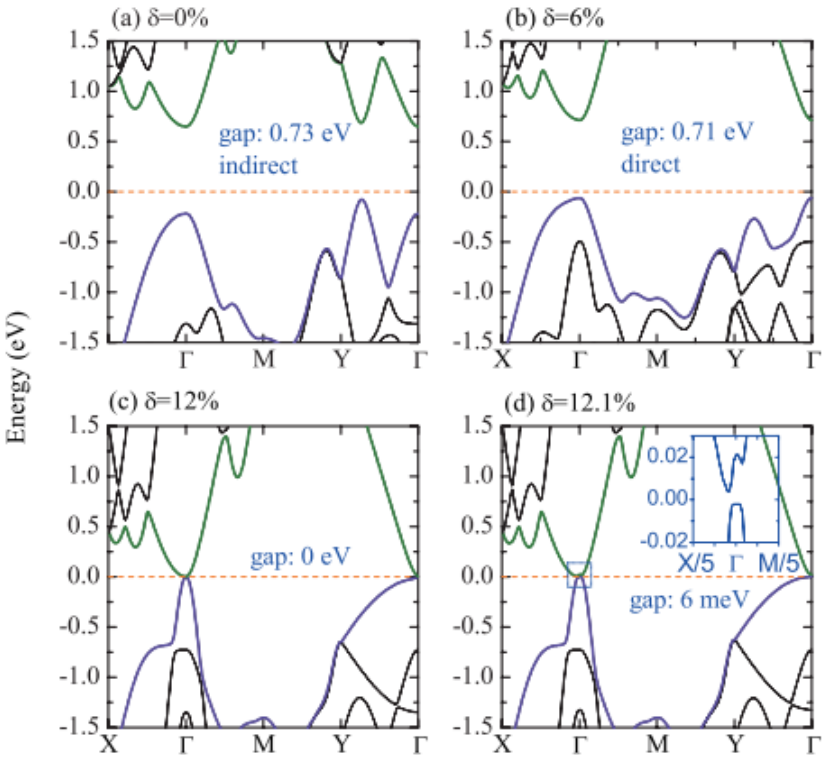

(a)-(d) The band structure of arsenene under zigzag-direction strain 0%, 6%, 12% and 12.1%.

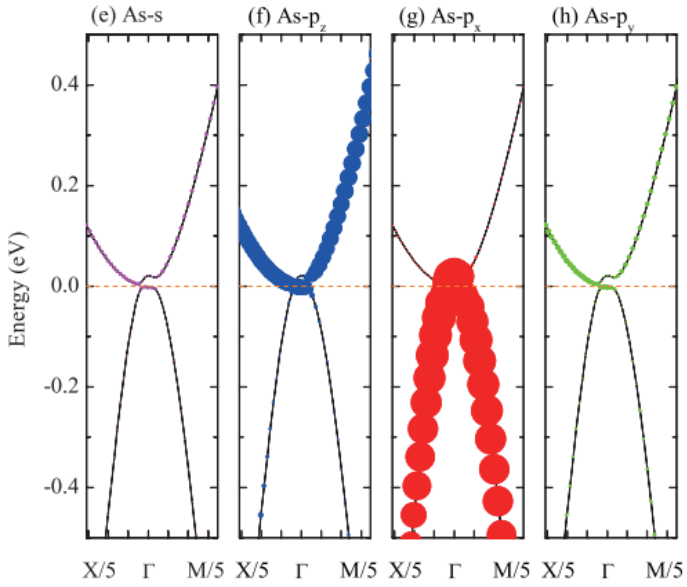

(e)-(h) The orbital-projected band structures under 12.1% strain.

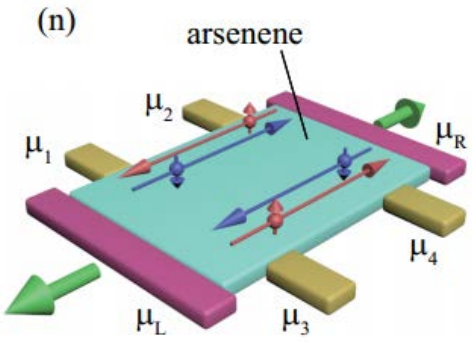

(n) Experimental setup for the detection of the topological phase transition in arsenene.

3.3、两层黑磷：

T. Zhang, J.H. Lin, Y.M. Yu, X.R. Chen, W.M. Liu, arXiv: 1502.01805

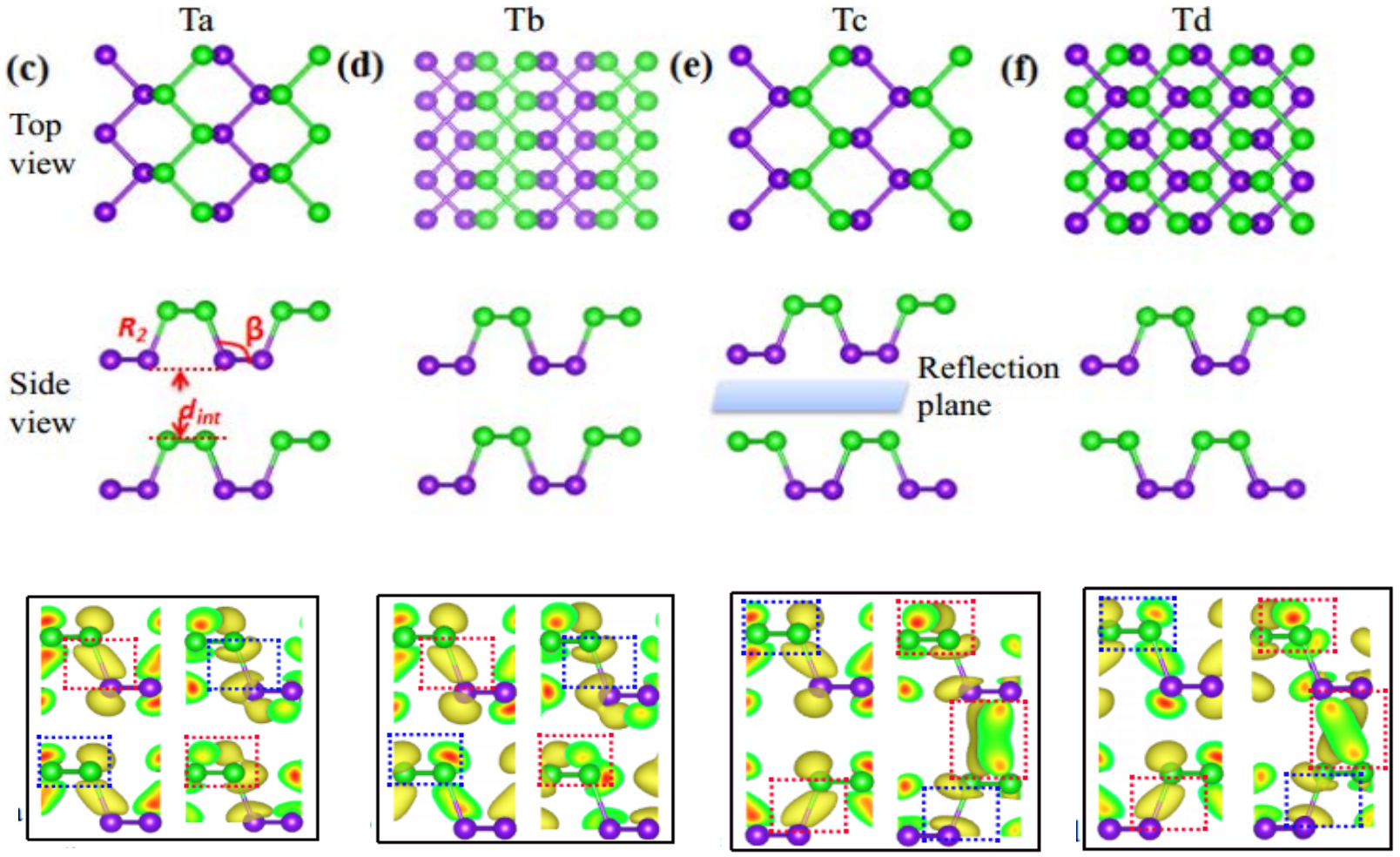

(e)-(h) The isosurface of band-decomposed charge densities on the $y-z$ plane of VBM and CBM at Γ point, A bond (antibond) is circled by red (blue) box.

Quantum topological phase transition

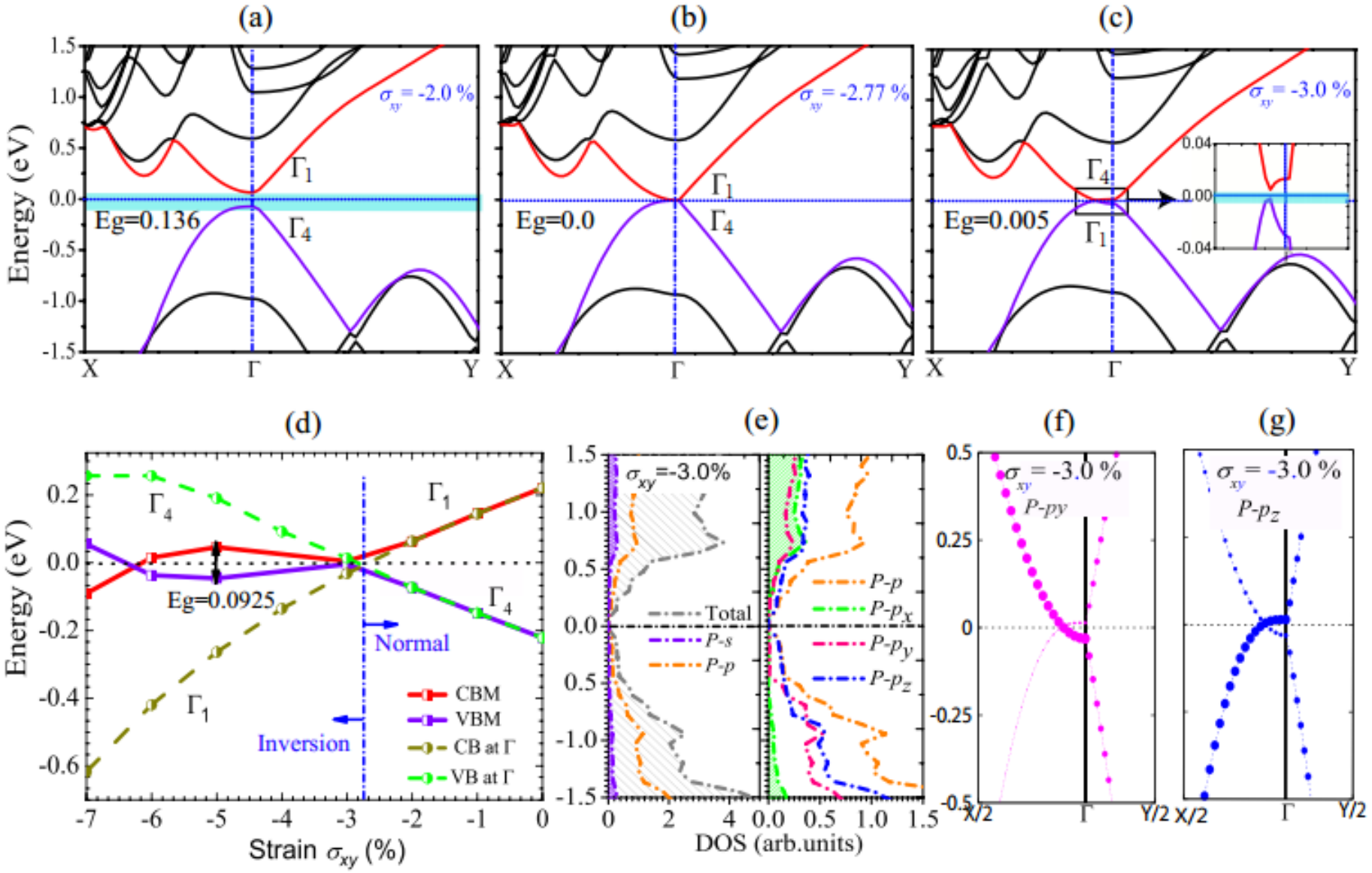

Figure 4 The electronic structures of the bilayer phosphorene for the Tb stacking order.

3.4、硅：

X.L. Zhang, L.F. Liu, W.M. Liu, Scientific Reports 3, 2908 (2013)

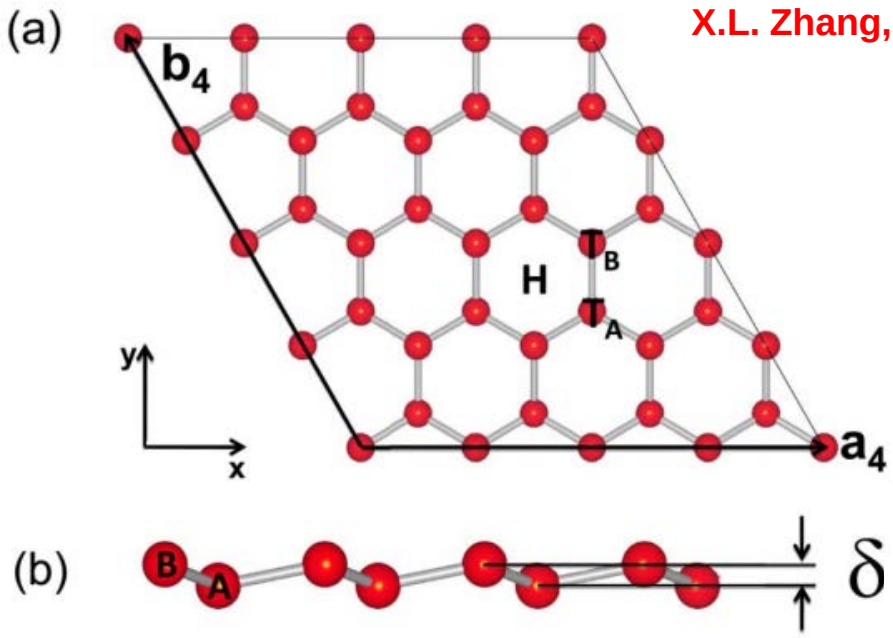

In the basis of $\{A, B\} : \{\uparrow, \downarrow\}$, the Hamiltonian reads:

$$H_{eff}^{\pm} = H_s^{\pm} + H_d^{\pm},$$

with

$$H_s^{\pm} = \varepsilon_{eff}\tau_0 : \sigma_0 \pm \tau_3 : h_{11} + \hbar v_F(k_x\tau_1 \mp k_y\tau_2 : \sigma_0,$$

$$H_d^{\pm} = \lambda_R^{ext}(\pm\tau_1 : \sigma_2 - \tau_2 : \sigma_1) + \Delta\tau_3 : \sigma_0 + M\tau_0 : \sigma_3,$$

$$h_{11} = -\lambda_{so}\sigma_3 - a\lambda_R^{int}(k_y\sigma_1 - k_x\sigma_2),$$

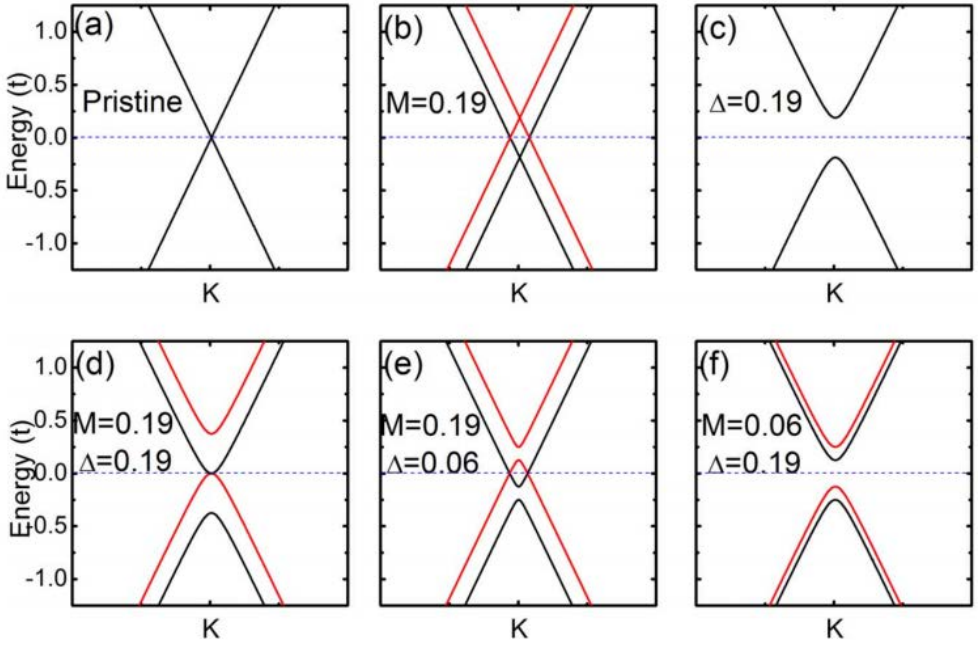

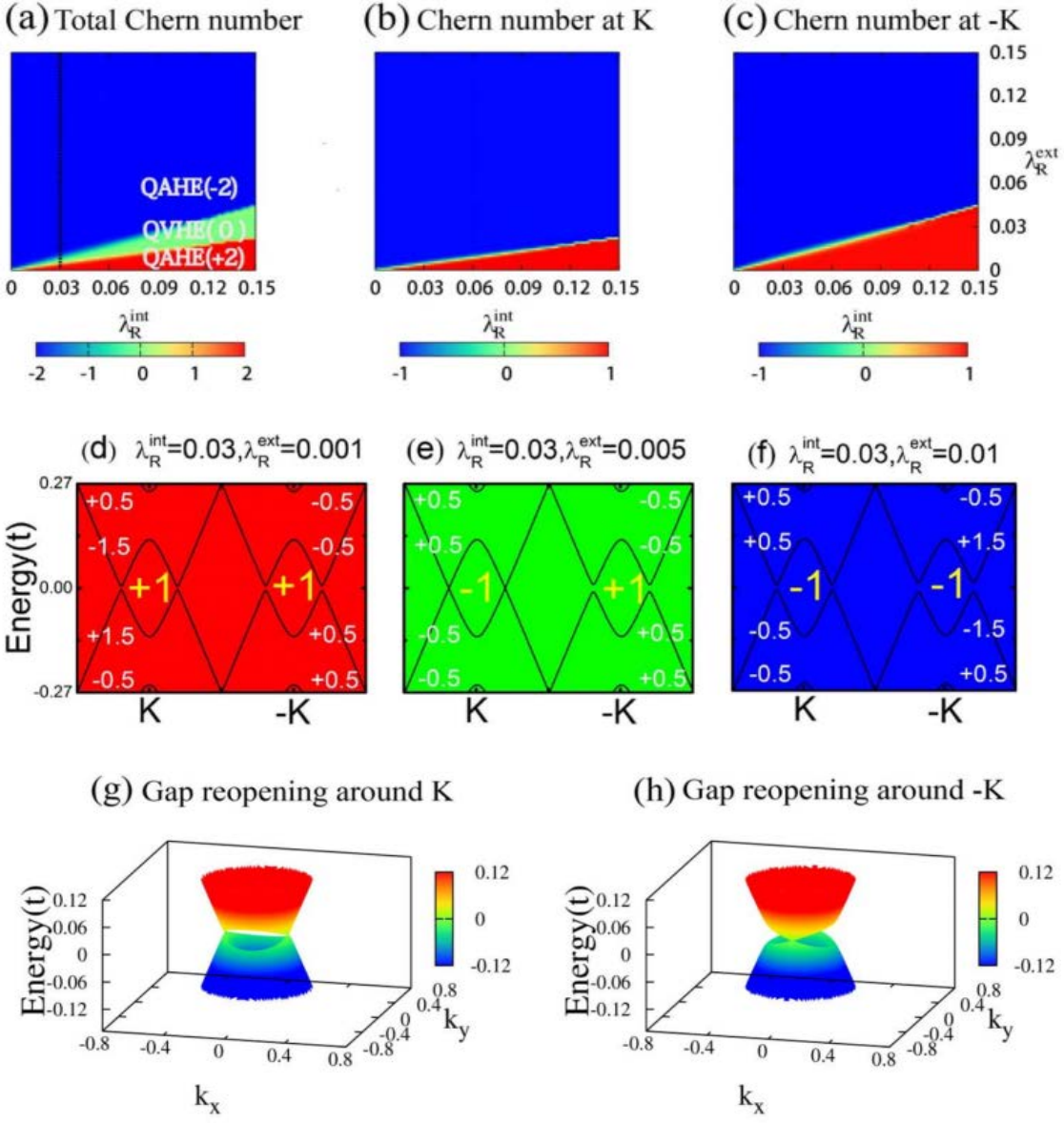

Figure 4 | The transition of Chern number by tuning Rashba SOC. The transition of Chern number by tuning λ_R^{ext} and λ_R^{int} (in unit of t). (a) Three topological nontrivial states, QAHE(2), QVHE(0) and QAHE(−2) with Chern number +2, 0, and −2, can be obtained from different combination of λ_R^{ext} and λ_R^{int}. (b) and (c) represent the the variation of $\mathcal{C}_K$ and $\mathcal{C}_{-K}$. (d), (e) and (f) depict the band structure along $k_y = 0$ line in BZ for the three topological states (QHE(2), QVHE(0) and QHE(−2)) in (a). The yellow integers (±1) represent $\mathcal{C}_K$ and $\mathcal{C}_{-K}$, corresponding to the sum of topological charge of each valence bands (the white ±0.5 and ±1.5). (g) and (h) show the gap closing around K and $-K$. They are the transition states from QAHE(+2) to QVHE(0) and from QVHE(0) to QAHE(−2), respectively.

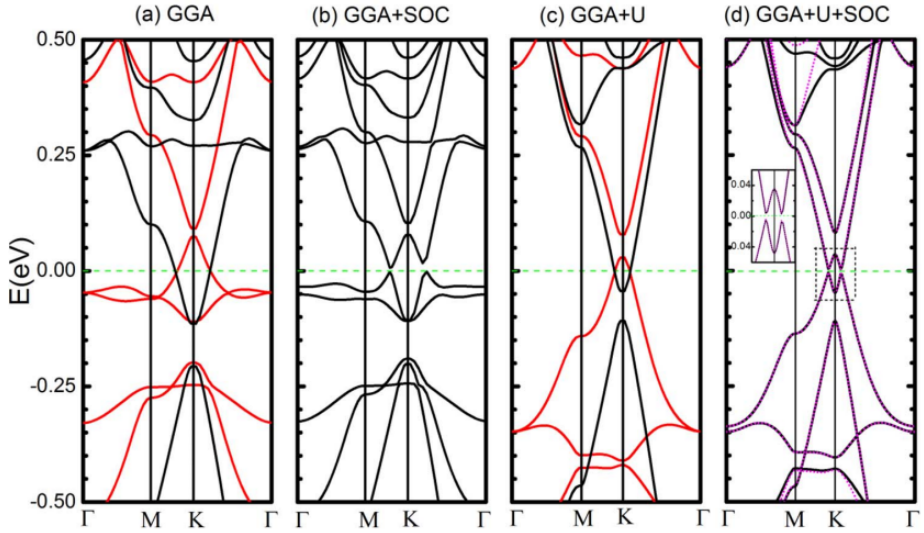

Figure 5 | The band structures of V doped silicene. (a) The band structures of V doped silicene from GGA ((a1)–(a2)) and GGA + U ((a3)–(a4)), respectively. The red (black) color in (a1) and (a3) correspond to majority spin (minority spin) subbands. After including SOC effect, a gap is opened at the Fermi level ((a2) and (a4)). In (a4), the band structure from Wannier interpolation is also shown in pink dashed lines.

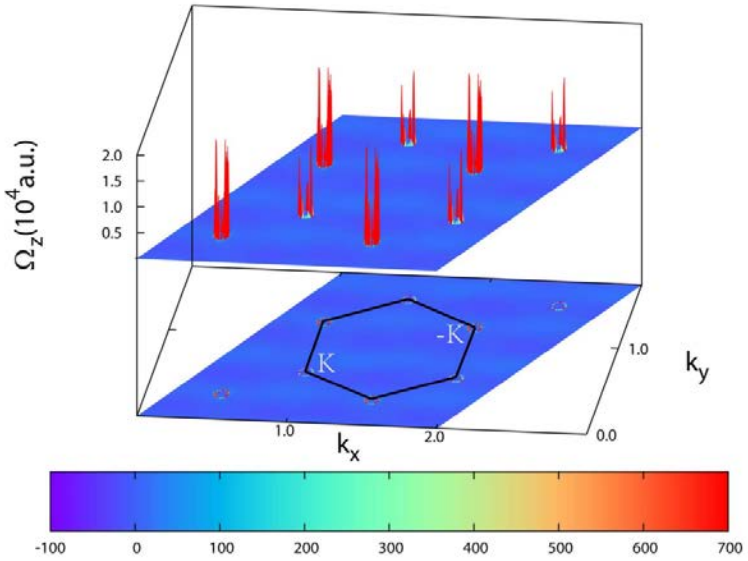

Figure 6 | The Berry curvature distribution of V doped silicene. The distribution of Berry curvature ($\Omega_z(k)$) of all occupied states in V doped silicene from GGA + U + SOC. The first Brillouin zone is marked out with black hexagon. The small red circles in the projection drawing represent the most non-zero values of Berry curvature.

3.5、方钴矿结构中的d-p反带拓扑绝缘体 IrBi3

M. Yang, W.M. Liu, Scientific Reports 4, 5131 (2014)

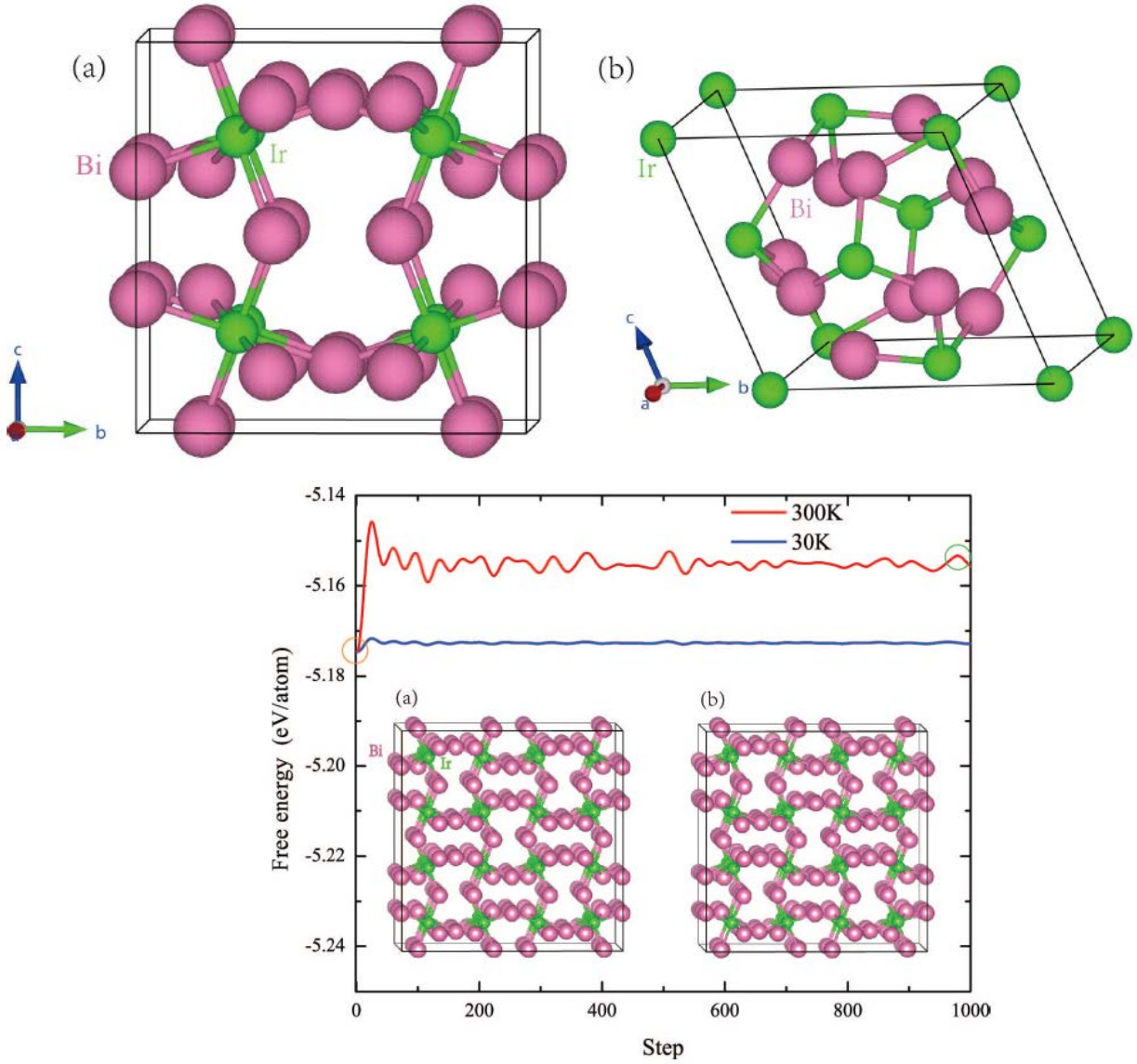

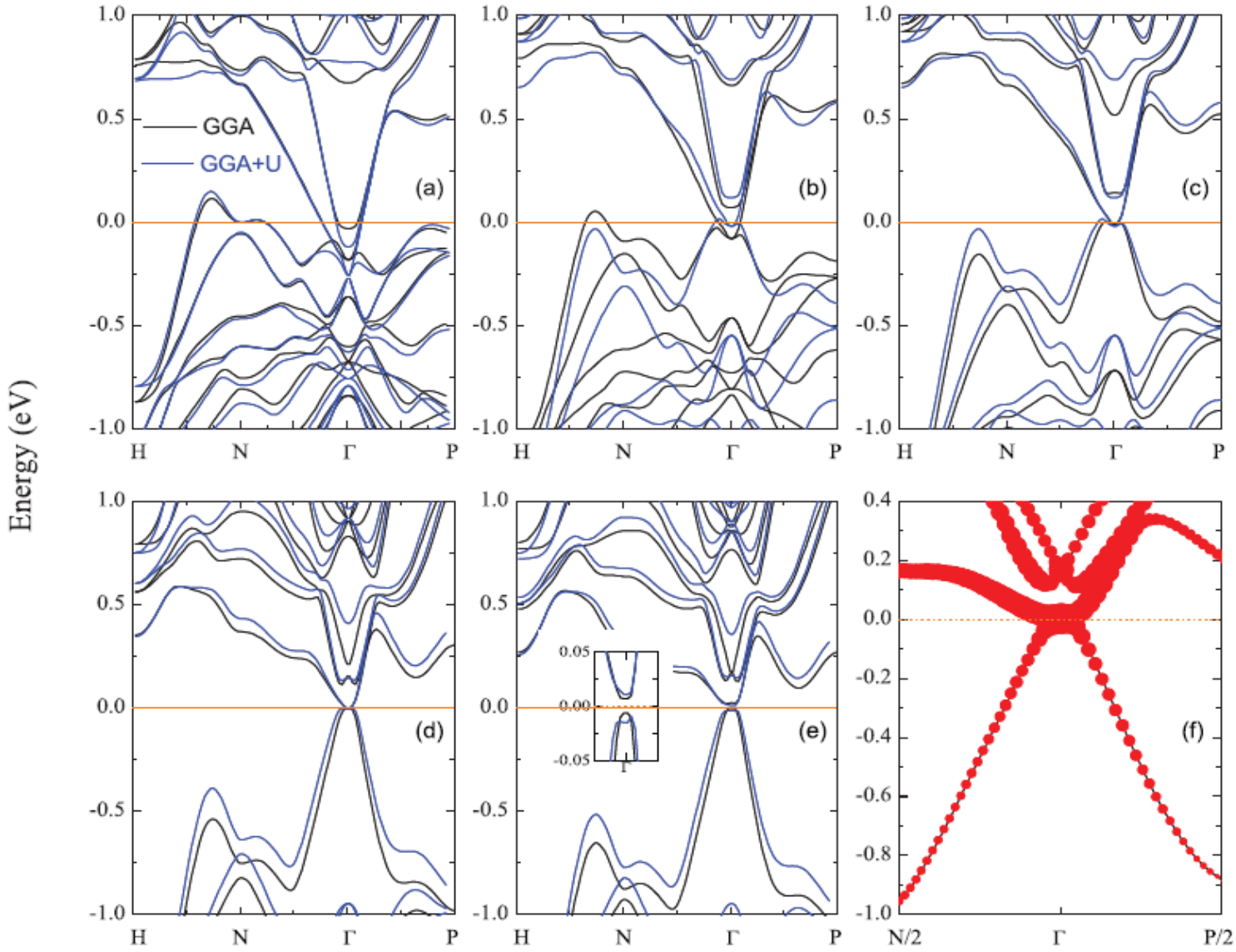

Figure 4 | Band structures of $IrBi_3$. The black and blue lines in all subfigures represent the GGA band structures and GGA+U band structures respectively. (a) band structure without exerting pressure, the system is in normal metal state with its bands go across the Fermi level several times. (b) to (d) represent the band structures at isotropic strain 3%, 6%, 9% respectively. With the increase of isotropic strain ((a) to (d)), the valence band crossing the E_F along H-N moves downwards gradually. In the band structure under 9% uniform strain (d), a zero gap metal state is obtained. (e) further impose a 2% suppression on the length of c-axis of the primitive cell, a gap appeared at the Fermi level due to the breaking of the cubic symmetry. The inset of (e) is the zoom-in of the band structure close to the Fermi level. (f) Ir-d projected band structure near Fermi level, the radii of red circles are proportional to the weight of Ir-d states, showing a significant band inversion.

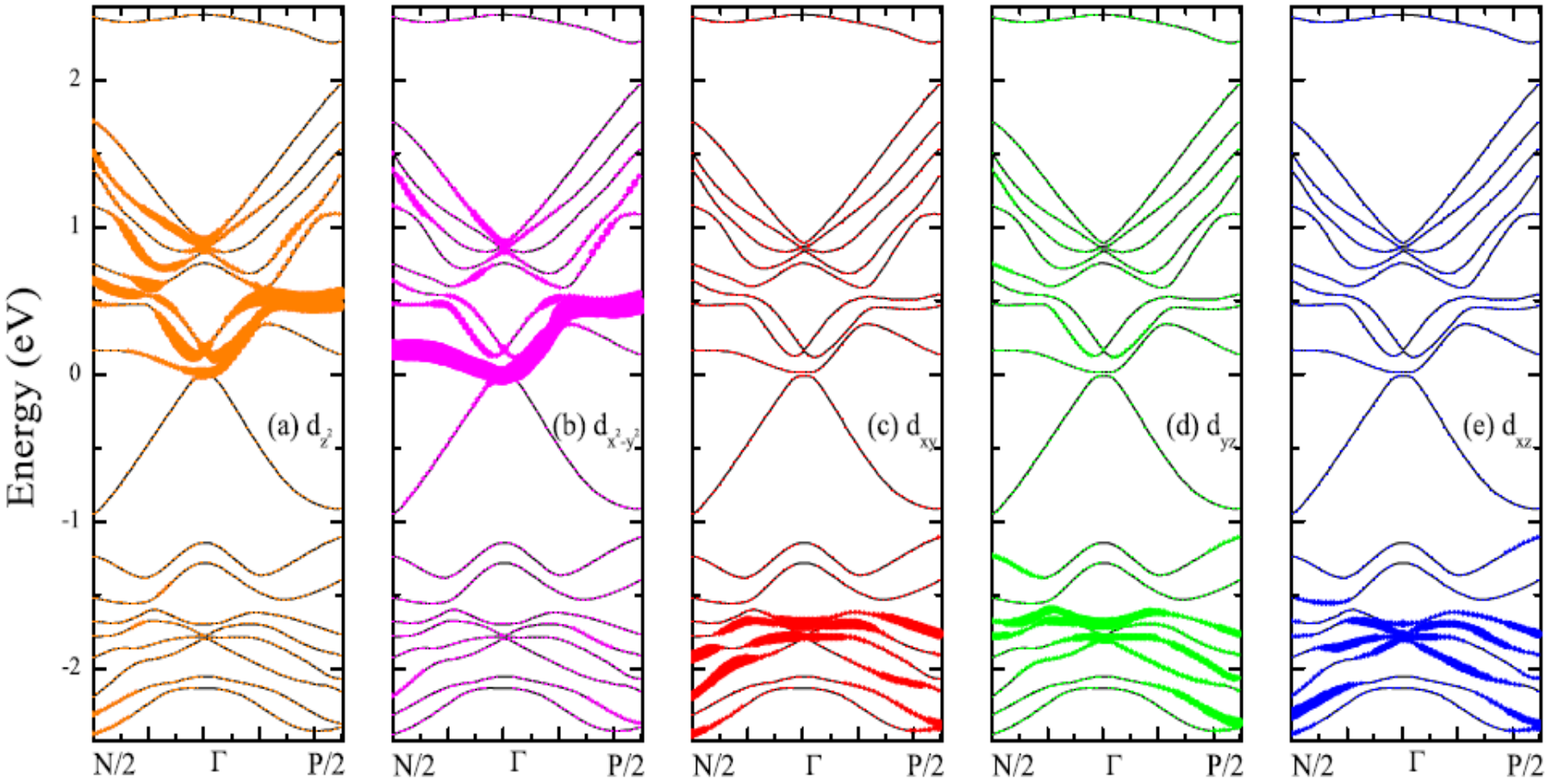

Figure 6 | Orbital-projected band structures. The orange, violet, red, green and blue colors in subfigures represent the d_{z^2}, $d_{x^2-y^2}$ and d_{xy}, d_{yz} and d_{xz} orbitals respectively. The radii of circles are proportional to the weights of corresponding orbitals. The Fermi level is set to be zero energy. It can be seen that, the t_{2g} orbitals (including the d_{xy}, d_{yz} and d_{xz} orbitals) reside far below the Fermi level and are fully occupied. While, the lowest three conduction bands are mainly contributed by the e_g orbitals (including the d_{z^2} and $d_{x^2-y^2}$ orbitals). More specifically, the $d_{x^2-y^2}$ orbital makes an even larger contribution than the the d_{z^2} orbital for the lowest conduction band.

结 论

1. 概况：量子相变
2. 强关联系统量子相变：
   - 2.1. 团簇动力学平均场方法
   - 2.2. 六角晶格：量子自旋霍尔效应、拓扑绝缘体
   - 2.3. kagome 晶格：Kondo金属
   - 2.4. Shastry-Sutherland 晶格：反铁磁金属
3. 自旋-轨道耦合系统量子相变：
   - 3.1. 第一性原理
   - 3.2. 单层砷：拓扑量子相变
   - 3.3. 两层黑磷：
   - 3.4. 硅：量子反常霍尔效应
   - 3.5. 方钴矿：反带拓扑绝缘体
4. 结论